HEINZ NIXDORF INSTITUT
UNIVERSITÄT PADERBORN

Claas Tebrügge

Towards Feasible Vehicular Visible Light Communication

Dissertation

April, 2022

Please cite as:
Claas Tebruegge, “Towards Feasible Vehicular Visible Light Communication,” PhD Thesis (Dissertation), Heinz Nixdorf Institute, Paderborn University, Germany, April 2022.

Distributed Embedded Systems (CCS Labs)
Heinz Nixdorf Institute, Paderborn University, Germany

Fürstenallee 11 · 33102 Paderborn · Germany

http://www.ccs-labs.org/

Towards Feasible Vehicular Visible Light Communication

Dissertation
zur Erlangung des Grades

DOKTOR DER NATURWISSENSCHAFTEN

vorgelegt von

Claas Tebrügge

geb. am 26. September 1990
in Wittmund, Deutschland

angefertigt in der Fachgruppe

Distributed Embedded Systems
(CCS Labs)

Heinz Nixdorf Institut
Universität Paderborn

In Kooperation mit dem E-LAB
und der HELLA GmbH & Co. KGaA

Betreuer:	**Prof. Dr.-Ing. habil. Falko Dressler**
Gutachter:	**Prof. Dr.-Ing. habil. Falko Dressler**
	Prof. Dr. Sinem Coleri
Tag der Abgabe:	**12. Januar 2022**
Tag der Promotion:	**4. April 2022**

Abstract

This thesis investigates the suitability of Vehicular Visible Light Communication (V-VLC) for the implementation of intelligent traffic systems and identifies, applies, and evaluates solutions to achieve reliable communication.

The general trend towards digitalization and networking offers opportunities to significantly increase efficiency and safety for future traffic. Among others, dynamic scenarios, the number of users, and the high demands on reliability and security result in extraordinary requirements on communication technologies. This is one reason why the question of the communication technology for networking vehicles is not solved at the time of this work. Different technologies and combinations thereof are being discussed. Besides traditional radio communication, V-VLC turned out to be a promising communication technology. Especially the combination of Visible Light Communication (VLC) and radio communication offers the potentials to achieve reliable communication for a diverse set of traffic scenarios.

This thesis identifies challenges in the field of visible light communication for the use of Inter-Vehicle Communication (IVC). Special attention is given to the appropriate control of vehicle lighting to achieve sufficient bandwidth and bandwidth efficiency, the analysis of legal regulations, especially the radiation characteristics, and the handling of disturbances on the hardware level. For this purpose, analytical considerations, experiments, as well as field tests on prototypes are performed. On the one hand, our investigations show the feasibility of V-VLC in an application-oriented approach, and on the other hand, we develop novel concepts and methods, such as Space-Division Multiple Access (SDMA) on matrix headlights, which represent a further step towards practicable and reliable V-VLC.

Kurzfassung

Im Rahmen dieser Arbeit wird die Eignung von Lichtbasierter Fahrzeugkommunikation (engl.: Vehicular Visible Light Communication (V-VLC)) für die Realisierung intelligenter Verkehrssysteme untersucht. Dazu werden technologische Lösungen entwickelt, implementiert und hinsichtlich einer hinreichend geeigneten, zuverlässigen Kommunikation zwischen Fahrzeugen bewertet.

Die grundlegenden Entwicklungen in der Digitalisierung und Vernetzung bieten Chancen, die Effizienz und Sicherheit im Bereich der Verkehrstechnologie maßgeblich zu erhöhen. Voraussetzung für die Realisierung dieser Zielsetzung ist eine Implementierung einer geeigneten Kommunikation zwischen Fahrzeugen. Unter anderem ergeben sich aus den dynamischen Szenarien, der hohen Anzahl der Nutzer und den hohen Anforderungen an Zuverlässigkeit und Sicherheit besonders hohe Ansprüche an die Kommunikation. Bisher ist nicht hinlänglich geklärt, welche Kommunikationstechnologie für die Vernetzung von Fahrzeugen eingesetzt werden sollte. Unterschiedliche Technologien und deren Kombination stehen zur Diskussion. Neben den traditionellen Funktechnologien zeigt sich die Lichtbasierte Kommunikation als eine vielversprechende Technologie, welche Probleme der Funktechnologie überwinden kann. Speziell die Kombination von Funk- und Lichtbasierter Kommunikation stellt eine erfolgversprechende Lösung zur Erreichung einer geeigneten, zuverlässigen Kommunikation in den vielfältigen Verkehrsszenarien dar.

In dieser Arbeit werden zunächst technische Hindernisse der Implementierung von Lichtbasierter Kommunikation für den Datenaustausch zwischen Fahrzeugen identifiziert. Besonders herausgestellt werden dabei die geeignete Ansteuerung der Fahrzeugbeleuchtung, um eine adäquate Bandbreite und Bandbreiteneffizienz zu erreichen, die Analyse der rechtlichen Rahmenbedingungen (z.B. die Richtlinien der Abstrahlcharakteristik), sowie die Handhabung von Interferenz auf Hardwareebene. Dazu werden analytische Betrachtungen, Experimente sowie Feldtests anhand von Prototypen durchgeführt. Im Ergebnis zeigen diese Untersuchungen die Realisierbarkeit von V-VLC in anwendungsnahen Szenarien. Darüber werden neuartige Verfahren präsentiert, die einen weiteren Schritt auf dem Weg zu einer praktikablen und zuverlässigen Lichtbasierten Fahrzeugkommunikation ebnen.

Acknowledgements

First, I would like to thank my PhD supervisor Falko Dressler. Thank you for the motivating supervision and your valuable advice. I was privileged to learn a lot from you. For me, you embody a great and ambitious way of working, which is characterized by high discipline together with great joy and motivation, which I was allowed to live out together with you and our team.

I would like to thank my friends and colleagues at the University of Paderborn, the CCS-Labs, TKN at TU Berlin, Hella, the L-Lab and the E-Lab. You have made a huge contribution to the success of the work and to the fact that it was such a wonderful time. I sincerely thank each of you.

Especially, I would like to thank my family; through our cohesion I always have a safe harbor to draw energy from.

Last but not least, I would like to thank my fiancée Hanieh Babaei. I was blessed to meet you during this work. You have made a big difference in my life. The joy I experienced through you gives me a lot of strength.

Contents

Chapter 1

Introduction

Since the invention of the automobile, traffic has been increasing rapidly. Only sophisticated safety systems have allowed the number of traffic fatalities to be kept within reasonable limits despite this increase. Initially, safety was increased by mechanical systems such as a crumple zone, passenger cell, or seat belts [1]. Then safety was further enhanced by electromechanical systems such as airbags [2]. Electronic systems and increased use of sensors made it possible to develop systems such as Adaptive Cruise Control (ACC) or the emergency brake assistant, which further increased safety [3]. Inter-Vehicle Communication (IVC) enables vehicles to perceive their surroundings more precisely and over a greater distance by exchanging data between vehicles and the infrastructure, thus obtaining information from the external environment in addition to the sensors on board. This enables them to react more reliably and early enough to avoid accidents [4] on the one hand, and to drive more efficiently by a smoother traffic flow on the other [5]. In the next step, cooperative automated driving can be realized [6] to empower vehicles to coordinate a cooperatively optimized solution to the driving task in advance instead of only reactively interacting with each other.

At present, various radio communications for the realization of intelligent traffic systems are under discussion. Dedicated Short Range Communication (DSRC) [7] and Cellular V2X (C-V2X) [8] are particularly popular. Due to high dynamics, widespread propagation, and the probable presence of many communication participants, these systems may not always be sufficient to enable safety-critical applications with the desired reliability [9]–[11]. One promising solution is to combine several communication technologies in order to complement each other positively. It seems to be particularly useful to combine physically different technologies so that their respective positive characteristics complement each other and cancel out the disadvantages [12]. For this reason, line-of-sight communication technologies such as Visible Light Communication (VLC) [13]–[16] or mmWave [17] are particularly

under discussion. Due to the high frequency in each case, the direct Line of Sight (LOS) path of communication dominates and the radiation can be easily isolated by objects [18]. This ensures that the signal is received by a limited number of receivers and therefore less multi-user interference occurs. This results in increased scalability [19], which makes these communication technologies suitable for dense traffic situations. VLC, as an advantage, has a license-free and mostly unused spectrum while the implementation costs are relatively low [20]. VLC gained popularity with the emergence of Light Emitting Diodes (LEDs) and their rapid switchability. In recent years, the LED caused a revolution in illumination technology and is now widely used in the lighting industry, because of its robustness, energy efficiency, and versatility. The rapidly increasing use of LEDs in headlights and taillights of vehicles enables the implementation of VLC for IVC, called Vehicular Visible Light Communication (V-VLC).

In general, VLC has made great progress in recent years, prototypes have impressively demonstrated the performance of VLC in terms of reliability and data rate, and the first VLC products are already on the market. However, these advances are mainly related to indoor communication. For outdoor communication, especially between vehicles, there are still challenges ahead.

1.1 Goals and Structure of the Thesis

The goal of the thesis is to examine the feasibility of V-VLC for reliable inter-vehicle communication, to identify possible challenges, and to identify appropriate solutions. To evaluate the feasibility of V-VLC, the following objectives are investigated and evaluated.

- Communicate over a typical distance occurring in traffic of 50 m with a bit error probability of less than 10^{-6}.
- Achieve a data rate that can send all vehicle data relevant to cooperative driving with a sufficient update interval.
- Performing the communication task while maintaining the main task of vehicle illumination and meeting acceptable component cost.
- Robust communication in real traffic scenarios

For this reason, the thesis is structured as follows. In Chapter 2, the technical fundamentals underlying V-VLC are presented. First, the current state of networking of vehicles across different communication technologies is presented. Then, the functional principle of VLC is explained step by step along the transmission chain. At the end of the fundamentals, the basics of vehicle lighting are given, since these have

a crucial influence on the behavior of V-VLC, as will concretely become apparent in the course of the work.

In Chapter 3, an analytical model is developed that is capable of providing information about the location-dependent RSS, channel capacity, and error probabilities of the communication, taking into account the hardware used. First, the model is verified empirically. Then, the model is used to investigate, for example, the influence of the type and mounting position of the transmitting light source or the behavior of the pitching due to the braking process. The chapter concludes with empirical measurements to determine the applicability of the model depending on the channel's characteristics.

Chapter 4 shows the implementation and evaluation of a prototype communicating with a commercial headlamp over 70 m with Orthogonal Frequency Division Multiplexing (OFDM) in a field test. The modulation is done with the Software Defined Radios (SDRs) and the open-source framework GNU-Radio. Depending on the distance, different Modulation and Coding Schemess (MCSs) prove to be reliably applicable. A comparison with the analytical model shows the success of the implementation through small deviations from the measurement.

Chapter 5 is addressed to the avoidance of interference. Two approaches are considered. First, a novel receiver prototype is presented and evaluated, which specifically suppresses spatial interference sources. Second, a prototype concept is presented in which individual LEDs are controlled using modern matrix headlights in order to emit information selectively into a limited solid angle. This reduces multi-user interference, enables the reuse of communication resources, and increases security against eavesdropping.

Chapter 6 summarizes the thesis and identifies future research questions. Thus, the thesis demonstrates the feasibility of V-VLC on an analytical and practical prototype-based basis. Limits and solutions are presented and evaluated. Potentials that further increase reliability are presented. Overall, this work takes a step towards a feasible V-VLC through the insight gained.

1.2 Publications

The work is based on the following publications:

- S. Kruse, C. Kress, et al., "Design of an Automotive Visible Light Communications Link using an Off-The-Shelf LED Headlight," in *16th GMM/ITG-Symposium ANALOG 2018*, Munich, Germany: VDE, Sep. 2018

  This publication is the result of the collaboration of the Schaltungstechnik (SCT) group led by Christoph Scheytt and the CCS-Labs group led by Falko Dressler. I could contribute by supporting to stabilize the circuit for real-

world usage. In addition, I performed the first measurements evaluating the properties of the circuit on the communication.

- A. Memedi, C. Tebruegge, et al., "Impact of Vehicle Type and Headlight Characteristics on Vehicular VLC Performance," in *10th IEEE Vehicular Networking Conference (VNC 2018)*, Taipei, Taiwan: IEEE, Dec. 2018

  In this publication, I contributed by developing an analytical model and validating it empirically. In addition, I assisted in the integration into Veins.

- C. Tebruegge, A. Memedi, and F. Dressler, "Empirical Characterization of the NLOS Component for Vehicular Visible Light Communication," in *11th IEEE Vehicular Networking Conference (VNC 2019)*, Los Angeles, CA: IEEE, Dec. 2019, pp. 64–67

  My contribution to this publication is the development of the analytical model. I was furthermore supported in the integration into Veins and performed measurements for the validation of the model.

- M. S. Amjad, C. Tebruegge, et al., "An IEEE 802.11 Compliant SDR-based System for Vehicular Visible Light Communications," in *IEEE International Conference on Communications (ICC 2019)*, Shanghai, China: IEEE, May 2019

  In this work, I was able to contribute by setting up the transmission chain with a focus on the electro-optical system. As well as the experimental design and execution of the collaboratively developed prototype.

- C. Tebruegge, Q. Zhang, and F. Dressler, "Optical Interference Reduction with Spatial Filtering Receiver for Vehicular Visible Light Communication," in *22nd IEEE International Conference on Intelligent Transportation Systems (ITSC 2019)*, Auckland, New Zealand: IEEE, Oct. 2019

  My contribution in this publication is the system design of the prototype, the experimental design and execution, and the support in the optical design.

- C. Tebruegge, A. Memedi, and F. Dressler, "Reduced Multiuser-Interference for Vehicular VLC using SDMA and Matrix Headlights," in *IEEE Global Communications Conference (GLOBECOM 2019)*, Waikoloa, HI: IEEE, Dec. 2019

  My contribution to this publication is the conceptual unification of the idea of locally separated radiation of the modulated light signal and modern matrix headlights. Furthermore, the planning and realization of the experiments for the evaluation of the system.

In addition, the following publication was produced as part of the research in the scope of the thesis:

- M. S. Amjad, C. Tebruegge, et al., "Towards an IEEE 802.11 Compliant System for Outdoor Vehicular Visible Light Communications," *IEEE Transactions on Vehicular Technology (TVT)*, vol. 70, no. 6, pp. 5749–5761, Jun. 2021

  I contributed to this publication mainly by building the transmission chain with a hardware focus, analyzing the bandwidth, and building an analytical analysis as a reference to the measurement results.

Chapter 2

Fundamentals

In the following, the fundamentals of this work are explained. Before describing in detail how V-VLC can improve modern traffic systems, the current status and basics of vehicle communication in general and intelligent traffic systems will be presented.

Light-based communication has made great progress in recent years, especially in the indoor area, and the first commercial products have been established. The basic functionality of VLC will be explained, and different versions will be compared. The components used in a typical VLC transmission chain are explained and their effects on communication are considered. In addition, the essential differences in outdoor and vehicle applications are explained and the challenges to be overcome are pointed out.

As it is a goal to use existing lighting systems of vehicles for VLC to ensure a cost-effective integration, the basics and fundamental aspects of vehicle lighting are presented. A short historical development of vehicle lighting systems is shown as well as the basic regulations that govern vehicle lighting.

2.1 State of the Art of Vehicular Communication

In consideration of the enormous possibilities connected vehicles promise to offer, there are several attempts to enable communication between vehicles. The individual technologies and the concept, in general, are described in the following. IVC describes the networking of vehicles. This can include the networking of vehicles with each other (Vehicle-to-Vehicle (V2V)), vehicles and infrastructure (Vehicle-to-Infrastructure (V2I)), and the networking of vehicles and everything else (Vehicle-to-Everything (V2X)). In Europe, the synonyms C2C, C2I, and C2X are also frequently used, with Vehicle being replaced by the word Car. IVC is an important component of Intelligent Transportation System (ITS) that can make future traffic safer [4], more efficient [5], and more comfortable.

The exchange of data between vehicles allows a multitude of new applications to be realized. The European Telecommunications Standards Institute (ETSI) already collects a large number of applications in its technical report [28]. The applications include warnings of special vehicles, such as emergency vehicles [29] or slow vehicles, of dangerous situations, such as construction sites or stationary vehicles, and dangerous maneuvers, such as threading into driveways or lane changes. In addition, some methods for increasing traffic efficiency are described, for example, a speed recommendation for traffic light controlled intersections, for which several field tests have already been conducted [30].

With cooperative driving, a new dimension of efficiency can be achieved. By combining automated driving with IVC, cooperative driving maneuvers can be realized [6]. Vehicles are enabled to organize themselves in platoons which are capable of lowering air drag due to reduced distances between the participants. Also, by utilizing cooperative optimization of the driving task vehicles can drive more anticipatory and thus safe fuel and enable a smooth traffic flow [31].

By sending Collective Perception Messages (CPMs) and a subsequent fusion of the data with further sensor data, a more reliable environment scenario with a greater range is created [32].

Several technologies can be used for data transmission. On the one hand, centralized infrastructure-based communication technologies such as UMTS or LTE. On the other hand, distributed ad-hoc communication such as 802.11p based standards (ARIB, WAVE, DSRC) or LTE-V2X as well as 5G based device-to-device communication. Due to the high-reliability requirements of safety-critical applications, the LOS-technologies like Millimeter-Wave (mmWave) or VLC is considered attractive because it could solve scalability problems to a large extent by its propagation characteristics in itself. The combination of an LOS technology, capable of higher range communication is particularly promising. At the time of writing, it has not yet been determined which technology or combination of technologies will be established.

Due to the mandatory integration of eCall systems in new vehicles in the EU since March 2018, a centralized communication technology is already widely used [33]. This is an automated emergency call in the event of an accident. The rapid sending of an emergency call together with the position of the vehicle should increase the chances of survival through a quick rescue. However, in order to take advantage of the great potential of connected vehicles and to prevent accidents before they happen, this communication technology will likely be increasingly combined with others.

In 2020, Volkswagen introduced networking based on 802.11p to the mass market with the Golf 8. Meanwhile, a trend towards 5G-based C-V2X technologies is emerging in the Chinese market through the allocation of 5.9 GHz for this technology in China.

2.2 Fundamentals of Visible Light Communication

Although VLC in its present form is a new technology, the concept of transmitting messages using light has been around for thousands of years. As early as 405 B.C., the ancient Greeks communicated between ships by deliberately reflecting the sun with the help of polished shields [34]. The use of smoke or fire signs is also known from primeval tribes.

A much more advanced way of transmitting messages based on light was shown by Alexander Graham Bell in 1880 with his photophone [35]. Bell modulated light by making a mirror vibrate in response to a speech signal. He received the signal with selenium cells located in the focal point of a parabolic mirror to convert the signal back into an audio signal.

An important basic building block for the VLC in the sense as it is treated here, i.e. for the transmission of data, was already laid in 1979 by Gfeller and Bapst [36]. The authors consider communication by infrared LEDs in buildings. Because infrared radiation is also in the range of optical wavelengths, there are many similarities to visible light. In general, communication with ultraviolet, visible, and infrared radiation can be summarized as Optical Wireless Communications (OWC) [37].

VLC is becoming increasingly popular because an increasing number of lighting tasks are being performed by LEDs [38], [39]. In recent years, LEDs have been able to further increase their performance and efficiency and, in particular, reduce production costs. At the same time, LEDs are energy-efficient [40], robust, can achieve high luminous fluxes with small dimensions, and can be controlled quickly and selectively. As a result, more and more light sources such as incandescent lamps, halogen lamps, or gas discharge lamps are being replaced by LEDs. The property of fast switchability together with the large and increasing spread of LEDs makes VLC feasibly for many applications.

A transmission chain for LED-based VLC can be constructed as shown in Figure 2.1. In many ways, the transmission chain corresponds to the transmission chain of RF communication [41]. Therefore, the differences will be highlighted in the following.

2.2.1 Coding

The generally known Forward Error Correction (FEC) methods from RF technology or wired communication can be applied for VLC. For example, Reed Solomon codes or convolutional codes are suitable [42]. A special feature of VLC is the existence of codes that regulate brightness and prevent flickering. For example, in the standard IEEE 802.15.7 [42], which is explained in more detail in Section 2.2.3, Run Length Limited (RLL) in the form of 4B6B or 8B10B is used to avoid flicker and achieve the desired dimming level. With 4B6B and 8B10B coding, 4 or 8 bits are mapped to 6

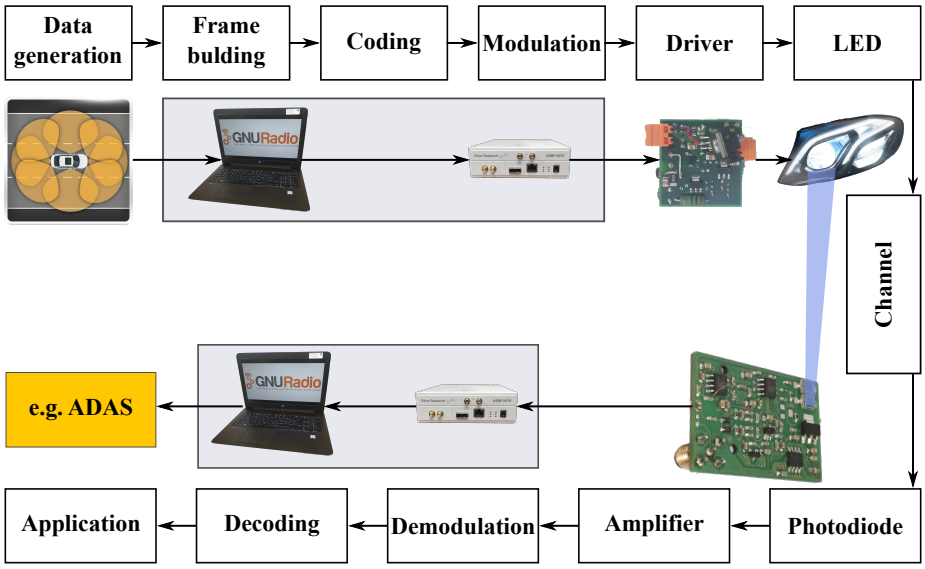

Figure 2.1 – Transmission chain of an VLC-system with exemplary hardware

or 10 bits respectively. The resulting codewords are made up of fixed ratios of zeros and ones to balance the dimming level. These special codes must generally be used when modulation is performed in the baseband and without additional methods of brightness control. For example, DCO-OFDM (cf. Section 2.2.2) with a sufficient carrier frequency does not require additional coding for brightness regulation and flicker prevention.

2.2.2 Modulation

Similar to coding, RF communication technologies can be consulted for modulation, but some of them have to be adapted since the light intensities are unipodal and real [43]. To meet these conditions, modulations can be used that are inherently unipodal and real such as On-Off Keying (OOK) and Pulse Position Modulation (PPM). Modulations that are generally complex and bipolar must be adapted, such as OFDM. There are different methods to make the signal unipodal. One solution is to add an offset to shift the signal to the positive range. This is called Direct Current-Biased Optical OFDM (DCO-OFDM) in this case of OFDM [44]. Alternatively, the negative-valued symbols can be cut off which causes predictable asymmetrical clipping, called Asymmetrically Clipped Optical OFDM (ACO-OFDM) [45]. To generate a real signal, a carrier frequency can be used to transmit real and imaginary signals with a phase shift of 90°. In baseband transmission, it must be ensured that exclusively real-valued signals are transmitted by selecting only the appropriate subcarriers that generate a real-valued signal for modulation.

Overall, several modulations are attractive for VLC. The appropriate modulation type often depends on the scenario and can vary depending on hardware, communication distance, or application. For example, ACO-OFDM can use the full amplitude compared to DCO-OFDM, but in the case of ACO-OFDM clipping causes interference on every second subcarrier, the full bandwidth cannot be used. Thus, Armstrong and Schmidt [45] proved a superior energy efficiency of ACO-OFDM compared to DCO-OFDM for low modulation orders on the basis of analytical and stimulative investigations, whereas DCO-OFDM is more energy efficient for high modulation orders. Islim and Haas [46] give an overview of attractive modulation schemes for VLC. These can be divided into Single Carrier Modulation (SCM), Multicarrier Modulation (MCM) and Color Domain Modulation (CDM). MCM can be further divided into non-OFDM based MCM, such as Hadamard Coded Modulation (HCM) [47] or Wavelet Packet Division Multiplexing (WPDM), and into OFDM based MCM. OFDM based modulation can be further divided into DCO-OFDM, inherent unipolar modulation (such as ACO-OFDM), superposition OFDM (such as Layered ACO-OFDM (LACO-OFDM) [48]), and hybrid solutions, which try to combine advantages and eliminate disadvantages the mentioned variants (such as Asymmetrically Clipped DC Biased Optical OFDM (ADO-OFDM) [49]). SCMs use a certain bandwidth without subdivision into subcarriers, which includes the less complex OOK or, for example, Carrier-less Amplitude Modulation (CAP) [50]. A special feature for VLC, which is distinct from RF communication, is CDM such as Color Shift Keying (CSK). In CSK, different wavelengths are modulated - this can be done using Red-Green-Blue (RGB)-LEDs, for example. The red, green, and blue components are varied according to the data to be transmitted so that the color point shifts. By switching the LEDs quickly and coding them accordingly, the inertia of the human eye produces a white color impression.

No single technology has yet emerged from the multitude of modulation technologies that is superior to all others. Rather, a modulation technology to be preferred results specifically for the application, which depends, among other things, on the required data rate, the communication distance, the type of light source, in particular bandwidth and linearity, as well as possible sources of interference.

2.2.3 Standardization

With the multitude of possible MCS as well as an advancing development of products, especially in the indoor area, there are already several efforts to standardize VLC. In particular, IEEE 80.15.7 [51], IEEE 802.11bb, and IEEE 802.15.13 are to be mentioned.

Already in 2011, the standard IEEE 802.15.7 was published. This standard focused on Medium Access Control (MAC) and physical layers of VLC. The avail-

able MCS are clustered in three Physical Layer Operation Modes. The Physical Layer (PHY) I is intended for outdoor use and provides OOK and Variable Pulse Position Modulation (V-PPM), uses Manchester coding or 4B6B for RLL and uses Reed-Solomon (RS)-codes and convolutional codes as FEC. Low optical clock rates of 200 kHz to 400 kHz are chosen to allow the use of high-power LEDs. The low bandwidth caused by low optical clock rates in combination with bandwidth inefficient modulation schemes leads to comparatively low data rates of 11.67 kbit/s to 266.6 kbit/s. However, the standard has not yet been established for the use of V-VLC and further adaptations should be made for this application [52].

The PHY II operation mode focuses on the application of indoor communication. It connects the modulation V-PPM and OOK with 4B6B and 8B10B as RLL. RS-coding is used for FEC. Among other things, the significantly higher optical clock rates of up to 120 MHz enable much higher data rates of up to 96 Mbit/s to be achieved. Such high optical clock rates cannot usually be achieved with vehicle lighting due to the low-pass behavior of high-power LEDs [53].

The operation mode PHY III targets RGB-LEDs, since the modulation scheme CSK is used. Optionally RS-coding can be used for FEC. With optical clock rates of up to 24 MHz, data rates of up to 96 Mbit/s can be achieved. RGB-LEDs are generally not used in vehicle exterior lighting.

IEEE 802.11bb is currently being developed by a task group that has set the goal of standardizing Light Fidelity (LiFi). Special emphasis is put on the fact that LiFi can be integrated very well into existing Wireless Fidelity (WiFi) networks. The standardization is not yet completed, current discussions suggest that OFDM will be used in the PHY. This increases overlap with other 802.11 standards and also achieves high bandwidth efficiency.

Since March 2017, a task group has been working on IEEE 802.15.13. In this task group, a physical layer and a MAC layer are being developed which will enable multiple Gigabit/s optical wireless communication. Wavelengths from 190 nm to 10 000 nm will be investigated, so that Ultraviolet (UV), Infrared (IR) and visible light will be considered. This standardization is also not yet completed and OFDM is also one of the promising candidates for the PHY.

2.2.4 VLC Driver

The modulated and coded signal must be converted into a current signal capable of driving LEDs in accordance with the signal transmission chain shown in Figure 2.1.

Some LED headlights and taillights are already modulated. Power Width Modulation (PWM) is used here, not for data transmission, but for adjusting the light intensity, i.e. dimming. PWM is experiencing great popularity because it achieves

linear dimming with low complexity. In contrast to a modified current supply, it also has the advantage that the color point does not shift.

Changing the current is another method of dimming LEDs. In terms of circuitry, however, this can be more demanding than PWM, where the current is switched on or off completely over time, as more levels have to be driven and possibly more power is lost at the electrical components that limit the current. In addition, the color point changes with the current [54]. This can have aesthetic disadvantages and, in the worst case, can lead to the color point no longer being within the range permitted for traffic.

With PWM, the LED is periodically switched on or off completely. This can be achieved even with simple semiconductor technologies such as a Metal-Oxide-Semiconductor Field-Effect Transistor (MOSFET)-circuit. Different brightness levels can be achieved by the ratio of the time being switched on or off, called the duty cycle. A sufficiently high frequency is selected so that the human eye perceives the light continuously and cannot resolve the temporal fluctuation. Since the human eye is comparatively slow, about 100 Hz are sufficient in static scenarios. To reduce flickering even with moving objects and in the peripheral visual region, lighting systems in automobiles typically use frequencies of around 500 Hz.

To achieve an adequate bandwidth for V-VLC, however, the LEDs must be switched much faster, for example in the tens of MHz range. These frequencies are usually not supported by current driver circuits because they were not required for the previous application of dimming and because, for example, capacitors are implemented on the boards for voltage stabilization, Electromagnetic Compatibility (EMC) and Electrostatic Discharge (ESD)-protection.

Acceptable switching frequencies can already be achieved with simple and inexpensive modification. In the first step capacitors connected in parallel to the LEDs should be removed. These are usually used for voltage stabilization, EMC and ESD protection. Corresponding actions must be relocated in front of the driver circuit. The measure reduces the low-pass behavior of the LED board and thus opens the possibility of driving at high frequencies, which increases bandwidth. This is also indicated by the faster slope of the LED when switched on.

An example circuit for fast switching between the states of an LED is shown in Figure 2.2. The first operational amplifier stage serves to raise the input signal, which could come from an SDR for example, to the desired level. This signal can be optionally amplified by a gate driver, so the gate of the following MOSFET can be switched faster by applying a higher current. Finally, the MOSFET switches the current of the LED, thus varying the brightness. This type of driver is used to switch the LED on or off hardly.

Intermediate brightness levels are only possible to a limited extent with this type of driver, as they are affected by non-linear behavior and cause a lot of waste

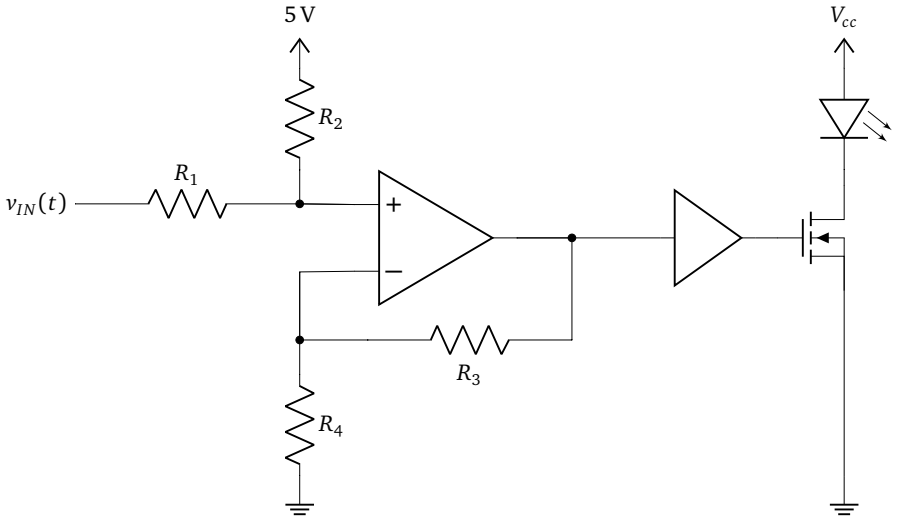

Figure 2.2 – Simplified schematic of an on-off VLC driver

heat at the MOSFET. However, this circuit can be used to transmit data by using modulation techniques that do not use a variety of amplitude levels to transmit data. The circuit has been successfully tested with OOK, PPM and Frequency Shift Keying (FSK). However, the data rates achievable with this type of driver circuit are limited because the usable bandwidth is limited by parasitic capacitors of the LED boards and the response time of the phosphor. To achieve higher data rates modulations with higher bandwidth efficiency must be used. This is usually done by enabling the variation of the amplitude. Thereby Pulse Amplitude Modulation (PAM) and Quadrature Amplitude Modulation (QAM) become possible. This allows more data to be sent per symbol, but on the other hand, more complex drivers are needed to drive the LEDs with different intensity levels as linearly as possible.

Within the scope of this research, a driver circuit capable of the previously mentioned characteristics was developed [21]. With this driver, a constant current passes through the LED to eliminate the problem of unipodal signals and to drive the LED in the linear range. A simplified schematic of this driver is illustrated in Figure 2.3. On the left side of the circuit, a Transconductance Amplifier (TCA) is used to generate a linear current signal i_{AC} which is highly linear to the input voltage v_{IN}. A bias tee separates the DC component (I_{DC}) from the high-frequency signal (I_{AC}). The bias tee consists of the inductance (L_1) which conducts the constant current and blocks the high-frequency signal and the capacitors (C_1 and C_2) which blocks the constant current and allows the high-frequency signal to pass. This circuit was successfully tested with a 70 m OFDM transmission in [24]. The field test is described in detail in Chapter 4.

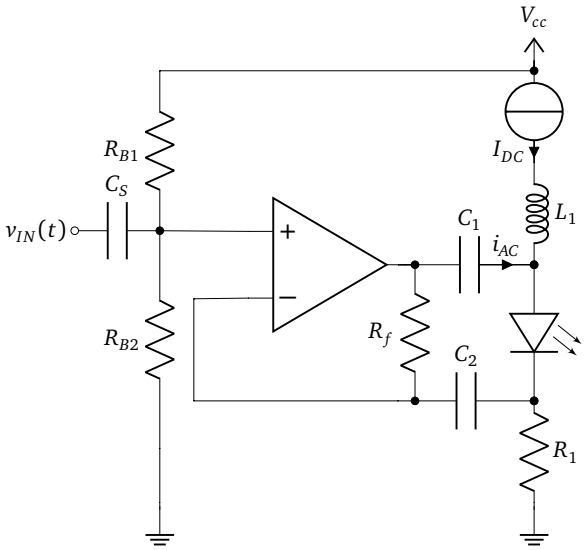

Figure 2.3 – Simplified schematic of a linear VLC-LED-Driver from [21]

Even if this circuit is already producing satisfactory results, further improvements can be achieved in the future if V-VLC is considered from the very beginning when developing headlamps and taillights. Higher bandwidths can be achieved by using short wiring to reduce inductance and avoiding parasitic capacitors due to large conductor areas, for example.

2.2.5 Light Source

For VLC with Intensity Modulation and Direct Detection (IM/DD) fast switchable light sources are essential. These are laser diodes, which are not widely used at present due to production costs, and LEDs, which have gained enormously in importance and popularity in the last decade. LEDs are semiconductors. LEDs have a PN junction where electrons are lifted from one level to another by applying a current. During this

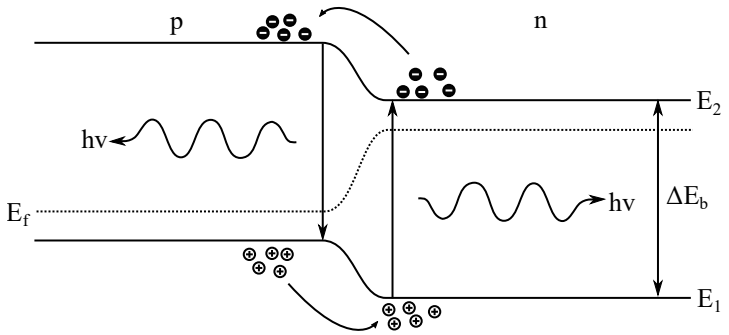

Figure 2.4 – Band model of a PN junction with applied voltage

process, a part of the energy is emitted in the form of photons. These are perceived by humans as light. The wavelength of these photons depends on the energy of the photon, which depends on the bandgap. This bandgap is determined by the choice of the semiconductor material.

The process is shown in Figure 2.4. A forward voltage is applied to the PN junction. The resulting excess of electrodes in the P region recombines with the holes. At the transition between the bands, photons are spontaneously imitated which have the energy of the bandgap (ΔE_b), the wavelength is given by the formula

$$\lambda = \frac{hc_0}{\Delta E_b}. \tag{2.1}$$

With the wavelength of the radiation λ, the speed of light c_0, and the Planck's constant h. To obtain red light aluminium gallium indium phosphide (AlGaInP) can be used. To obtain white light, blue LEDs with indium gallium nitride (InGaN) are used usually. These are then converted to white light using phosphor and additive color mixing. A typical spectral wavelength distribution of a phosphor-converted blue LED is shown in Figure 2.5.

The first peak at about 452 nm is caused by the blue LED and the wide peak at 570 nm is caused by the phosphate coating. The wavelengths correspond to blue or yellow light. Humans perceive the superposition of these colors as white light.

The light generated in the semiconductor is often already directed in the desired direction on the chip with appropriate optics. For example, reflectors on the underside of the substrate are used to increase efficiency and direct light in the intended direction. Sometimes the chip is fitted directly with a lens to further influence the beam angle. In vehicle lighting, additional optics are used to optimize the beam pattern for its specific task, this is described in more detail in Section 2.3.

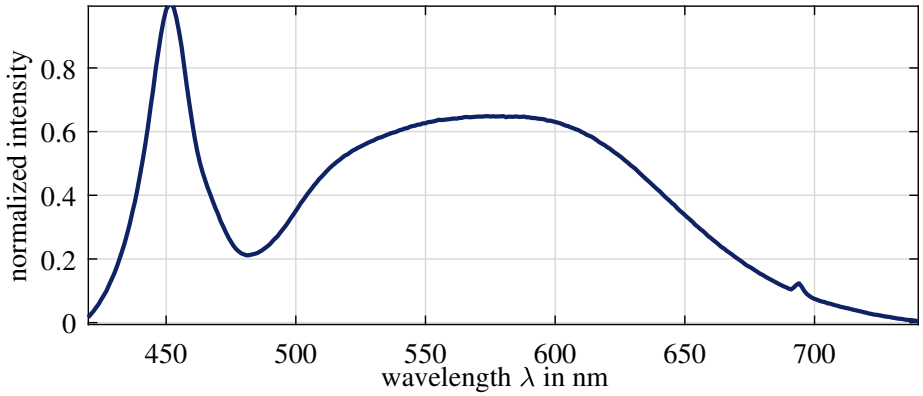

Figure 2.5 – Band model of a PN junction with applied voltage

2.2.6 VLC Channel

The signal, which has been converted to an intensity-modulated light signal by the light source, is transmitted via the wireless optical channel. This channel differs significantly from the usual channels of radio communication as very high wavelengths are used [55]. These high wavelengths result in a high directivity of the signal, so the signal can easily be blocked. Another special feature of the IM/DD is the different carrier frequencies that occur. On the one hand, the medium-light is in the terahertz range at very high frequencies. On the other hand, in relative terms, intensity modulation takes place at very low frequencies, either in the baseband or at carrier frequencies in the kilohertz or megahertz range. This is a special feature so that two carrier frequencies are used simultaneously, the carrier frequency of the intensity modulation and the frequency of the medium light. These occurring frequencies are very far apart and therefore have different effects on the communication link. The carrier frequency of light in the terahertz range together with incoherent radiation and a comparatively large receiver surface compared to the wavelength ensures that usually no multipath fading in the domain of the light can be observed at the receiver [56]–[58].

Intensity modulation takes place at comparatively very low frequencies, as they are limited by the low-pass behavior of the LEDs. A variety of work is investigating the indoor channel with respect to multipath propagation. [59], [60]. The multipath propagation for vehicle applications is examined in detail in Section 3.6.

Another big difference to radio-based communication is the shaping of radiation. While in RF communication a certain directivity can be achieved by geometrically arranging the antenna, in V-VLC optics can be used to create very precise and sharp radiation patterns with a high degree of freedom. This is discussed with a focus on vehicle applications in Sections 2.3 and 3.3.

2.2.7 VLC Receiver

There are two main concepts for VLC available for the receiver. On the one hand, camera sensors are used which have a spatial resolution [61]. Due to lower sensitivity, lower bandwidth and higher costs [62], this type of receiver will not be considered further for the use of V-VLC in the following. The other main concept is the reception with photodiodes. A photodiode converts the received light flux into an electric current. This is then converted via a Transimpedance Amplifier (TIA) into a voltage signal which can be further processed. There are different types of photodiodes available, such as PN photodiode, PIN photodiodes, and avalanche photodiodes. In addition, different material types such as silicon or indium gallium arsenide are possible. Furthermore, the design of the photodiode, such as the receiving surface, influences the behavior of the photodiode.

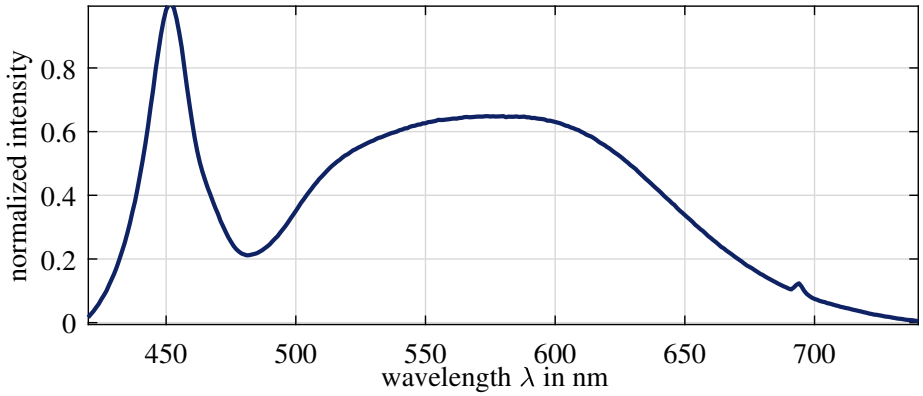

Figure 2.6 – Band model of a PIN photodiode

The functionality of PN and PIN photodiode is rather similar. Impinging photons in the junction layer are absorbed and generate charge carriers through their energy which generates a current flow. In PIN photodiodes, the space-charge region is extended by a layer of intrinsically conducting semiconductor between P and N doped layers. This allows the space charge to expand and thus achieve a higher sensitivity by collecting more photons. However, a PIN photodiode needs a bias voltage to build up the space-charge region. Figure 2.6 shows the structure of a PIN photodiode with the space-charge region in which incoming photons cause electrons to rise to a higher band level.

In avalanche photodiodes, avalanche multiplication also takes place in the barrier layer due to the photogenerated charge carriers. This multiplication process leads to an internal current amplification. Although avalanche photodiodes are generally more sensitive than PN photodiodes and PIN photodiodes, they suffer from saturation and higher noise. Therefore, PIN photodiodes are chosen for further investigations in the following.

In front of the photodiode, an optical system can enable desired reception characteristics. Optics can increase the signal strength by offering a larger entrance pupil and thus capture more light. On the other hand, they can determine the angle of incidence or the field of view. In Section 5.1 the design of a specific adaptive receiver optics is presented in detail.

2.2.8 Receiver Signal Processing

Subsequently, the signals can be processed in a similar way to RF communication. Therefore the signal should be amplified with a low noise amplifier. Due to the high dynamic range of RSS, an amplifier with automatic gain control is useful. If the intensity-modulated signal has been mixed to a carrier frequency, the signal should be downmixed and filtered. After that, demodulation and decoding, and

forwarding to the higher communication layers can take place in a similar way as with RF communication. Chapter 4 presents a prototype of the structure based on SDRs, including a detailed description of the hardware used.

2.3 Basics of Vehicle Lighting

A basic idea of V-VLC is to modify existing vehicle lighting systems in such a way that they can transmit wireless data in addition to their current task, lighting, or signaling. Vehicle lighting systems have been optimized over many years in terms of their main task of illumination or signaling, robustness, and efficiency.

Additionally, the lighting systems are regulated strictly. On the one hand, traffic, in general, is highly regulated in most parts of the world, due to the still not negligible potential danger in traffic. Vehicles have a large mass and can travel at high speeds, which means high kinetic energy, which can cause great damage and can be fatal. At the same time vehicles are used by almost the entire population.

On the other hand, to cope with the driving task, visual perception is one of the most important senses. In order to ensure a high level of safety for the human driver even when driving at night, the vehicle lighting is particularly detailed and strictly regulated. Essentially, the aim is to ensure that the driver can see well on the one hand and that other drivers are not glared by the vehicle on the other. These rules are described in more detail in Section 2.3.2.

2.3.1 Evolution of Vehicle Lighting

Driving a vehicle requires the driver's sense of sight in particular. For this reason, even before the invention of the automobile, lighting equipment was installed in carriages. At that time, these consisted mainly of candles, oil lanterns, and acetylene gas lamps. These technologies were also used to illuminate the car when the automobile came into the market. Shortly after the turn of the century, the first electric light bulbs were considered for lighting in vehicles. However, it could only gradually replace the established lighting systems. In addition to the light source, the optics are also crucial for fulfilling the lighting task. In 1908, the Westfälische Metall-Industrie Aktiengesellschaft (WMI AG) combined a reflector system and a lens for a vehicle lighting system for the first time and was thus able to increase the range. This product was named Hella after the nickname of the wife of the founder of the company, which at the same time creates an association with the German word "heller" (Engl. "brighter"). Later in 1986, this company was renamed to the name of the former product, Hella. Over the years, the bulb became more and more popular as a light source. In 1936, the Bilux light was introduced, which had two filaments and could therefore produce low beam and high beam from one light source.

In 1971 the H4 lamp was introduced, which made it possible to achieve an increased range of vision of the high and low beam by halogen technology. In 1991 the first xenon light for vehicles came into series production, which in turn provided improved illumination and a longer range due to a higher luminous flux. LED lights were initially used in rear lights because low luminous flux and a red wavelength were initially easier to master with LEDs. In 2007 and 2008, respectively, the first vehicles with headlamps featuring LED technology or a fully LED headlamp went into series production. Currently, there are multiple new developments driven by LED technology, for example, Matrix LED headlamps which can emit light in a very targeted way in selectable beam angles. Such a system will be presented and examined for the application of V-VLC in Section 5.2.

Since 2014 lasers are partly used for illumination to further increase the range for an extended high beam [63]. In addition, very high-resolution headlamps are investigated using matrix LED technology as well as micro-LED chips, Liquid Crystal (LC) headlamp systems, and Digital Micromirror Device (DMD) headlamp systems, all of which reach resolutions that enable the possibilities of symbol projection. A prototype of a combination of a high-resolution headlamp and a fiber-bound laser is presented in by Hansen [64].

2.3.2 Fundamental Vehicle Lightning Regulations

Since good sight is essential for road safety, vehicle lighting is strictly regulated. In North America, the Society of Automotive Engineers (SAE) standards are available for this purpose. In Europe, the Economic Comission for Europe (ECE) standards regulate vehicle lighting. Regulations in other countries are often based on these two standards, for example, in Japan, an adapted form of the ECE standard is used. These standards include a detailed set of limit values and characteristics for vehicle lighting. A luminous flux limit is also defined, above which a headlamp cleaning system and automatic headlamp leveling must be installed. In addition, upper and lower limits of luminous intensity are defined depending on the beam angle.

Figure 2.7 shows the limit values of a low beam distribution where the light distribution is mapped onto a plane at 25 m. An asymmetry can clearly be seen, which reduces glare for oncoming traffic employing the cut-off line. In addition, special measuring points such as point B50L are shown, which are measured particularly meticulously, as this point is particularly critical for glare from oncoming vehicles. The different zones or measuring points have either minimum light intensities or maximum light intensities accordingly, to ensure either no glare or sufficient illumination, respectively. In this way, depending on the type of headlamp, at least 1700 cd must be reached at each point in Zone IV, while 625 cd must not be exceeded in Zone II. The point B50L must have a light intensity of only 350 cd. Further values

are described in the ECE standard R112 for static and in R123 for Adaptive Front-Lighting System (AFS). Further requirements such as a value range for permissible gradients are additionally defined.

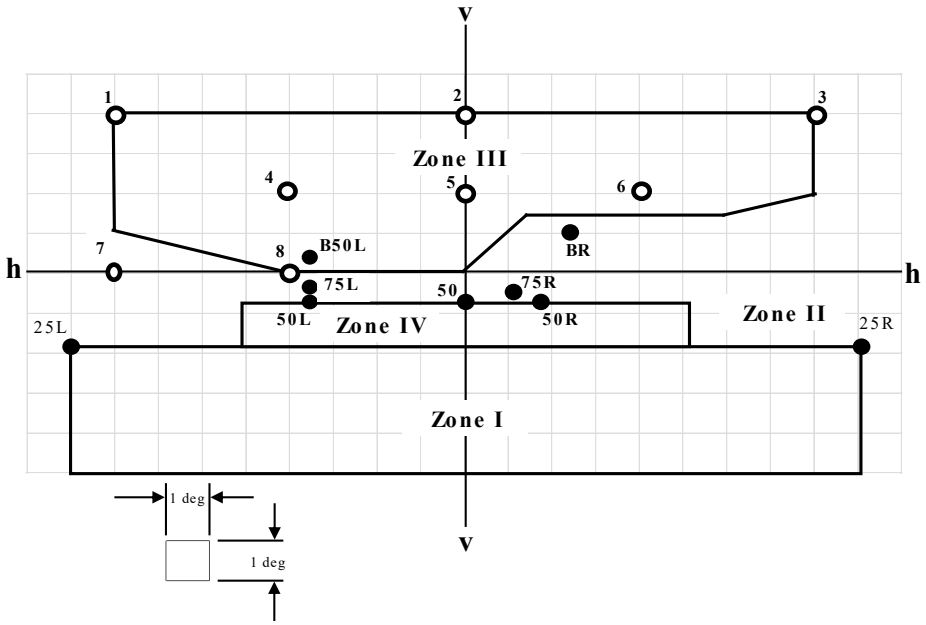

Figure 2.7 – Angular positions for the required photometric values of the low beam. Reproduced from eur-lex.europa.eu under CC BY 4.0 licensing

Chapter 3

V-VLC Channel Characterization

V-VLC has the potential to solve problems that arise with pure RF communication in networking, such as limited bandwidth or multi-user interference in rapidly varying scenarios. On the other hand, difficulties arise when using V-VLC. Especially when using V-VLC as an additional function to the existing lighting functions, several specifications, regulations, and requirements result in limits for V-VLC. In the following, the physical limits resulting from conditions as well as from the characteristics of the systems are first shown in an analytical way and then validated empirically.

Existing characterizations of the channel in the literature are often based on simple models like Lambert's law. This law represents the radiation characteristic in a homogeneous radiating surface as it occurs in an LED without further optical moments sufficiently well. However, single LED chips without further optical elements are rarely used for vehicle lighting. This results in deviations [65]. Viriyasitavat, Yu, and Tsai [66] reduced this error by combining several Lambertian emitters. However, even models of multiple Lambertian emitters suffer from sharp edges of certain light radiation pattern such as low beams. Other approaches from the literature are based on intensive measurement campaigns that record characteristics of the channel (e.g. the received signal strength) at a large number of measurement positions [65], [67]. Extrapolation of these measurements may not be applicable to changes in parameters such as mounting height or pitch. In contrast to these approaches, the following presented approach offers as a contribution a model which takes into account a precise characteristic light source in the form of an optical measurement or simulation and on the other hand offers the possibility of applying various parameters such as other mounting heights, inclinations or hardware parameters. Through empirical measurements, the model is validated with respect to LOS and Non Line Of Sight (NLOS).

3.1 Analytical V-VLC Model

An advantage of V-VLC is that it can be combined with existing lighting systems. The aim is to use existing headlights and taillights and to enable them to transmit data with as little modification as possible. However, vehicle lighting is strictly regulated as described in Section 2.3. This regulation is important because vehicle lighting has a decisive influence on safety. However, in addition to the strict regulation of lighting, there is some freedom to use different technologies and designs, which allows for variation of radiation characteristics within the limits. Since the signal strength and thus the probability of errors and the possible data rate depend directly on the illuminance, an analytical model is presented in the following which calculates the signal strengths at the receiver from real light distributions. Furthermore, the signal strengths can be used to determine local error probabilities, channel capacity, or optimal modulation schemes. In line with this, Gurbilek, Koca, et al. [68] proposed an adaptive physical layer design, which selects an optimal MCS according to the Signal-to-Noise Ratio (SNR) depending on the location.

The real light distributions can be generated by measurements with a photogoniometer or by detailed optical simulations. A photogoniometer is a device that measures the luminous intensity of a light source as a function of the angle of radiation. Usually either the light source is rotated step by step and the illuminance is measured at a fixed position with a calibrated photodiode or the photodiode is rotated around the fixed light source. Taking into account the distance and the properties of the photodiode, the light intensity can be reconstructed. An alternative measuring method with some limits in terms of dynamic range and angular range is the detection of light distribution on a measuring screen by a luminance camera.

Optical simulations are usually based on ray tracing. A common procedure is to first measure the bare light source, e.g. an LED chip, itself in great detail, or to assume a model of the radiation (e.g. a Lambertian distribution) in order to obtain a model of the distribution of the light source's outgoing rays. In the simulation, these rays are then traced in a CAD model of the entire luminaire with all optical elements such as lenses, apertures, or reflectors. The interaction according to the geometry and optical properties of the elements, such as the refractive index, is considered. The data recorded in this way is stored as light intensities for the relevant angles.

To determine the power applied to the photodiode, the light intensity must first be integrated over the solid angle Ω, which corresponds to the angle that the receiving area A_{ep} spans from the viewpoint of the transmitter with the distance r.

$$\Omega = \frac{A_{ep}}{r^2}. \tag{3.1}$$

In the simplest case, the receiving area A_{ep} is equal to the area of the photodiode A_{PD}, or in the case of a tilt by θ, the projection onto the plane orthogonal to the direction of propagation of the signal.

$$A_{ep} = A_{PD} \cdot \cos(\theta). \tag{3.2}$$

If a receiving optic is used, the receiving area corresponds to the aperture pupil of this optic. In the case of a simple biconvex lens, this would be the area of the lens.

The integration of the luminous intensity ($I_V(\alpha_h, \alpha_v)$) over the receiving surface results in the luminous flux ($\Phi_{V,\Omega}$) which reaches the receiver.

$$\Phi_{V,\Omega} = \iint_{\Omega} I_V(\alpha_h, \alpha_v)\, d\Omega \tag{3.3}$$

Both the magnitude of luminous intensity and luminous flux are photometric units. They are well suited to describe the human perception of light since the wavelength-dependent sensitivity of the human eye is taken into account with the $V(\lambda)$ curve. This is useful for the analysis of lighting and signaling tasks of lamps. For communication, however, the actual radiant power is relevant, so the photometric unit of luminous flux ($\Phi_{V,\Omega}$) must be converted into the radiometric unit of radiant flux ($\Phi_{E,\Omega}$). This conversion is done by integration of the spectral distribution of the luminous flux $d\Phi$ and the sensitivity curve of the eye $V(\lambda)$ under consideration of the photometric radiation equivalent K_m

$$\Phi_{E,\Omega} = \int_0^{\infty} \frac{d\Phi_{V,\Omega}(\lambda)}{K_m \cdot V(\lambda)\, d\lambda}\, d\lambda = K^{-1} \cdot \Phi_{V,\Omega}\ . \tag{3.4}$$

The relationship between photometric and radiometric quantities is constant for a constant spectrum. Therefore, the conversion for a constant spectrum, which we can assume for an LED, can be realized by multiplication with the factor K^{-1}.

The radiation flux ($\Phi_{E,\Omega}$) indicates the power of the radiation reaching the receiver. The receiver, which can be realized for example by a photodiode, must first convert this radiation power into a current for further processing. This process can be described by the photodiode specific responsivity curve $\mathcal{R}(\lambda)$. The responsivity curve indicates the wavelength-dependent conversion of radiation flux into electric current. So the photodiode current can be calculated with

$$I_{PD} = \int_0^{\infty} d\Phi_{E,\Omega}(\lambda) \cdot \mathcal{R}(\lambda)\, d\lambda\ . \tag{3.5}$$

Usually, the photocurrent is then converted into a voltage with a TIA and amplified. For a linear TIA with the amplification G the following results

$$V_{PD} = I_{PD} \cdot G. \tag{3.6}$$

The current signal needs to be converted by the TIA to a voltage signal in order to be processed further. For example, it can be further amplified, downmixed, filtered, or converted directly from analog to digital. Usually, these stages have an input impedance of $50\,\Omega$. So that the power at the next stage results in

$$P_{PD} = \frac{V_{PD}^2}{50\Omega}. \tag{3.7}$$

This form of analytical analysis of the signal strength provides the option to calculate the local distribution of the signal strength from real light distributions. This allows, for example, the influence of mounting heights of the receiver to be investigated. In addition, the variation of different headlights with the same light function can be investigated (cf. Section 3.3). Also, different lighting functions can be compared with each other and the optimum lighting function can be determined for a specific application or situation. The combination of a noise model allows further statements about communication. For example, bit error probabilities can be calculated depending on the modulation and coding schemes by creating the dependency between SNR and BER analytically or by Monte Carlo simulations. A further achievement of this model is the connection to VEINS, an open-source vehicular network simulation framework [69], which, with the use of OMNeT++ [70] and SUMO [71], allows large-scale simulations of connected driving. Thus, Memedi, Sommer, and Dressler [72] were able to analyze multi-user interference in realistic environments and emphasize the need for a multi-user access technique.

3.2 Empirical Validation of the LOS-Model

The analytical model is validated in [22] with empirical measurements. Additionally, the model was integrated into the simulation framework VEINS VLC and different light distributions are compared within the framework in the paper. In Section 3.3 an investigation of light distributions by the bare analytical model in Matlab is performed, the agreement shows a successful integration.

The empirical validation was carried out in the HELLA Lichtkanal. The HELLA Lichtkanal is a 145 m long, 11 m wide two-lane road including road markings in a hall. The walls are painted with black, light-absorbing paint and the light channel can be completely darkened to eliminate disturbing light. For the measurement, a pair of LED headlamps with low beam and high beam were operated stationary. The

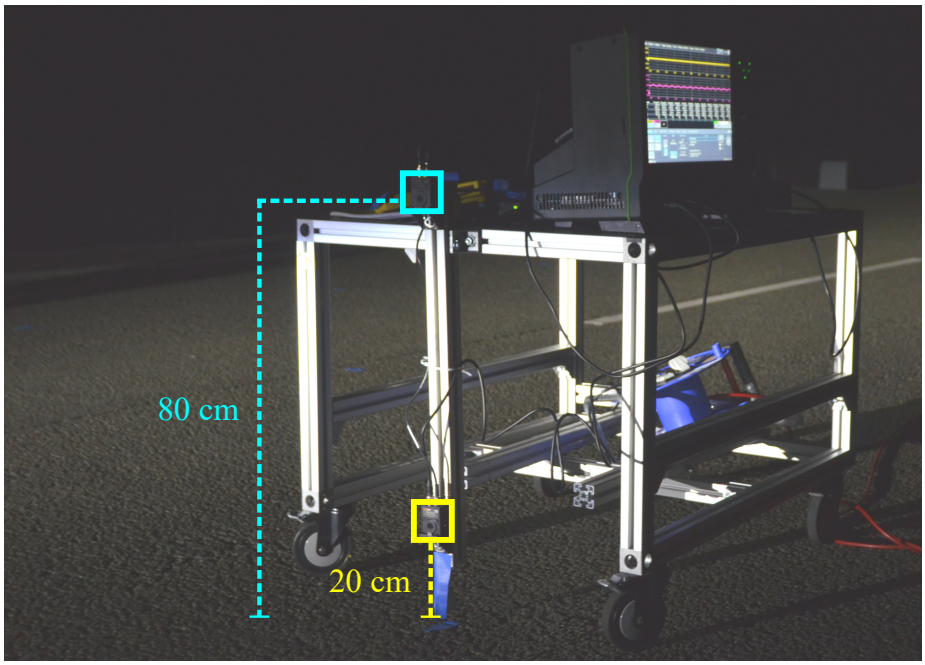

Figure 3.1 – Cart equipped with two photodiodes to perform measurements in the HELLA Lichtkanal. (Reproduced from [22], © 2018 IEEE.)

pair consists of two ECE-conform full LED-Headlights for right-side traffic. The two headlights are mounted 1.50 m apart at a height of 65 cm. On the receiving end, we used a cart with two Thorlabs PDA100A Photo-Detectors (PDs) connected to an oscilloscope, to simultaneously measure the voltage at two different heights, as it is shown in Figure 3.1. One photodiode was mounted at a height of 20 cm, which is the lowest mounting height of a license plate permitted in Germany. The second photodiode was mounted on 80 cm, which corresponds to the usual mounting height of a tail light.

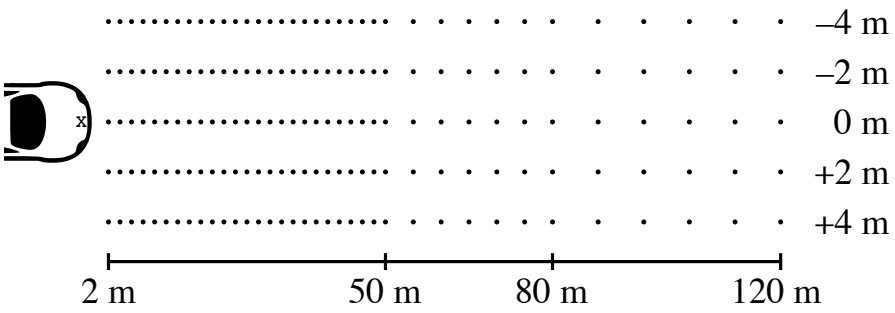

Figure 3.2 – Diagram of the measuring points in the light channel, with the longitudinal distance on the x-axis and the lateral displacement on the y-axis. The reference point X is at $x = y = 0$. (Reproduced from [22], © 2018 IEEE.)

The measuring points are shown in Figure 3.2. The reference point is located centrally between the two headlamps. Five lateral displacements were measured. One row of headlamps in the middle and 2 m and 4 m displacement to the left and right respectively. For 2 m to 50 m longitudinal displacement a high resolution of 2 m step size was measured, because the gradient of RSS is highest for short distances. For distances between 50 m and 80 m, the resolution was reduced to 5 m. A resolution of 10 m is sufficient for distances of 80 m to 120 m.

The measurement results are compared in Figure 3.3 with the result of the analytical calculation. For the analytical calculation, the light distributions of the identical headlamps were used and the signal strength at the corresponding measuring points was calculated. In general, the calculation corresponds well with the empirically measured values. For a mounting height of the photodiode of 20 cm, the signal strength first increases with increasing distance until it reaches its maximum at about 5 m (cf. 3.3a). Since the photodiode is initially located at small vertical angles where the radiation characteristic has low luminous intensity. After reaching the maximum at 5 m, the signal strength decreases steadily with increasing distance, which is mainly caused by the quadratic distance law.

Measurements with a negative lateral shift, i.e. a shift to the left, show similar behavior, but with a consistently lower RSS. With a positive displacement, i.e. a displacement to the right, the signal strengths are lower than in the middle but higher than with a displacement to the left. This is since an ECE-compliant low beam was used, which has a strong asymmetry. This asymmetry is characterized by low luminous intensity on the left side for positive vertical angles in order not to glare oncoming traffic. On the right side, high luminous intensity also occurs for larger vertical angles to ensure illumination of the own lane over long distances (c.f. Section 2.3).

With a mounting height of the photodiode of 80 cm (cf. 3.3b), the behavior of an initially increasing intensity with increasing distance does not occur, as with the mounting height at 20 cm, so that the maximum occurs at the minimum measuring distance of 2 m. This happens because with the higher mounting height we are not in an angular range with lower luminous intensity so that at least for the middle path the signal strength decreases continuously according to the square distance law. Also, in this case, a difference between left and right lateral displacement is noticeable, specifically more signal strength is measured on the right side.

In general, the signal strength is much lower with a high mounting height. This becomes clear when looking at the Y scale in Figure 4.5, the maximum value of the photodiode at 80 cm is 6.06 mV at 1 m distance with no lateral shift, while the maximum value at a mounting height of 20 cm is about 8 times higher and located 6 m distance with no lateral shift. The reason is that in this case, the photodiode is higher than the headlamps. However, since a low beam has a cut-off line and

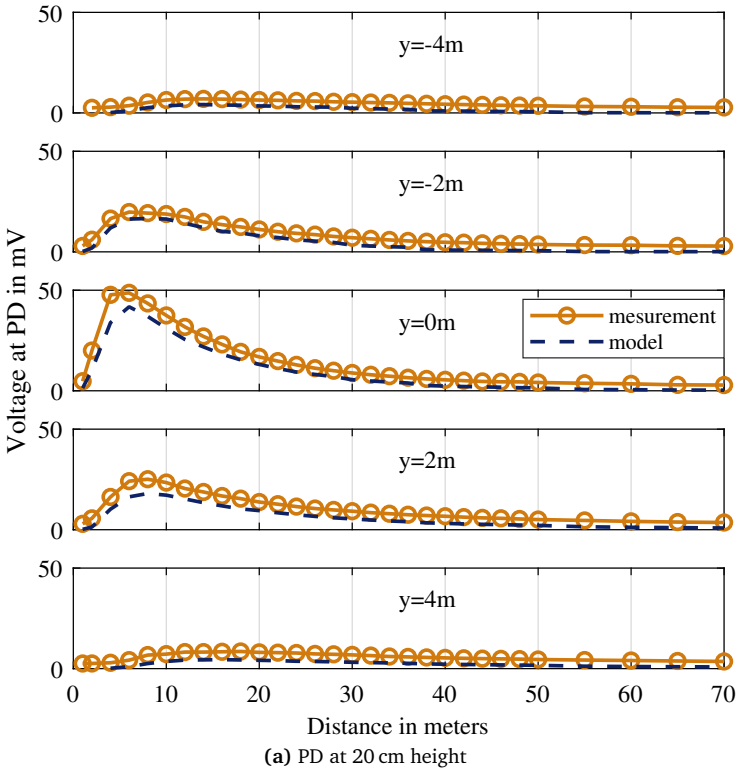

(a) PD at 20 cm height

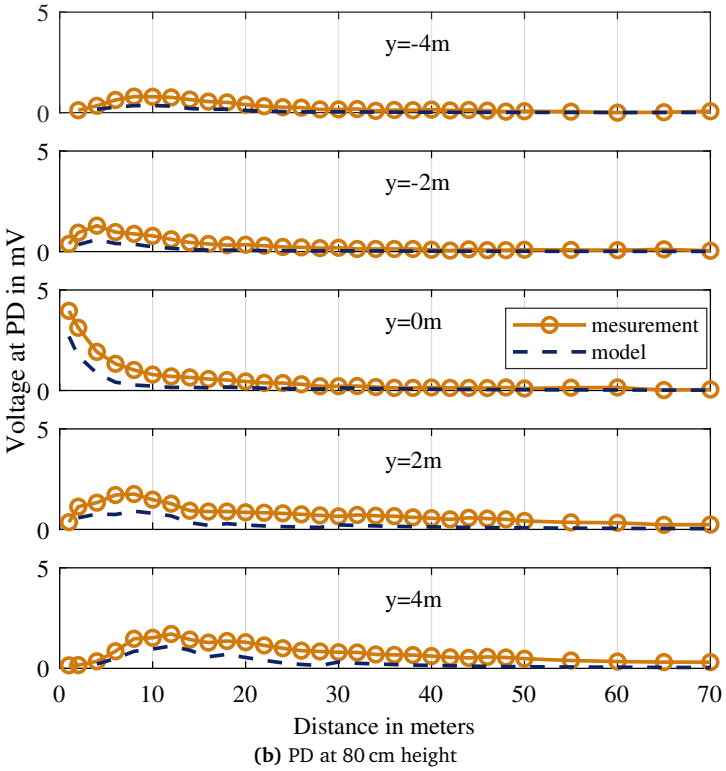

(b) PD at 80 cm height

Figure 3.3 – Measured voltage and calculated voltage for different PD heights. (Reproduced from [22], © 2018 IEEE.)

this line has a negative horizontal angle (usually 0.57° corresponds to 1%), the headlamp emits little light into the solid angles in which the photodiode is located in the case of the mounting at 80 cm.

In general, the measurements are very close to the analytical calculation, so that an Root-Mean Squared Error (RMSE) of 1.7 mV occurs for the photodiode at 20 cm mounting height and of 0.39 mV at a mounting height of 80 cm over all measurements. In addition, a positive deviation of the measurement from the simulation can always be seen. This could be caused by a reflection, which is discussed in more detail in Section 3.6. Another possibility for this deviation is, for example, a deviation in the components or a smaller deviation in the measuring environment of the light distribution and the measurement of the signal strength such as a different temperature or a slight variation of the power supply. Furthermore, a small part of the measured signal power may be caused by noise, such as thermal noise of the photodiode or a common offset of the photodiode.

3.3 Comparison of RSS for Different Light Functions and Models

In the following, three different low beams and two main beams are compared with each other concerning their signal strength distribution according to the model introduced in Section 3.1. These are two LED low beams of sedans and one LED low beam of an Sport Utility Vehicle (SUV). In addition, two full-LED high beams of the sedans are compared. Figure 3.4 shows the corresponding light intensity distributions on the left side and the corresponding signal intensity distributions on the right side. The luminous intensity distribution is shown as an isocandela plot so that one line represents a constant luminous intensity in the plane defined by horizontal and vertical angles. For space reasons, only the luminous intensity distributions of the right headlamp are shown. Generally, the radiation characteristics of the left and right headlamp are similar. The radiation pattern is not mirrored as could be wrongly assumed.

On the right side of Figure 3.4, the signal strength distributions are shown according to the model. For this purpose, a mounting height of the headlights of 65 cm each and a photodiode height of 20 cm was assumed. In this case, the resulting signal strength of right and left headlights are added up. Therefore; a distance between the headlights of 1.5 m would be assumed for all pairs of headlights. The parameters of the PDA100a from Thorlabs were used to parameterize the receiver. This includes a receiver area of 1 cm^2 and the silicon photodiodes typical responsibility as well as a TIA gain of 0 dB (750 V/A).

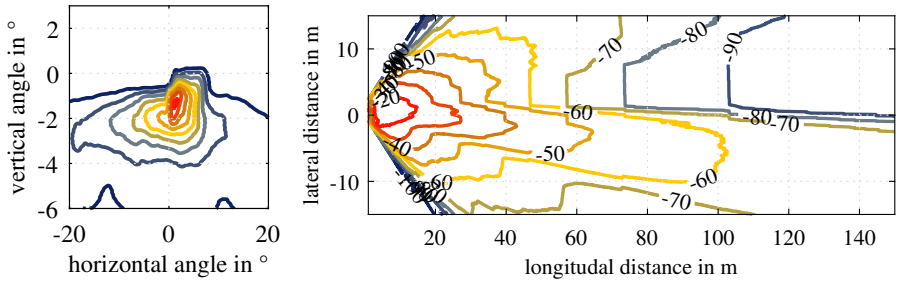

(b) Low beam sedan 1

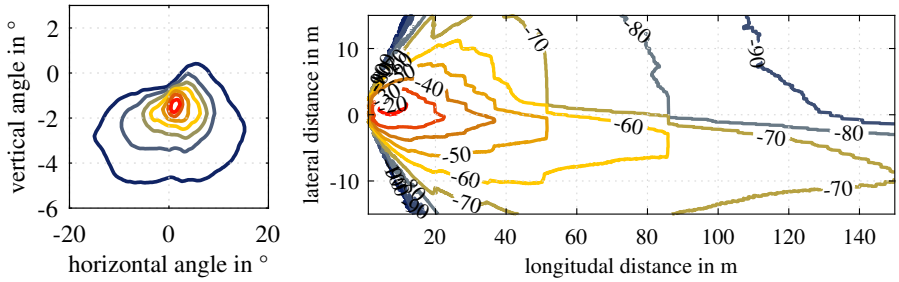

(d) Low beam sedan 2

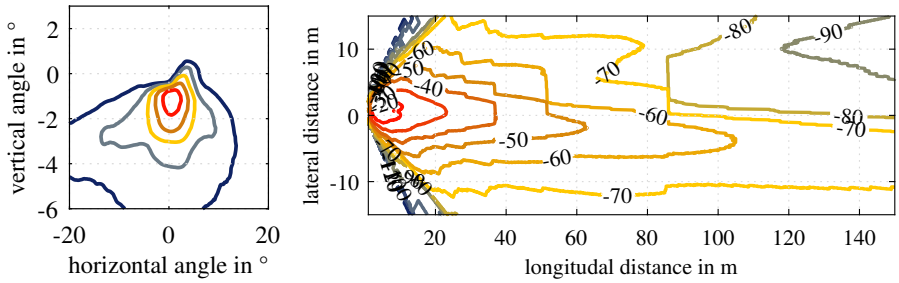

(f) Low beam SUV

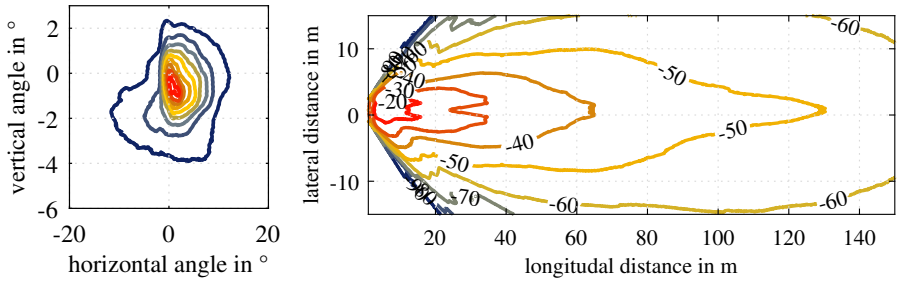

(h) High beam sedan 1

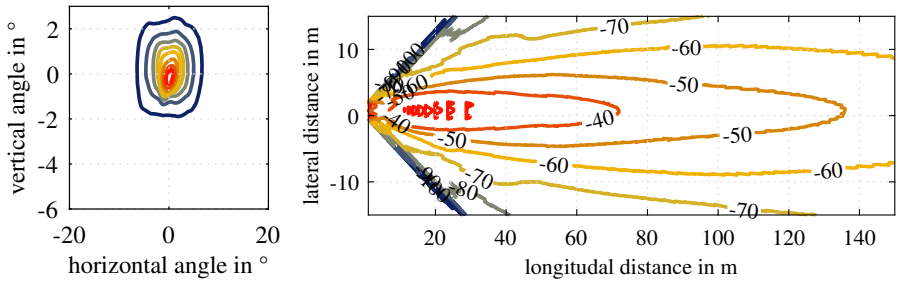

(j) High beam sedan 2

Figure 3.4 – Isocandela plot (of the right lighting module) and corresponding radiation pattern (of both modules) for the considered headlights. Isocandela plots show the luminous intensity, whereas the radiation patterns show the RSS at the PD. (Reproduced from [22], © 2018 IEEE.)

When comparing the light distribution on the right-hand side, clear differences between the low beams Figures 3.4b, 3.4d and 3.4f can already be seen. The light distribution of the first sedan shows sharp edges. Thus the cut-off-line forms an almost rectangular plateau at small positive horizontal angles. The light distribution of the second sedan shows softer contours, and higher light intensities can also be seen a little further to the right of the center. The light distribution of the low beam of the SUV is similar to that of the second sedan. However, lower vertical angles contain higher luminous intensities.

The signal strength distribution behaves equivalently. For example, the signal strength distribution of the low beam of the first sedan shows a sharp-edged, rectangular beam on the right side. The signal strength distribution of the second sedan's low beam is also directed towards the right-hand side of the road and does not extend as far as that of the first sedan in the longitudinal direction. However, higher signal strengths can be observed further to the right in about 20 m to 60 m. On the left side of the road, the signal strength distribution is very similar. The beam pattern of the second sedan has slightly higher values near the middle, which is caused by the slightly softer light. The low beam distribution of the SUV is similar to the shape of the second sedan, but slightly less light is emitted to the right side and the signal level is generally higher so that the -70 dBm line reaches up to about 135 m while the second sedan reaches less than 120 m. The -70 dBm line of the first sedan reaches similar distances as the SUV but is slightly more open due to its rectangular shape.

The high beams differ significantly from low beams. A high beam does not have to guarantee the compromise between illumination and no glare for oncoming traffic. The high beam just has to illuminate as well as possible. In the event of oncoming traffic, the high beam must be switched off or it is automatically switched off on modern vehicles. For this reason, there is no need for a cut-off line or restriction of the light intensity on the left-hand side. High luminous intensity can also be observed for vertical angles greater than 0°. This ensures in the signal strength distribution that high signal strengths are achieved even at much greater distances. Thus -70 dBm can also be reached far beyond 140 m. An asymmetry as required for low beam due to right-hand traffic is not provided for high beam. The two high beams differ in that the first sedan has more light even in small vertical angles and the light distribution is generally broader. This could be caused by the fact that the high beam consists of a low beam and additional light sources while for the high beam of the second sedan a special module is used.

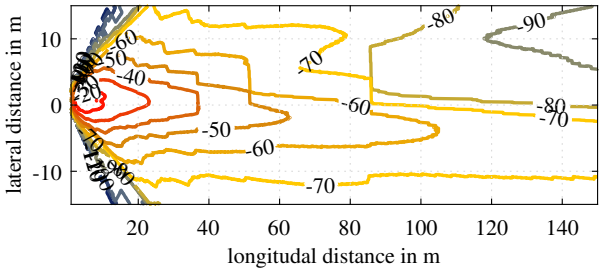

(a) Low beam SUV 55 cm-mounting

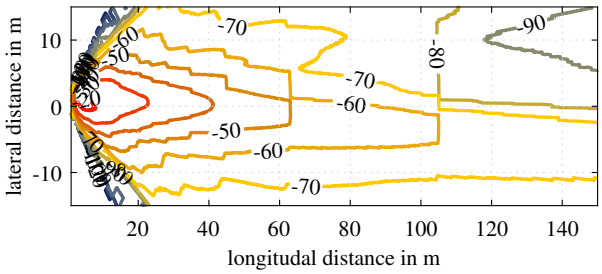

(b) Low beam SUV 75 cm-mounting

Figure 3.5 – RSS-distribution of the SUV low beams with different mounting heights, while the photodiode is mounted at 20 cm.

3.3.1 Impact of Mounting Height

Besides the type of headlamp, the mounting height also influences the distribution of the received signal strength. In Figure 3.4, all headlamps are assumed to be mounted at a height of 65 cm for better comparability. Especially for special vehicle classes such as sports cars, the mounting heights differ from those of SUVs. A typical mounting height for a sedan is 65 cm while an SUV can also have 75 cm. Figure 3.5 shows the signal strength distribution of the SUV low beam lights for 75 cm and 55 cm mounting heights. Compared to 65 cm, the 75 cm installation height achieves in general higher signal strength even at greater distances, while 65 cm installation height results in shorter ranges. This is due to the fact that the cut off-line is placed at a low negative angle. As a rough rule of thumb, a centimeter higher mounting height corresponds to a range that is about one meter longer due to the cut-off line.

3.3.2 Influence of Pitching

Due to the high directivity and the sharp edges in the radiation pattern, the pitching movements of the vehicles can also have a strong effect on the spatial signal strength distribution. Especially the low beam, which is interesting for medium distance communication got a sharp edge at the cut-off line, as it can be seen in the Figure 3.4.

Car manufactures try to keep pitching small by using special geometries of the suspension system to achieve a high comfort for the passengers and to guarantee a

stable driving behavior [73]. Never the less during strong acceleration or breaking there still is pitching.

Pitching occurs during the braking process because the inertia force of the vehicle at the center of mass and the braking force create a balance of forces at different points of attack. This creates a moment that builds up forces on the suspension, causing the vehicle to dive in at the front and rebound at the rear, cf. Figure 3.6. This creates the pitch angle γ.

Kardelke, Diederichsen, and Weinberger [74] proceeded an experimental study to evaluate the pitching during breaking. Therefore a set of 51 vehicles was tested. Each was braking with different deceleration from a speed of around $v_0 = 40\frac{km}{h}$. A set of sensors measured front the height changing of front and back and the deceleration. It was figured out, that the pitch after some transient behavior stays constant for a constant deceleration. Besides the finding that the height changes of front and back are almost linear to the deceleration. In [74] the deceleration of a range of $a = -3\frac{m}{s^2}$ to $a = -9\frac{m}{s^2}$ is investigated. To model the influence of braking on the signal strength a car's mediocre pitching behavior was chosen, the Mercedes

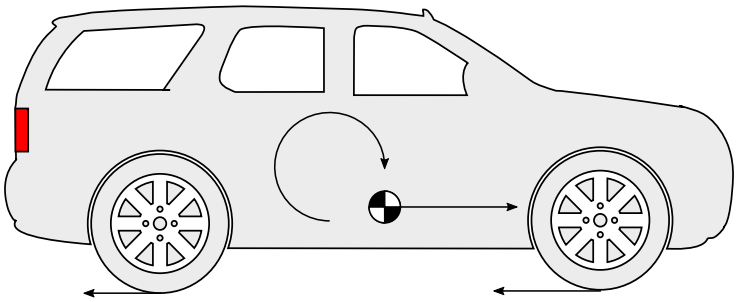

Figure 3.6 – Drawing of the forces and the resulting moment while braking.

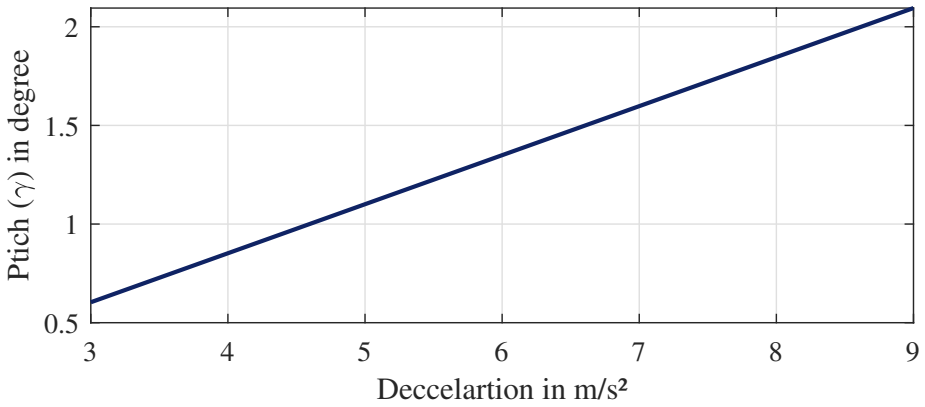

Figure 3.7 – Linear model of the relation between negative deceleration and pitching angle

Benz CLK. The pitching was calculated for this vehicle in combination with the wheelbase and the linear fitted function, as it is shown in Figure 3.7.

If the car accelerates the beam pattern will be shifted by a positive degree. During braking or deceleration, the pattern will be shifted by a negative factor in the vertical axis. In most cases, acceleration increases the signal strength while breaking decreases it. In Figure 3.8a the signal strength distribution of low beam is shown for Pitch of 0°. The transmitter is attached at 20 cm which is the lowest allowed position for the license plate in Germany, while the headlights are at a height of 65 cm. In Figure 3.8c the same scenario is shown with a negative acceleration (breaking) of $a = 3\frac{m}{s^2}$, which results is an overall power drop. Especially in more far distance, the signal drops strongly. For example 25 m in front of the left headlight there is a drop of 21.21 dB from −33.3 dBm to −54.51 dBm. This can be explained by the high gradient of the cut-off line. Without breaking the PD is in the high-intensity area below this line, while breaking the line moves down and the sensor finds itself in the low intensity non-glaring area above the cut-off line. Even stronger breaking, as shown in Figure 3.8h, increases the effect.

Other light functions show a different influence on pitching. The DRL has a smoother beam pattern, with a lower angle dependence and no hard edge like the cut-off line of the low beam. This causes that the signal strength barely changes during braking, cf. Figures 3.8i to 3.8l. Overall, however, the signal strength of the daytime running light is significantly lower, which is associated with a shorter communication range. This makes the modulation of the DRL function attractive for short-distance applications like platooning.

The high beam (cf. Figures 3.8b, 3.8d, 3.8f and 3.8h) shows a noticeable, generally negative change in the signal strength distribution during braking. However, the change is not as significant as with the low beam. This is due to the fact that the high beam has no cut-off line to avoid glare. Therefore, a vertical rotation of the light distribution caused by the braking process results in a less severe change by not shifting a large gradient as with the cut-off line. This becomes evident when the occurring gradients of the isocandela curves (left side) in Figures 3.4b and 3.4j are considered. Additionally, the RSS is overall higher than the RSS of the low beam, as discussed in Section 3.3. Without further measures, however, a simple high beam can only be switched on when there are no other road users in front of the vehicle. For this reason, this light function in its form is only suitable for communication with the infrastructure.

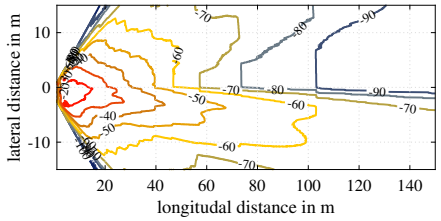

(a) Low beam deceleration of $0\,\mathrm{m/s^2}$

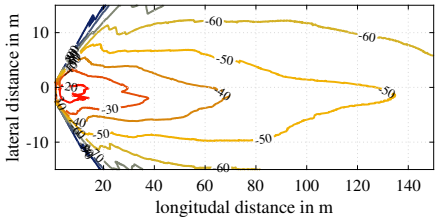

(b) High beam deceleration of $0\,\mathrm{m/s^2}$

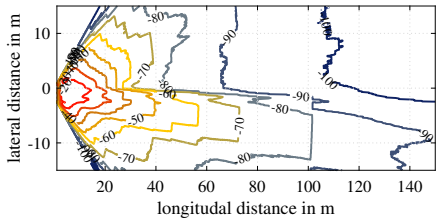

(c) Low beam deceleration of $-3\,\mathrm{m/s^2}$

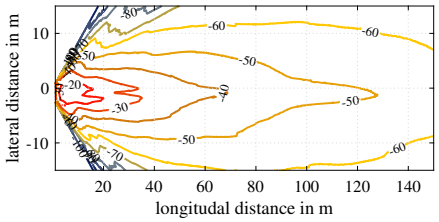

(d) High beam deceleration of $-3\,\mathrm{m/s^2}$

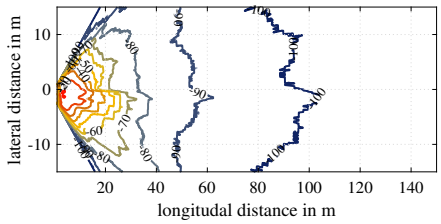

(e) Low beam deceleration of $-6\,\mathrm{m/s^2}$

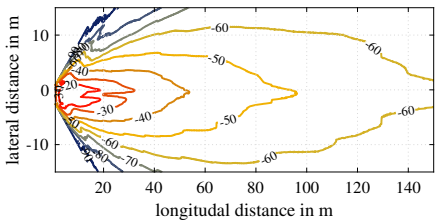

(f) High beam deceleration of $-6\,\mathrm{m/s^2}$

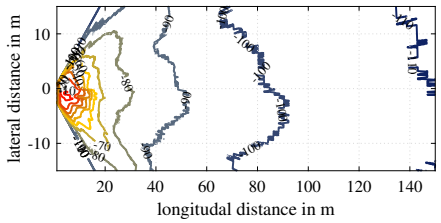

(g) Low beam deceleration of $-9\,\mathrm{m/s^2}$

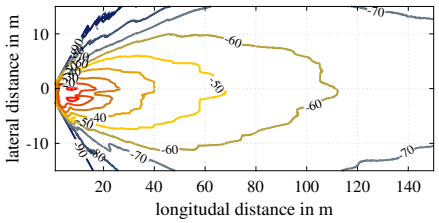

(h) High beam deceleration of $-9\,\mathrm{m/s^2}$

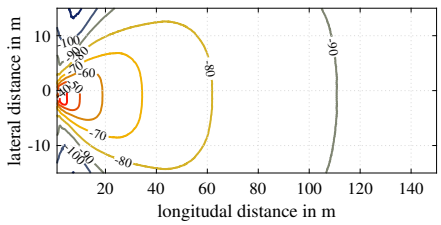

(i) DRL deceleration of $0\,\mathrm{m/s^2}$

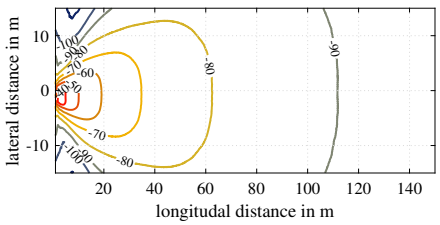

(j) DRL deceleration of $-3\,\mathrm{m/s^2}$

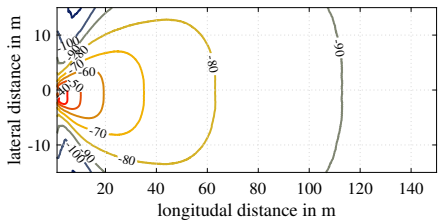

(k) DRL deceleration of $-6\,\mathrm{m/s^2}$

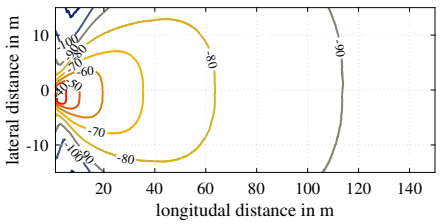

(l) DRL deceleration of $-9\,\mathrm{m/s^2}$

Figure 3.8 – RSS distribution of different light modules during deceleration introduced pitching

3.4 Implications of the Light Distribution on Communications

Together with an adequate noise model, the spatial distributions of the received signal strength can be used to calculate potential bit error ratios for specific modulation and coding schemes. Analytical calculations or Monte Carlo simulations based on the signal-to-noise ratio can be used.

3.4.1 Noise and Communication Model

A possible noise model for light-based communication was presented by Komine and Nakagawa [58]. The noise consists mainly of thermal noise which is composed of the temperature T, the load resistance R_L and the noise figure F_n and the Boltzmann constant k_B.

$$\sigma^2_{thermal} = \frac{4k_B T}{R_L} B F_n \ . \tag{3.8}$$

The other component of the noise is the shot noise which is induced by the current at the PN junction of the photodiode. It is composed of the bandwidth B of the receiver, the responsivity $\mathcal{R}$ of the photodiode, the received optical power P_r, and the dark current I_{dark}. The dominant part of the shot noise is attributed to sunlight in daytime outdoor conditions, due to its high power.

$$\sigma^2_{shot} = 2qB(\mathcal{R}P_r + I_{dark}) \ . \tag{3.9}$$

The following investigations are based on the noise of the photodiode from the datasheet used in the prototypes. This has the advantage of better comparability of the analytical model to the communication properties actually achieved in our field tests.

Using the Shannon-Hartley theorem for determining channel capacity, allows to investigate the theoretical limit of the data rate with the given hardware and an Additive White Gaussian Noise (AWGN)-channel with optimal modulation and coding.

$$C = B \log_2 (1 + SNR) \tag{3.10}$$

If the noise is white and Gaussian in the relevant frequency range, the error probability can be calculated with the following formulas [75].

$$BER_{NRZ-OOK} = \frac{1}{2} \ \mathrm{erfc}\left(\frac{\sqrt{SNR}}{2\sqrt{2}} \right) , \tag{3.11}$$

where erfc is the error function. For Pulse Position Modulation (L-PPM), the BER is calculated with [75]

$$BER_{L-PPM} = \frac{1}{2}\,\mathrm{erfc}\left(\frac{\sqrt{SNR\,\frac{L}{2}\,log_2\,L}}{2\sqrt{2}}\right), \tag{3.12}$$

with L the modulation order of the L-PPM.

For an QAM as used in Chapter 4 the BER is calculated by [76]:

$$BER_{QAM} = \frac{2}{\sqrt{M}\log_2\sqrt{M}} \sum_{k=1}^{\log_2\sqrt{M}} \sum_{i=0}^{(1-2^{-k})\log_2\sqrt{M}} \left\{(-1)^{\left\lfloor \frac{i2^{k-1}}{\sqrt{M}} \right\rfloor} \cdot \left(2^{k-1} - \left\lfloor \frac{i2^{k-1}}{\sqrt{M}} + \frac{1}{2} \right\rfloor\right) Q\left((2i+1)\sqrt{\frac{6\log_2 M\, E_b}{2(M-1)N_0)}}\right)\right\} \tag{3.13}$$

with M, the size of modulation constellation, $k = \log_2 M$, number of bits per symbol and $\frac{E_b}{N_0}$, energy per bit-to-noise power-spectral-density ratio with is proportional to the SNR with [77]

$$SNR = \frac{E_b}{N_0}\frac{f_b}{B} \tag{3.14}$$

with f_b, the channel data rate, and B, the channel bandwidth. $Q(x)$ is the complementary cumulative distribution function of the standard normal distribution, with [78]

$$Q(x) = \frac{1}{\pi}\int_0^{\frac{\pi}{2}} \exp\left(-\frac{x^2}{2\sin^2\theta}\right) d\theta. \tag{3.15}$$

In packet-based communication Packet Error Rate (PER) is a meaningful metric. Disregarding other methods to improve communication, such as retransmissions, and sources of interference other than the AWGN, the dependence of the PER on the BER can be described by [79]:

$$PER = 1 - (1 - BER)^l \tag{3.16}$$

with l the packet length in bit.

3.4.2 Spatial Dependency of Channel Capacity

The presented analytical model described in the previous chapter, together with the realistic light distribution allows all kinds of statements to be made about the performance of V-VLC. With Equation (3.10) and the real radiation patterns, theoretical limits of V-VLC in terms of data rate can be calculated considering specific hardware. The Bandwidth B is assumed to be 2 MHz in the following.

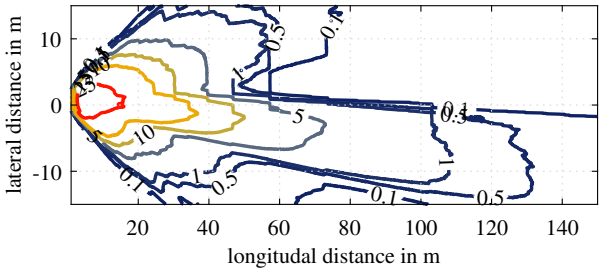

(a) Low beam

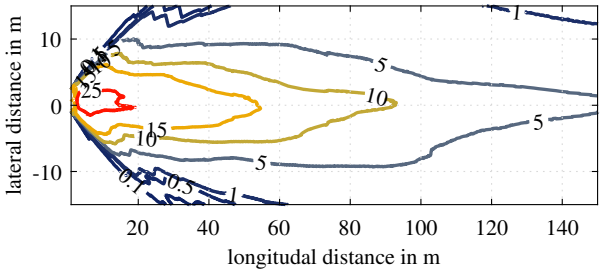

(b) High beam

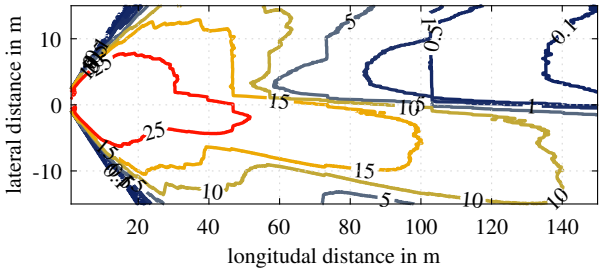

(c) Low beam with receiver optics

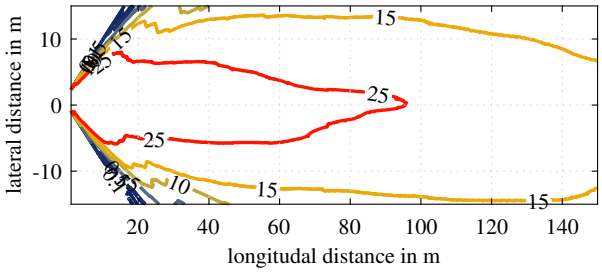

(d) High beam with receiver optics

Figure 3.9 – Channel capacity according to the Shannon–Hartley theorem for realistic radiation patterns with an AWGN-channel

The channel capacity for the low beam is shown in Figure 3.9a, once again showing that higher data rates for longer distances are available on the right side. So, 500 kbit/s can still reach up to about 130 m. On the left side of the headlamp, i.e. for positive lateral distances, 500 kbit/s are reached at about 50 m.

With a high beam, significantly higher channel capacities are possible. Even in large longitudinal distances but also for lateral shifts, high channel capacities of more than 1 Mbit/s are possible. In a large area, a channel capacity of more than 5 Mbit/s is available. With such data rates, many applications in the field of intelligent traffic systems can already be implemented.

A significant increase in channel capacity is achieved by using receiver optics. A simple receiver optic consisting of two biconvex lenses with a diameter of 43 mm, as used in Chapter 4, is assumed. This is shown in Figures 3.9c and 3.9d. With the low beam and receiver optics (cf. Figure 3.9c), channel capacities of 10 Mbit/s can be observed over 130 m on the own lane. On the left lane, 500 kbit/s up to 100 m are possible. With the high beam (cf. Figure 3.9d) 15 Mbit/s are possible up to over 140 m. 25 Mbit/s bits extend to over 80 m, while there is no asymmetry as with low beam. Thus, theoretically, a large amount of data can be transmitted with the high beam over a long-range with suitable modulation and coding. However, as a restriction, it must be ensured that nobody is glared, as outlined before.

3.4.3 Analytical Investigation on the BER

If an actual MCS is considered, the analytical calculations of the bit error probability presented in Section 3.4.1 can be used to determine the local distribution of the bit error probability. Since we assume here an infinitely long transmission length, the bit error probability is equal to the bit error rate according to the law of large numbers. Figure 3.10 shows the bit error ratio for a low beam and a high beam. For this purpose, the shot noise caused by ambient light of 100 klx as well as the shot noise induced by the signal strength and the noise of the photodiode from the datasheet (254 µV) were assumed as noise sources. Two headlight modules with a distance of 1.5 m to each other are assumed. The headlights are located at a height of around 65 cm. The photodiode is at 20 cm height. The 0 dB-setting of the TIA is used and no optical gain by optics is considered.

Using FEC, a reliable communication link can be established with a pre-FEC BER of 10^{-3} or lower [80]. The asymmetrical behavior of the low beam is displayed in Figure 3.10a. The 10^{-3}-BER-threshold is reached at about 30 m on the left side of the light distribution. Slightly offset to the right, however, the threshold reaches up to 47 m. The high beam (cf. Figure 3.10b) reaches much higher distances within the 10^{-3}-BER-threshold. The beam is relatively narrow. But still, it reaches a width of more than 40 m, which covers the entire width of a two-lane road. The increased

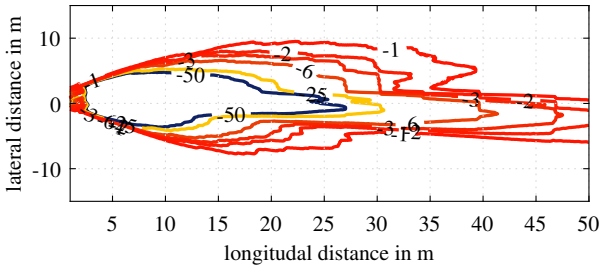

(a) Low beam

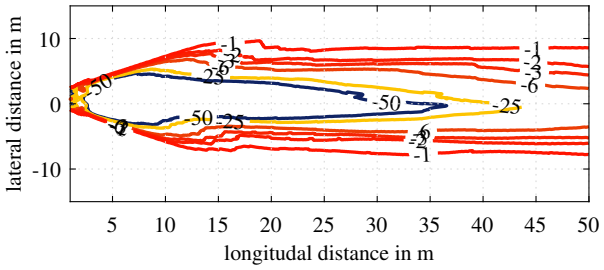

(b) High beam

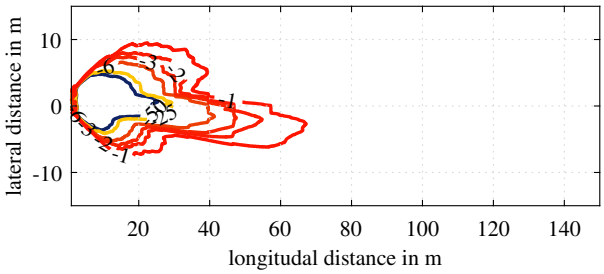

(c) Low beam zoomed out

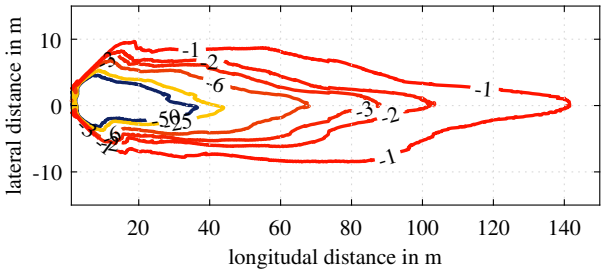

(d) High beam zoomed out

Figure 3.10 – BER of different light functions. The Iso-BER-curves show the exponent to the power of 10 for the BER of 4-PPM

range becomes particularly clear when comparing Figures 3.10c and 3.10d. They show the same scenario as in Figures 3.10a and 3.10b are shown but for a higher longitudinal distance of up to 150 m. It becomes clear that the 10^{-3}-BER-threshold for the high beam extends over 80 m. Also in this case the use of optics is essential to increase the communication range, this is not explicitly shown here to avoid repetition.

3.5 Conclusion of the Analytical Model

In Section 3.1 an analytical model was presented which can evaluate the properties of the V-VLC with respect to channel capacitance, error probability, and signal strength. Different light functions were compared with each other and for example changes in hardware or different modulation and coding schemes were investigated. The basic suitability of light-based communication for applications in intelligent traffic systems was highlighted, but also limits were shown and the necessity to further improve the hardware.

This investigation already helps in the implementation or prosecution of the V-VLC approach. The model can also contribute to the development of light-based communication in the future. The fact that on the one hand the properties of the communication can be estimated without the need for expensive and time-consuming hardware and on the other hand simulation can be carried out on a large scale allows fast and efficient development of improved systems. For this purpose the model presented here was inserted into the simulation framework Veins, which was published in [22]. The integration called veins-vlc is open source software and is available to the public[1]. It allows to investigate large-scale traffic scenarios with many participants equipped with light-based vehicle communication. Concrete applications like Advanced Driver Assistance System (ADAS), platooning [16] or cooperative driving can be analyzed. Especially promising is the investigation of heterogeneous communication in V-VLC combined with radio-based communication, e.g. 802.11p with LTE-V2X or in the future with 5G.

3.6 Empirical Characterization of the NLOS Component

Similar to the model used in Section 3.1, the literature often exclusively considers the LOS-component for V-VLC. This is since light is easily shielded and usually a high amount of the signal is absorbed in case of a reflection. Usually, the main component of reflections of V-VLC is the reflection on the road, as this can vary considerably

[1] `http://ccs-labs.org/software/veins-vlc/`

depending on the material, roughness, and weather, such as rain or snow, a variation of NLOS component is also expected. To estimate the effects of the NLOS component on V-VLC, the signal strength ratio of LOS and NLOS is characterized empirically in the following section.

To be able to exploit a new communication technology in terms of data rate, latency and reliability it is essential to know the channel. Therefore, a certain amount of preliminary work is carried out to characterize the channel. This will be discussed in the following.

Two very special properties of V-VLC are the directional propagation and the asymmetric propagation behavior resulting from the very different light distribution of front and rear lights [67].

Reflections can usually be understood as a superposition of diffuser and specular reflection [81]. Luo, Ghassemlooy, et al. [81] takes advantage of this to describe the reflection on the surface of the road, using Bidirectional Reflectance Distribution Function (BRDF) [82], which come from the field of photometry. Within an BRDF coefficients describing the ratio of incident and reflected light for each angular combination are used to describe different road conditions. With an analytical approach, the authors find that a wet road has a strong NLOS component, while the LOS component is independent of the road condition. In addition, the authors estimate the ratio of NLOS and LOS at 10%.

Simulations are another way to characterize the channel. Lee, Kwon, et al. [55] uses raytracing simulations, which allow to calculate a Power Delay Profile (PDP) by different propagation paths. The raytracing takes place in different traffic scenarios, which were created with commercial Computer Aided Design (CAD) programs. The raytracing is based on a pure Lambertian radiation pattern for the reflection on all materials. The authors observe that a higher dispersion of the channel occurs in metropolitan scenarios because of a large number of propagation paths with different propagation times.

Miramirkhani [83] treats in his dissertation a similar procedure of raytracing in combination with CAD models. However, he additionally considers the different reflection properties, consisting of specular and diffuse reflection, for different materials, such as different asphalts, steel, and car paint. Furthermore, he also takes into account different weather influences, such as rain or fog. He concludes asphalt, which has a low specular reflection, causes small portions in the channel response.

In [22] and Section 3.2 we validated the model shown in Section 3.1 with intensive measurements. It turned out that the analytical model based purely on the LOS component always calculated the signal strength as slightly too small. One reason could be the NLOS component that was not taken into account.

Due to the multitude of propagation paths and parameters, NLOS propagation is very complex and difficult to analyze. This leads to the fact that it has not yet been

extensively investigated in the literature. Especially an empirical validation is often missing. This gap shall be filled with the following experimental setup. Which was presented in [23].

3.6.1 Measurement Setup

The individual paths of the non-line-of-sight are difficult to measure in isolation. This is due to the large number of different propagation paths created by reflection from surrounding objects or surfaces. The LOS component is much easier to isolate. This behavior is exploited in our experimental setup.

Figure 3.11 shows an illustration of our experimental setup. The signal source is an LED low beam, which is modulated in intensity by a suitable driver circuit and a function generator. A square wave signal with 100 kHz was used. This modulation was chosen so that the signal can later be easily separated from the ambient light or noise. On the receiver side, the signal is received by two identical photodiodes. One of the photodiodes has a structure that blocks the NLOS component. For this purpose,

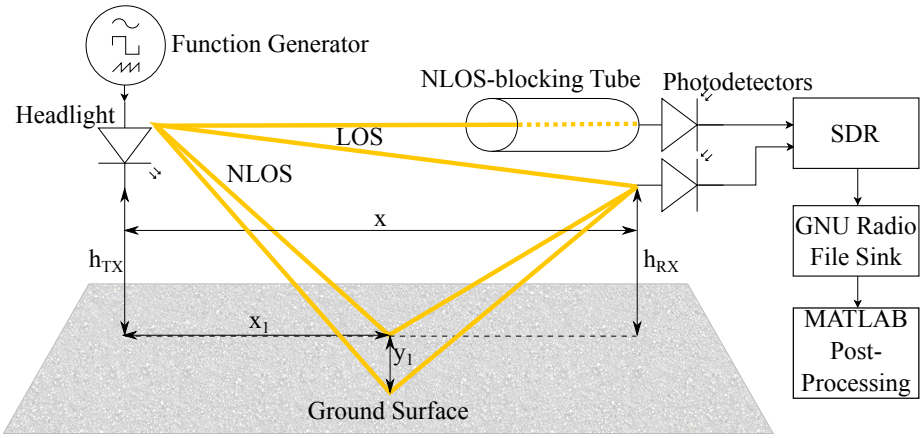

Figure 3.11 – Illustration of the measurement setup. (Reproduced from [23], © 2019 IEEE.)

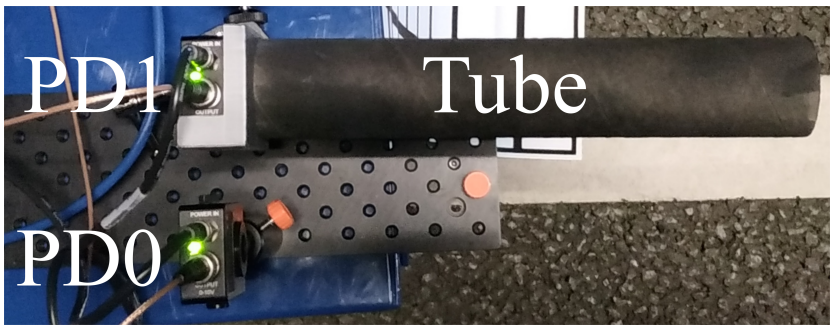

Figure 3.12 – Top-view photo of the receivers with and without NLOS-blocking tube. (Reproduced from [23], © 2019 IEEE.)

a 3D printed holder and a black tube of about 30 cm length were mounted on the photodiode. This tube is precisely aligned with the signal source so that it allows the LOS-component to pass through, but shields reflection that hits the receiver from other angles. The other photodiode is placed without a mount so that it can receive both LOS and NLOS signals. The light received is converted into a photocurrent in the photodiodes and this is converted into a corresponding voltage by the integrated TIA. This output voltage of the photodetectors is converted from analog to digital by a software defined radio (USRP X310), sampled and stored by a GNU Radio flow graph. The signal was recorded with a sample rate of 3 MSamples/s for 10 s at each position. The samples generated in this way are then further evaluated using Matlab.

The signal was analyzed in the frequency domain and the signal strength of the 100 kHz-square wave signal was evaluated and compared. The experiment was performed in two very different environments. One environment is the HELLA light channel. This is a 140 m long covered road, which is made of standard asphalt and also has the usual road marking of a two-lane road. The walls of the light channel are painted with black paint that absorbs light to a high degree so that the reflection on the road is viewed in isolation. The HELLA light channel is used to evaluate new headlamp systems. The basement of the Heinz Nixdorf Institut (HNI) in Paderborn was chosen as the second environment because there is a long corridor with a highly reflective linoleum floor. This high reflectivity should emulate a wet or icy road surface.

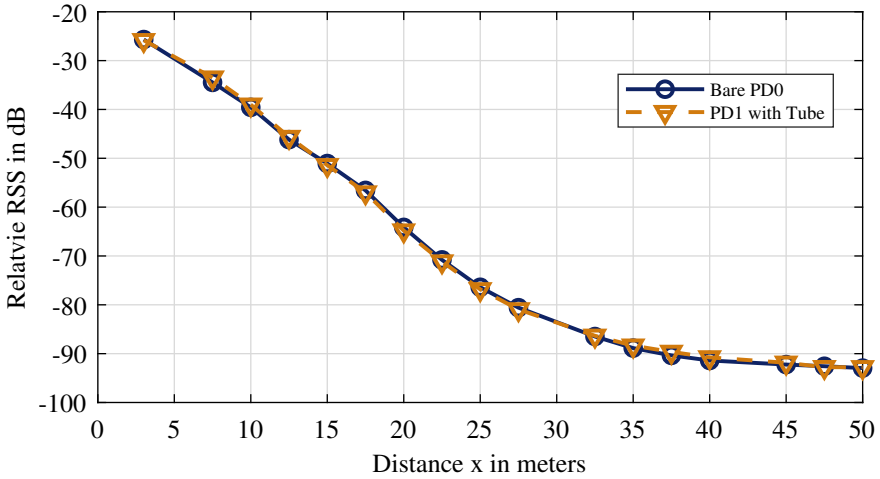

Figure 3.13 – RSS of LOS and LOS+NLOS with dry asphalt. (Reproduced from [23], © 2019 IEEE.)

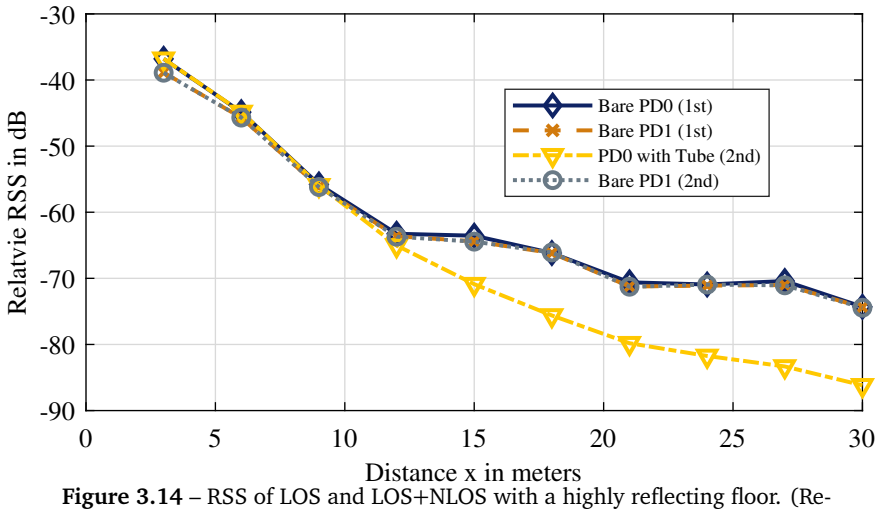

Figure 3.14 – RSS of LOS and LOS+NLOS with a highly reflecting floor. (Reproduced from [23], © 2019 IEEE.)

3.6.2 Evaluation of Signal Strength

Figure 3.13 shows the signal strength over the distance in the light channel. The signal strengths of the two photodiodes with and without tube are almost at the same level. From this, it can be concluded that the NLOS component is very low. The slight deviations between the two signal strengths do not follow a trend and are most probably the result of measurement inaccuracies, such as the exact alignment of the receivers. In this case, the influence of the distance between transmitter and receiver is many times stronger than that of the NLOS component. This measurement indicates that the NLOS component plays no significant role in dry asphalt, which is similar to that in the light channel and can be neglected.

Completely different behavior can be observed in the second measurement environment, the basement of the HNI. In Figure 3.14 the signal strength is plotted over the distance in the HNI. Since the ground here has a higher reflectivity, the NLOS component can be clearly observed. For small distances the signal strengths with and without tube almost the same. From a distance of about 12.5 m, the signal strength with NLOS blocking tube is significantly lower than the signal strength of the bare photodiode, which detects both LOS and NLOS components. This behavior is mainly due to two effects. On the one hand, a low beam was used for the measurement, which has a sharp cut-off line. At about 12.5 m the photodiode crosses this line and leaves the range where the LOS component is particularly strong. This increases the impact of the NLOS component by the relation between LOS and NLOS component. As a second reason, the angle of incidence and reflection on the ground decreases with increasing distance. Investigations by Köhler and Neumann [84], for example, show that the intensity of the reflection usually increases with a smaller angle.

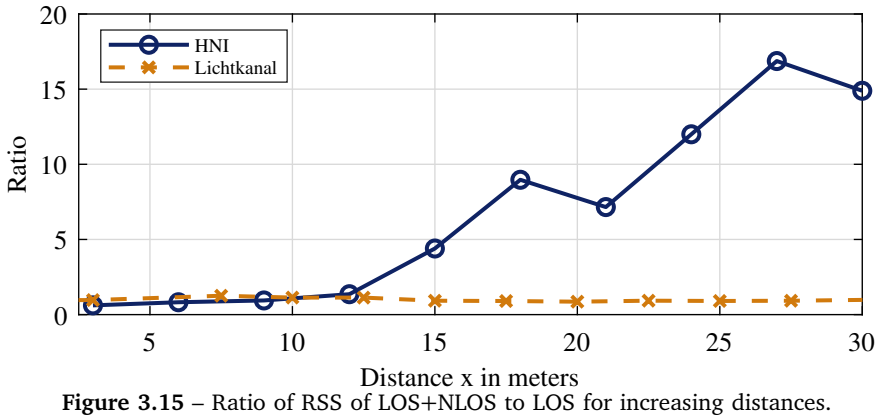

Figure 3.15 – Ratio of RSS of LOS+NLOS to LOS for increasing distances. (Reproduced from [23], © 2019 IEEE.)

The behavior becomes even clearer when the dependence of the distance is calculated by considering the ratio of with and without tube, which corresponds to the ratio of NLOS and LOS to LOS, cf. Figure 3.15. While the ratio in the light channel is almost one, i.e. there is hardly any measurable NLOS component, the measurement in the HNI shows a strong NLOS component. In some cases, the ratio of NLOS+LOS is more than 15 times larger than that of the isolated LOS component. This means that most of the signal strength reaches the receiver via reflections.

In order to be able to better analyze possible measurement inaccuracies of the setup, a total of four measurements were compared in the HNI experiment. First, both photodiodes were measured simultaneously without a tube to ensure that the slight local offset of the photodiodes would not falsify the measurement result. Then one of the photodiodes was fitted with the tube. The signal strengths of both photodiodes were measured again to detect the isolated LOS component on the one hand and to ensure a temporal invariance of the system with the other photodiode on the other hand. The small deviations between the three measurements without NLOS-blocking tube, confirm that no significant errors occur due to temporal as well as the small local deviation between the photodiodes.

3.6.3 Evaluation of Path Length Difference

In addition to the pure signal strength of the individual reflection paths, the propagation time of the paths is also relevant for multipath propagation. If the ratio between symbol duration and the delay time difference is unfavorable, destructive interference also called fading, occurs. In order to estimate whether destructive interference occurs in V-VLC scenarios, a geometric analysis of the delay is carried out in the following.

For the analysis, the reflection at the road, as shown in Figure 3.11, is considered. Reflection paths emitted by the headlamp at the height h_{TX} are considered, reflected

at the reflection point $R_1(x_1, y_1)$ and then received by the photodiode at the height h_{RX}. The reflection path difference on the straight line between headlamp and photodiode can be determined with

$$\Delta s_1 = \sqrt{x_1^2 + h_{TX}^2} + \sqrt{(x - x_1)^2 + h_{RX}^2} - x \tag{3.17}$$

If additionally a lateral shift of the reflection point is considered, the formula expands to:

$$\Delta s_1 = \sqrt{x_1^2 + h_{TX}^2 + y_1^2} + \sqrt{(x - x_1)^2 + h_{RX}^2 + y_1^2} - x \tag{3.18}$$

Together with the speed of light c, the transit time difference τ can be calculated from the reflection path difference:

$$\tau = \Delta s \cdot c \ . \tag{3.19}$$

Figure 3.16 shows the path differences in time and space domain for a distance of 20 m plotted over the longitudinal position of reflection and for selected lateral positions of reflection. Reflections without lateral shifts show very small path differences of less than 80 cm. With a larger lateral displacement (larger y_1), however, the path difference also increases. Nevertheless, this consideration does not take into account that a larger lateral displacement usually causes a significantly weaker reflection.

With a lateral displacement of $y_1 = 3$ m there is a time difference of 18 ns. This is significantly shorter than the usual symbol duration in a V-VLC system. Turan, Gurbilek, et al. [53] measured a large number of LED sources and determined

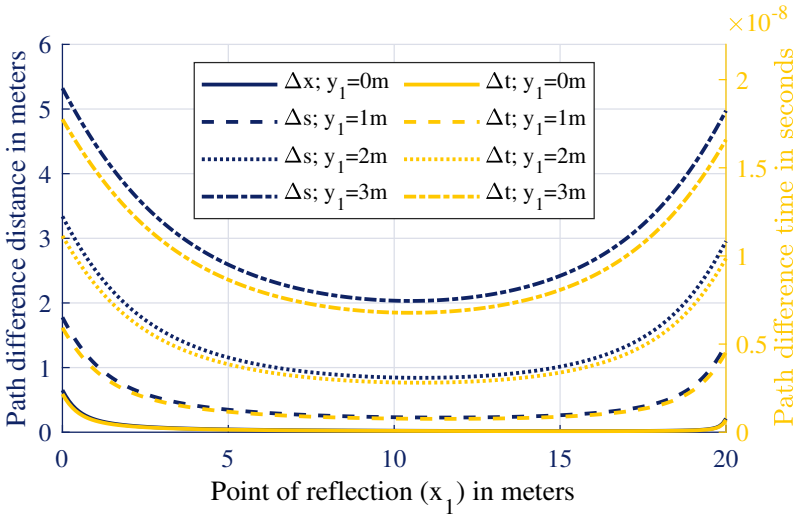

Figure 3.16 – Length of reflection Path in time and distance. (Reproduced from [23], © 2019 IEEE.)

the maximum 3 dB bandwidth with 2.311 MHz. This means that when the whole bandwidth is modulated with a single carrier modulation, a symbol duration of 0.432 µs is achieved. So no fading is to be expected. Multi-carrier methods like OFDM further increase the robustness against fading.

3.6.4 Conclusion of the NLOS-Experiment

In this experiment, the influence of the NLOS component, which mainly consists of the reflection at the road, was empirically analyzed. A very strong dependence on the road condition was found. Thus, when the asphalt is dry, the NLOS component is insignificant and can be neglected in most cases. On the other hand, the NLOS component was even significantly stronger than the LOS component when the ground had a high reflectivity. This is consistent with the observations of Köhler and Neumann [84], who measured forward reflectivity in wet asphalt, which was three orders of magnitude higher than in dry asphalt. An analytical, geometric observation was used to investigate the impact on communication caused by potential fading. It was found that no fading is to be expected with usual symbol durations of V-VLC. For simulations or calculations that only include the LOS component, this means that with dry asphalt you have only a very small error and with higher reflectivity, you fundamentally underestimate the channel quality, which is useful for worst-case considerations.

Chapter 4

Proof-of-Concept

Taking the challenges of V-VLC into account, this chapter examines a prototype that communicates reliably in an outdoor environment with commercially available headlights. The prototype is based on SDRs for modulation and coding, using OFDM in compliance with the 802.11 standard. This relation to 802.11(p) means on the one hand that established and mature methods for frame building, coding for modulation, filtering, equalization, and further signal processing can be used. OFDM is particularly suitable for V-VLC because it is robust against narrowband noise, which can occur from other modulated light sources, and because equalization of the signal is comparatively simple because individual subcarriers can be assumed to be flat in frequency. OFDM allows the combination of several multiple access schemes like Time Division Multiple Access (TDMA) and Frequency Division Multiple Access (FDMA) with comparatively little effort [85]. Another advantage is potential compatibility to future standards based on OFDM 802.11p for example.

4.1 Related Work of V-VLC-implementations

Even though V-VLC is a rather new, emerging field, several prototypes were implemented during the last years. In this chapter, these prototypes are introduced and the differences to our outdoor prototype with Commercial Off-The-Shelf (COTS)-headlamps and an applicable data rate are highlighted.

A prototype based on 802.15.7 is presented by Gavrincea, Baranda, and Henarejos [86]. It uses COTS hardware while modulation and encoding are done with SDRs and GNU Radio. The implementation is compliant with the PHY I 802.15.7 standard. This is intended for outdoor communication as described in Section 2.2.3. It achieves data rates from 11.67 kbit/s to 266.6 kbit/s depending on the operation mode and is based on OOK and PPM. By using a single high power LED they achieve an error rate

of less than 10^{-3} depending on the operation mode for communication distances of up to 2 meters.

A higher range of 40m could be shown by Kumar, Lourenço, et al. [87] with a prototype by using Direct-Sequence Spread Spectrum (DSSS). The low bandwidth efficiency of DSSS combined with the low pass behavior of LEDs results in a data rate of 20 kbit/s. On the other hand, the redundancy added by the chip sequences resulted in higher reliability and lower error rates at low SNR. The signal processing takes place on both the transmitter and receiver side by using an Field-Programmable Gate Arrays (FPGA).

Even though fading is usually not a problem of V-VLC, MCM are attractive for visible light communication as they are robust against narrowband interference and the equalization can be easily done with a single tap filter. This is especially attractive for dynamic channels.

MCM has already been widely used for indoor applications. In addition to high-performance prototypes [88], [89], commercial products already exist on the market [90] and first Application-Specific Integrated Circuits (ASICs) dedicated for VLC based on OFDM have been introduced [91].

Due to the challenging environment for communication between vehicles, fewer prototypes in this area than in the indoor area and no product yet. However, Shen and Tsai [92] were able to test a prototype based on OFDM on a 108 km drive, achieving 70% symbol reception rate over communication distance of 45 m. To achieve this range, the system uses a lens system with an aspherical lens with a diameter of 5cm and a plano-convex spherical lens, which causes an amplification of the signal by 15 dB. On the other hand, the comparatively low frequency of intensity modulation (200 kHz sampling rate with a carrier frequency of 200 kHz) increases the signal strength by reducing the effect of the low-pass behavior of the LED. In addition, 50 times repetition of each OFDM symbol is used to ensure reliable reception even at low SNR. This aspect suggests a low data rate for the first experiment of this kind.

In the following, based on [24] V-VLC communication with OFDM using SDRs and COTS headlights over distances relevant for traffic is investigated. With detailed long-term tests, the BER behavior of the prototype was already examined in a laboratory setup in [93]. The linear driver of the prototype was presented in [21].

In contrast to the prototypes known from the literature, the prototype presented in the following simultaneously achieves large distances of up to 75 m, as they occur in real traffic scenarios, and practicable data rates in the range of 0.15 Mbit/s to 1.35 Mbit/s or, after optimization for short distances, up to 8.1 Mbit/s. This performance combination is a novelty, emphasizing that a modified series headlamp was used for communication.

4.2 System Design of the OFDM Prototype

In general, a very similar transmission chain as shown in Figure 2.1 (page 10) was used. A random ASCII code was generated for data generation. The modulation and coding or the demodulation and decoding, as well as the equalization and partial filtering, was realized in GNU-Radio using Universal Software Radio Peripherals (USRPs). For this purpose, the 802.11 a/g/p implementation for GNU Radio by Bloessl, Segata, et al. [94] was used and adapted for the use of light as the transmission medium. According to the 802.11 a/g/p standard, the implementation includes corresponding MCSs: BPSK, QPSK, 16-QAM, and 64-QAM with the code rates 1/2, 3/4, 2/3 which are achieved by convolutional codes and puncturing. Interleaving is also used for increased robustness against burst errors. Packets are provided with a header that is constantly modulated with BPSK. In contrast to 802.11 a/g/p communication, which communicates in the 2.4 GHz or 5.9 GHz band, a carrier frequency of 2.4 MHz was selected to meet the low-pass behavior of the LED and to avoid interference signals at low-intensity modulation frequencies. The bandwidth was also reduced by using a sample rate of 1 MSample/s and a filter with a two-times interpolation.

On both the receiver and transmitter side is a laptop running the corresponding flowgraph on GNU Radio. On the transmitter side, the samples generated by the laptop are transferred via an Ethernet cable to the USRP ETTUS N210, which converts the digital sample into an analog voltage signal and mixes the signal up to 2.4 MHz. The resulting high-mixed signal is converted into a corresponding current signal by the driver introduced in [21]. It is important to note that the output signal of the USRP is bipolar and mean value free. Due to the integrated bias-T in the current driver, the signal is provided with an offset so that an exclusively positive current signal is generated. This results in a hardware-generated DCO-OFDM signal.

The setting to an adequate bias current is crucial for the performance of DCO-OFDM, as this determines the range of the linear amplitude [44]. An incorrectly set bias can either cause distortion due to non-linear behavior or clipping or result in a lower controllable amplitude and therefore less signal strength. The bias is adjusted by measuring the linearity of the ratio of current to illuminance. For this, an operating point with the largest possible linear operating range was selected. The bias is about half the maximum luminous flux. The linear range could be increased by pre-equalization, resulting in an increase of the signal strength. A COTS full LED headlamp of a VW Passat was used as the light source. For the experiment in this chapter, the low beam was used. It is a static headlight. The light shaping is done by a reflective optical system.

The Intensity Modulation (IM) light generated in this way is transmitted via the optical free space channel. This channel was discussed in detail in Section 3.1. For

the measurements, the receiver is placed centrally and 40 cm lower in front of the left headlight. Distances from 2.4 m to 75 m are investigated.

The receiver contains a receiver optic which consists of two convex lenses (cf. Figure 4.1). This optic serves to increase the signal strength. By increasing the entrance pupil, the received luminous flux increases according to the area ratio of entrance pupil and photodiode area,

$$G_{optic} = \frac{\Phi_{\text{ep}}}{\Phi_{\text{PD}}} = \frac{A_{\text{ep}}}{A_{\text{PD}}} = \frac{\pi \frac{d_{\text{ep}}^2}{4}}{d_{\text{PD}}^2}. \tag{4.1}$$

In this way, the effective area has been increased from 100 mm^2 to 1452 mm^2, which corresponds to a luminous flux increase of 11.6 dB. Since the optical power is initially converted into a current by the photodiode in a nearly linear fashion, amplification by the optics results in an increase in electrical output power of 23.24 dB. This fact may seems counterintuitive compared to RF communication, it is caused by the following dependence:

$$I_{LED} \propto \Phi;\ \Phi \propto I_{PD};\ I_{PD}^2 \propto P_{PD} \Rightarrow \Phi \propto \sqrt{P_{PD}} \tag{4.2}$$

with the LED current I_{LED}, the luminous flux Φ, the photocurrent I_{PD} in the photodiode, and the power P_{PD} at the output of the photodiode. With Equation (4.1) follows

$$P_{PD} \propto G_{optic}^2 \cdot \Phi_{PD}^2. \tag{4.3}$$

Since some components of the noise are not related to the incident light, such as thermal and quantization noise, a higher SNR is achieved by this optical amplification. The second task of the optics is to limit the Field of View (FoV). The optics, in conjunction with the ambient light-blocking cover could prevent disturbing light sources from interfering with or even saturating the transmitted signal.

The light concentrated by the optics is converted into a current by a pin-photodiode (see Section 2.2.7). This current is converted into a proportional voltage by a

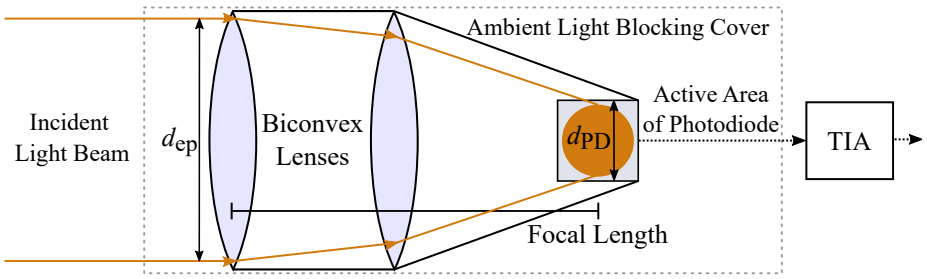

Figure 4.1 – Schematic illustration of the receiver optics.

TIA in the next step. The Thorlabs PDA 100 A photodetector was used for these tasks. It is characterized by a large active area and a high bandwidth, which leads to high sensitivity. A gain can be set on the integrated TIA, whereby gains of 0 dB to 70 dB are possible. If not mentioned differently, a gain of 0 dB is used in the following measurements, which corresponds to a current to voltage conversion of 750 V/A.

Behind the TIA a Direct Current (DC) blocker in the form of a capacitor was connected. This reduces the risk that the Analog-to-Digital Converter (ADC) of the following USRP runs in saturation. In principle, a DC blocker could also be used right behind the photodiode before the TIA. This would reduce the risk of the TIA running into saturation. However, this modification is not applicable when using an integrated TIA. Though, it could be an improvement for future receiver circuit designs.

The next step is to mix the signal into the baseband in the USRP. The baseband signal is then sampled into a digital signal using the ADC of the USRP. A sampling frequency of 1 MHz was selected. The Ettus N210 has a 14-bit ADC. The static amplification might result in limited utilization of the range of the ADC. An AGC stage connected ahead could reduce the quantization noise in future designs.

The digital baseband signal is transmitted to the receiver notebook where the GNU-Radio flowgraph reconstructs the transmitted data. In the flow graph, the signal is first normalized. With the help of an autocorrection and the setting of a threshold value, the sequence that marks the beginning of a frame is detected [94], [95]. Only if a frame is detected, the following samples are further processed. In the next step, a correction of the frequency based on the algorithm of Sourour, El-Ghoroury, and McNeill [96] is applied to the short training sequence [94]. Then a 64-FFT is executed to resolve the individual subcarriers. In the next step, LS, LMS, STA, and Linear Combiner are available for the equalization of the individual subchannels. Tekoepe2018poster the LS was shown to be the best choice for the equalizer due to its complexity and low error rate. Followed by the training sequences, each frame consists of a BPSK which contains the length and coding of the subsequent symbols. With this information, the other symbols are demodulated, deinterleaved, decoded and descrambled, in order to reconstruct the original data in case the transmission was successful [94].

4.3 Measurement Setup

To evaluate the prototype, measurements were taken over a long distance. A parking garage was chosen for this purpose. This choice was made to avoid a varying influence of ambient light on the communication by constant lighting achieve an increased reproducibility and keep the number of influencing parameters low. At the

Figure 4.2 – Measurement environment. (Reproduced from [24], © 2019 IEEE.)

same time, this environment offers a long free distance of 75 m and a floor made of concrete paving stones as used on roadways. The influence of the fluorescent tubes was observed to be negligible, as they are not modulated in the frequency range of our IM. Extensive measurements were made to determine the reliability of the communication. For this purpose, the transmitter unit with the headlight was placed on one side of the parking lot, while the receiver side was mounted on a trolley in order to cover different distances. In addition to the laser distance meter and tape measure, the marking of the parking bays was helpful for the distance measurement, as these are exactly 2.7 m wide and thus served as an additional orientation reference. For each measuring point, 1000 OFDM packets were transmitted. Each packet consists of 250 bytes, so 2 million bits were transmitted per measuring point.

An overview of the measurement parameters is given in Table 4.1. The Headlight's relatively low 3 dB bandwidth of only 1.3 MHz is noticeable. This is due to the high-power LEDs in combination with parasitic inductances and capacitances of the headlamp PCBs. However, a carrier frequency of 2.4 MHz was nevertheless chosen for the IM signal to avoid the negative influence of modulated artificial light sources. This is a trade-off that achieves higher robustness against interference at the expense of signal strength and thus range. By using an improved adaptive receiver, as described in Section 5.1.5, this consideration could be omitted, as interference sources are optically filtered.

4.4 RSS of the OFDM Prototype

The performance of the system is highly dependent on the SNR. For this reason, the RSS is first compared with the noise over distance. In Figure 4.3, you can see that the noise is almost constant over the distance at about −85 dB. Measurements

have shown that internal noise sources, such as quantization noise from the ADC or thermal noise, dominate the noise, and noise sources such as shot noise from ambient light are rather negligible. The signal strength, on the other hand, is strongly dependent on the distance between transmitter and receiver, it varies continuously with the distance. The RSS is influenced by the inverse square law of distance on the one hand and additionally by the specific radiation characteristic of the headlamp on the other hand. This behavior means that an SNR of 46 dB can be achieved at short distances, while the SNR is reduced to 13 dB at long distances of over 60 m. This variation of the SNR implicates there are different optimal MCSs depending on the distances. As described in Section 3.1, the RSS shows a high degree of dependence on the geometry of the scenario, i.e. the alignment of transmitter and receiver to each other. As described in Section 3.6, fading usually does not play a role.

Table 4.1 – Hardware specific parameters for the measurements. (Reproduced from [24], © 2019 IEEE.)

Headlight	VW Passat 18 W LED-based low beam
Headlight's 3 dB bandwidth	1.3 MHz
PD	Thorlabs PDA100A
PD's 3 dB bandwidth	2.4 MHz
PD gain	750 V/A at 0 dB
Optics gain (G_{optic})	11.6 dB
Distance between RX/TX	2.4 m to 75 m
Relative height RX/TX	40 cm
Center frequency	2.3 MHz
Sampling frequency	1 MHz
Data rates	0.15 Mbit/s to 1.35 Mbit/s

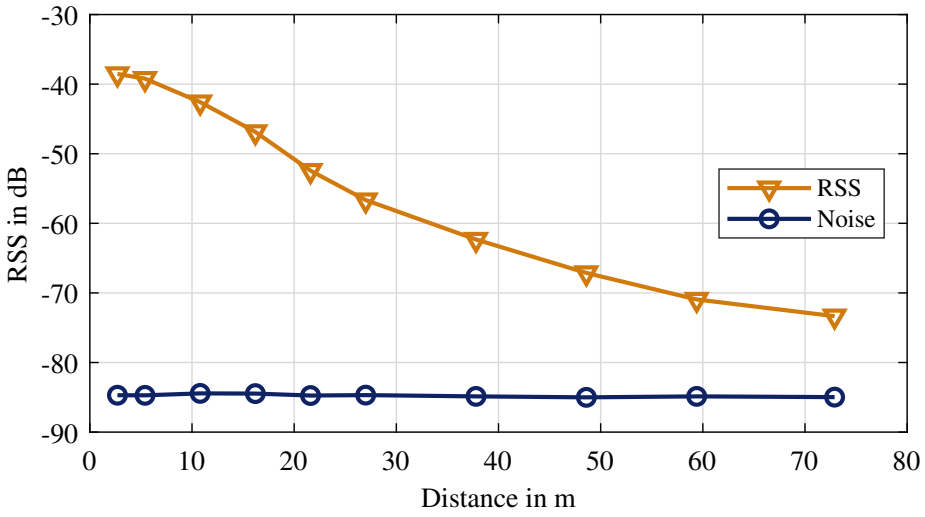

Figure 4.3 – RSS and noise over distance.

4.5 Reliability of OFDM

With the help of the measured SNR values, the reliability of the communication can already be estimated, taking the used modulation and coding into account. Only white Gaussian noise is used as a source of interference, other influences such as imperfect synchronization are neglected, respectively assumed to be perfect. The models of this calculation agree with the fully analytical consideration from Section 3.1. So that the error probabilities can be calculated in an analytically closed way. Figure 4.4a shows the BER over distance according to the SNR of Figure 4.3 when the modulations of the 802.11a/g/p standard are used but no coding takes place. Low modulation schemes, such as Binary Phase-Shift Keying (BPSK), allow long ranges even without coding. A BER of 10^{-6} is achieved at about 65 m. Higher modulation schemes, which also allow higher data rates, reach shorter distances. With 16-QAM, the BER threshold of 10^{-6} is reduced to 40 m, for example. By using coding, allowed distance for reliable communication can be greatly increased - even 64-QAM achieves error probabilities that allow reliable communication for distances over 40 m. A convolutional code with the constraint length of 7 and the generator polynomial $[171\ 133]_8$ was chosen as coding. The BER was estimated with Matlab using a tree search algorithm as in [97]. As code rate $R = \frac{1}{2}$ was chosen, this code rate is also used in 802.11 standards, including 802.11p.

The BER already gives a good impression of the dependence of distance on the reliability of communication. Since the 802.11 standard represents a packet-based communication, PDR is also particularly relevant for later applications. It indicates the ratio of correctly transmitted packets to sent packets. Without taking other factors into account, the PDR can be described with Equation (3.16) from Section 3.1. This allows the PER or PDR to be estimated based on the measured SNR and the calculated BER, as shown in Figure 4.5. The packet length l was chosen identically in the field test with 250 B respectively 2 kbit. The clear drop at a specific distance for the respective modulation and coding shows more clearly up to which distance reliable communication can be expected. For example, 64-QAM without coding still achieves a PDR of 1 at the 27 m, while at the next measuring point (37.8 m) it has dropped to almost 0, cf. Figure 4.5a. Even without coding, BPSK still achieves a PDR of 1 at about 60 m. The respective FEC result in a range increase of about 10 m, cf. Figure 4.5b. With a code rate of one half BPSK and Quadrature Phase-Shift Keying (QPSK) achieve a PDR of 1 over the entire measured distance.

Figure 4.6 shows the PDR measured in the field test. For this purpose, the received packets are compared with the transmitted packets and the ratio of correctly received packets to transmitted packets is formed. Especially the low modulations reach long distances of about 60 m with a very reliable PDR of almost 1. For higher MCS, which provide higher data rates, the distance of reliable communication reduces. For

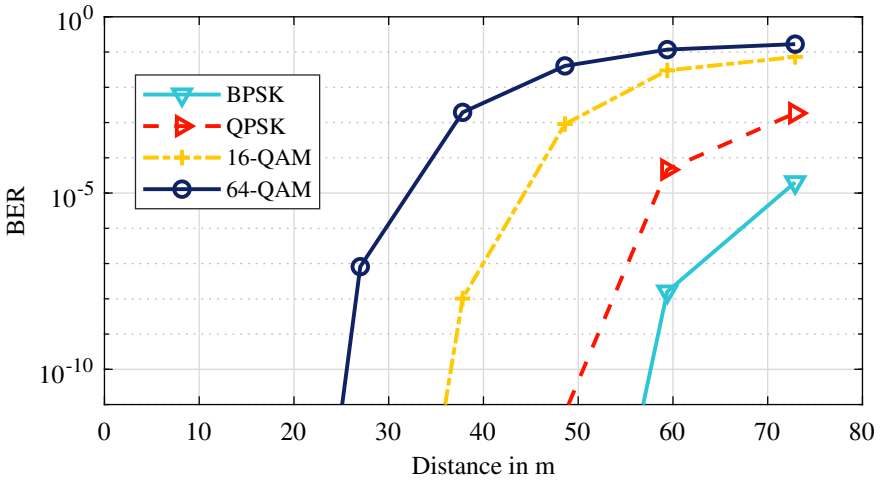

(a) BER without coding applied

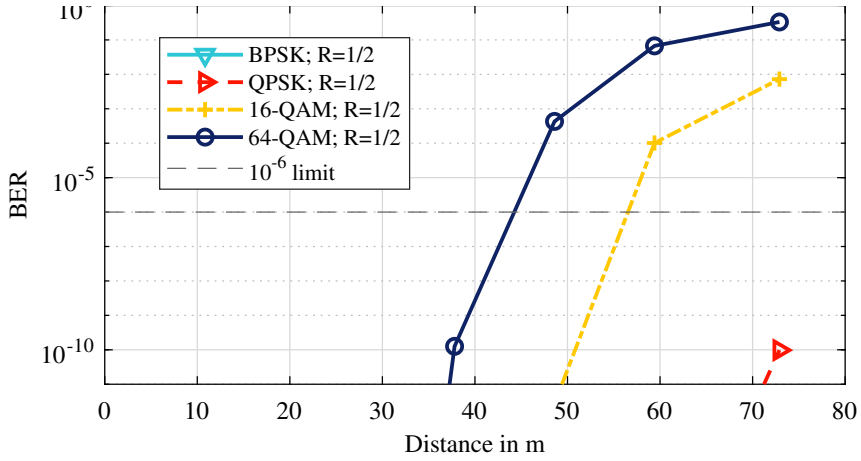

(b) BER with convolution coding applied

Figure 4.4 – Measured PDR over distance at the parking lot in front of the HNI at different times with different ambient light levels.

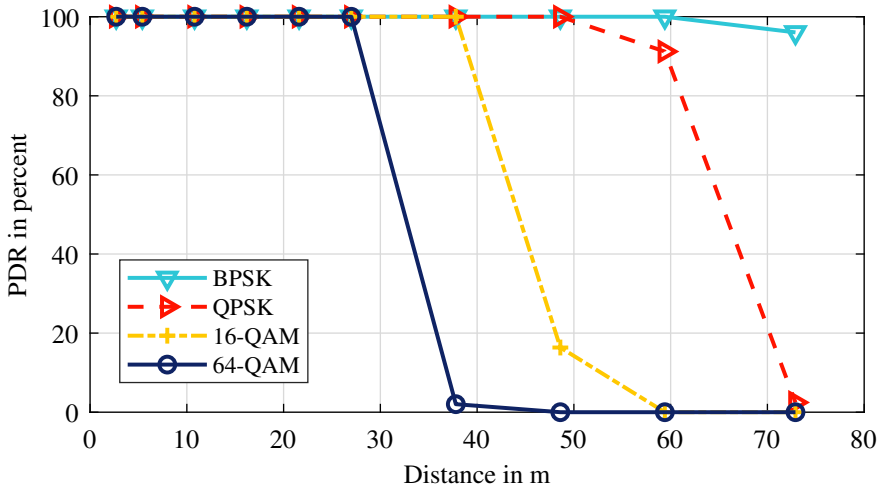

(a) PDR without coding applied

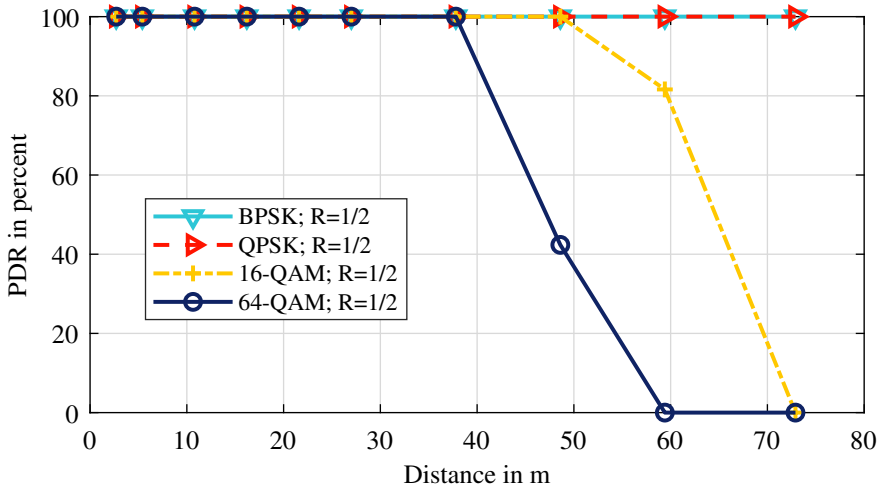

(b) PDR with convolution coding applied

Figure 4.5 – Analytical estimation of the PDR over distance under consideration of the measured SNR.

example, the reliability for 16-QAM for the code rates $R = 1/2$ and $R = 3/4$ drops sharply already at about 50 meters. If bandwidth efficiency is further increased by using 64-QAM, the distance is reduced to less than 40 m before the PDR drops sharply.

Apart from this behavior, fluctuations of the curves are also noticeable. When analyzing the clock drift in [24] it became clear that this error is mainly caused by insufficient synchronization of transmitter and receiver caused by clock drift. No external synchronization takes place for this field test. Teamjad2019compliant the setup was operated with an external synchronization to investigate the reason in more detail, whereby this kind of error, which is caused by a difference in sampling, could be eliminated. The synchronization must be improved for a later application. This can be done by using external synchronization signals such as GPS, by using more accurate clocks to reduce clock drift, and by applying methods for improved synchronization such as a Costas-loop to the system in an optimized way [98].

When comparing the empirically measured PDRs with the analytically determined PDRs from the SNR, a large agreement is noticeable. The distances at which a significant packet loss begins are almost identical for 64-QAM and 16-QAM in both cases. The analytically determined values of the PDR for BPSK and QPSK exceed the values measured in the field test. Since the analytical model does not consider sources of error that occur in the real world, the analytical model could be regarded as the upper limit of the field test. This is true for most graphs, but the performance of the field test exclusively for 16-QAM with a code rate of $1/2$ at distances of 59.4 m and 72.9 m slightly exceeds that of the analytical model. A possible reason for this could be that the analytical model and the field test are very close to each other. At the same time, a finite number of packets of 1000 is used for the field test, so that small deviations are possible. A further factor of the deviation could be inaccuracies in the measurement of the SNR. Because the amplitude of the received samples is used for this purpose, the SNR measurement itself is subject to noise. The fluctuations which occur especially in the field test for 64-QAM do not occur in the analytical observation. These deviations are caused by potential imperfections which are not considered in the analytical analysis. These certainly include to a large extent the deviations during sampling, other influences could be, for example, imperfect linearity or inaccuracies in the determination of the SNR. However, the generally small difference between the analytically determined packet error rate and the many rates measured in the field underlines the almost optimal implementation of the communication chain and the assumption that errors are mostly determined by the SNR.

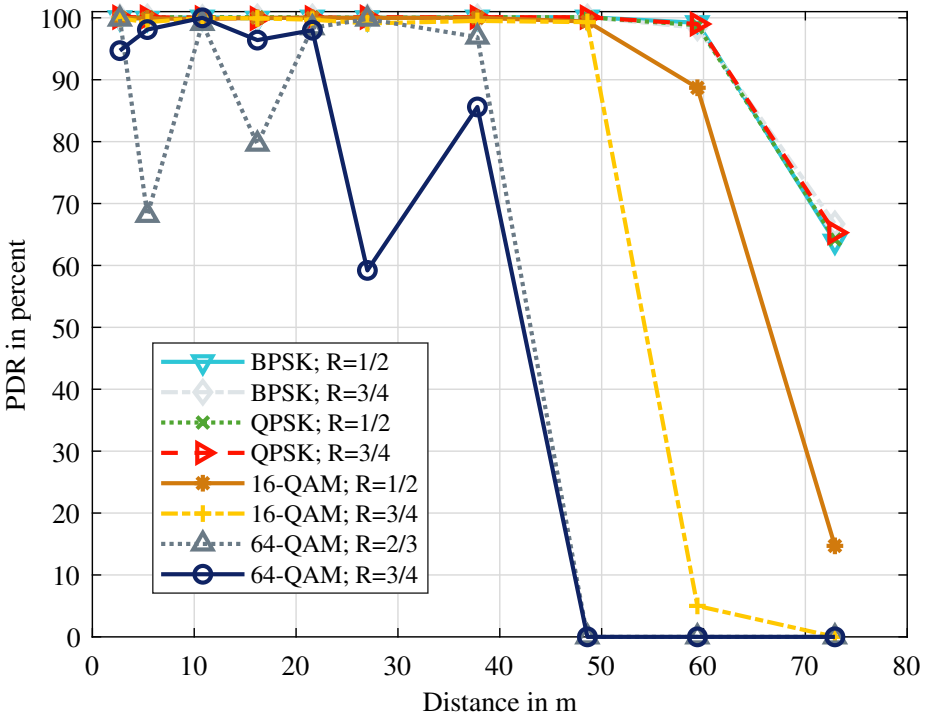

Figure 4.6 – Measured PDR over distance.

4.6 Investigation on Data Rate

As in the previous chapter, the potential selection of the MCS results from the available SNR under the condition of an acceptable error rate. The MCS determines the data rate in addition to the influence on the error rate. Data rate and error probability are competing goals. A robust MSC such as BPSK with a code rate of 0.5 has a lower data rate than, for example, 64-QAM with a code rate of 0.75, which in turn has a higher error probability with the same SNR. For this reason, adaptive switching between MCS makes sense. In this way, a high data rate can be achieved at a high SNR.

While at low SNR a robust MCS is chosen to maintain a reliable connection at the expense of the data rate. One possible way to set the switching thresholds between the MCS is to specify a desired maximum error probability. In Figure 4.4b 10^{-6} is drawn as a threshold. Based on this, it is now possible to determine data rates through the corresponding MCSs which, as a function of distance, have a lower probability of error than the maximum required. Figure 4.7 shows these data rates while maintaining the error threshold based on Figure 4.4b. It can be seen that up to a distance of 37.5m data rates of 1.35 Mbit/s are possible while maintaining the desired maximum error probability. Up to 48.6m it is data rates of 600 kbit/s

and beyond that 150 kbit/s. Two methods are conceivable for adaptive switching between MCS. On the one hand, an optimal MCS can be selected by the feedback of the receiver from e.g. the SNR. Since the signal strength depends significantly on the geometry of the scenario, as shown in Chapter 3, a position-based selection of the MCS can also be considered.

Since the prototype is based on 802.11 a/g/p, the set of established modulation schemes and code rates shown in Table 4.2 is implemented, which can be selected for the prototype. While the MCS, pilot symbols/carrier and guard blocks are identical to 802.11 a/g, the bandwidth of the systems differs, resulting in a different data rate. 802.11 a/g has 20 MHz bandwidth while the prototype was operated with a bandwidth of 500 kHz. The bandwidth results from 1 MHz sampling frequency and an interpolation filter with a factor of 0.5.

Additionally, the data rate can be increased by establishing a higher bandwidth. While in radio-based applications the bandwidth to be used is strictly regulated in

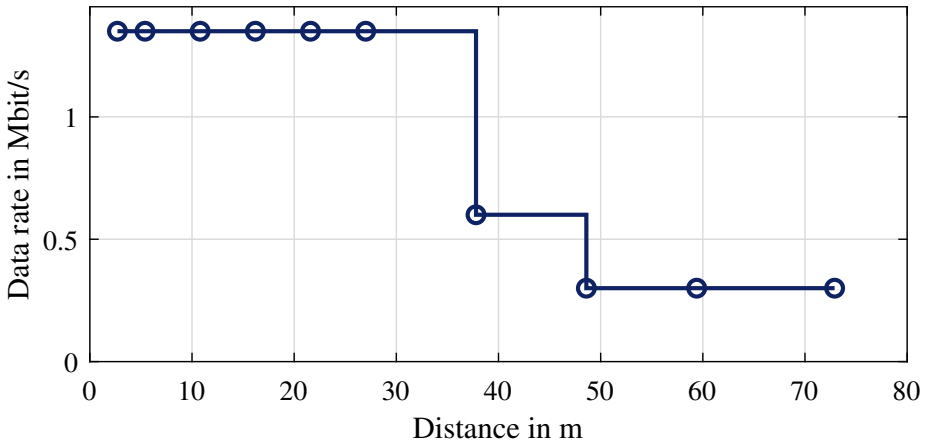

Figure 4.7 – Highest data rate with an BER of $< 10^{-6}$ depending on the distance.

Table 4.2 – Modulation and Coding Schemes Available for the Prototype with Corresponding Data Rates)

Modulation Scheme	Bit per Symbol	Code Rate	Data Rate in Mbit/s
BPSK	0.5	0.5	0.15
BPSK	0.75	0.75	0.225
QPSK	0.5	1	0.3
QPSK	0.75	1.5	0.45
16-QAM	0.5	2	0.6
16-QAM	0.75	3	0.9
64-QAM	$0.\overline{6}$	4	1.2
64-QAM	0.75	4.5	1.35

order not to interfere with other channels or services, this regulation does not apply to VLC. However, the usable bandwidth is limited by the low-pass behavior of the system. The bandwidth of 500 kHz was chosen, because this bandwidth with the corresponding carrier frequency is on the one hand indoor and outdoor robust against other light sources, like fluorescent tubes, and on the other hand is less attenuated by the low pass behavior of the system. Thus, regardless of the environment, long ranges can be achieved with an acceptable data rate. However, larger bandwidths are also possible, especially for shorter ranges. Figure 4.8 shows the receiving spectra of the receiving OFDM signal with 500 kHz and 3 MHz bandwidth, respectively. The distance of the signal plateau to the off-band noise in the normalized spectrum shows that the additional bandwidth is at the expense of reduced SNR. Especially due to the low pass behavior the signal strength drops strongly with higher frequency. A transmission over 5 m with 3 MHz bandwidth and 64-QAM with code rate 0.66 could be performed successfully with a PDR of 100%. This translates into a possible data rate of 8.1 Mbit/s.

However, the focus of this field test was not on achieving the highest possible data rate, but on communicating over a distance that is common in traffic with a reasonable data rate and hardware that is feasible for automobiles. If the data rate is to be increased further, the implementation of bit loading would be particularly interesting in addition to the bandwidth increase. In accordance with the low-pass ratio, strong signals, essentially lower frequencies, could be modulated with bandwidth-efficient MCS, while frequency ranges with low SNR could be modulated with robust MCS so that these are utilized but do not harm the communication due to bit errors. In this way, the spectrum as a whole can be used robustly and bandwidth-efficiently.

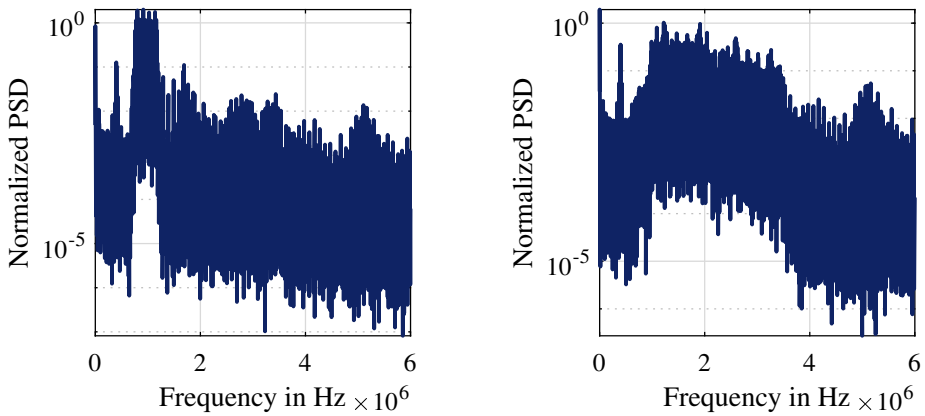

(a) Bandwidth of 500 kHz

(b) Bandwidth of 3 MHz

Figure 4.8 – Received OFDM Spectrum

4.7 Conclusion of OFDM Field Tests

In conclusion, this chapter shows that V-VLC with COTS hardware and only minor hardware modifications already allow performant communication with satisfactory ranges. With this prototype, which is based on SDRs, an open-source driver circuit, and the open-source framework GNU Radio, a platform is created which allows fast prototyping and can be used for collaborative development of V-VLC. The high flexibility of the signal processing with GNU Radio and SDRs allows real-time modifications of the signal processing and the MCS. By using high-level languages for the development of GNU Radio blocks and the graphical configuration of the transmission chain, even complex signal processing operations can be carried out with a manageable effort for a wide range of users. For this experiment a very promising transmission chain was chosen, which is highly compliant with the 802.11 standard. This has the advantage on the one hand that the foundation of the transmission chain is well established, thoroughly analyzed, and optimized to the greatest extent, and on the other hand that a combination with other technologies such as 802.11p can be easily implemented to achieve complementary communication.

Depending on the modulation order, communication over long distances of more than 70 m and communication with data rates satisfactory for many applications could be shown. The importance of adequate receiver optics was emphasized by the fact that even a relatively simple converging lens increased the received signal power by more than 23 dB without increasing the noise significantly. Thus, SNR was increased to enable communication over longer distances. A comparison with an analytical consideration of the error probabilities showed that both calculated values and values measured in the are nearly consistent, which speaks for a successful implementation. Furthermore, it shows that bit errors are primarily caused by AWGN and that the assumption of an AWGN channel is reasonable for the V-VLC scenario. Overall, this prototype provides a foundation for further investigations and measurements of VLC communication where a variety of other parameters like weather or dynamics but also the optimization of signal processing like diversity combining can be investigated.

Chapter 5

Communication in Presence of Interference

Another fundamental difference between V-VLC and Radio Frequency (RF) communication is that the light spectrum is currently barely used for communication, while the RF spectrum is heavily utilized. For reliable communication, however, potential interference must be carefully considered.

Interference can be caused by other light sources even if they are not modulated for the communication task. First of all, the sun is an obvious source of interference; it is characterized by its high intensity. At the same time, the sun is not modulated in intensity. The frequency of intensity fluctuations of the sun, for example, due to changing clouds, is very small compared to communication, they are in the range of a few Hertz. This influence can easily be eliminated with a high-pass filter so that the influence of the sun is not as strong as the intensity might suggest.

However, due to the enormous intensity in Scenario during the day, the sun can still influence communication. On the one hand, precautions must be taken to ensure that none of the components are running at saturation. This is achieved by placing the high pass filter as early as possible in the transmission chain. The first possible location is after the photodiode and before TIA. Experiments have shown that placing the filter at later locations will cause different components to run in saturation. A software high-pass filter in GNU Radio after the USRP and before further signal processing let the ADC run in saturation in the presence of strong sunlight. No communication was possible. Placing the high-pass filter between TIA and USRP may cause the TIA to run in saturation.

Even if the photodiode does not run in saturation, the operating point can shift due to an increased DC component and thus reduce the useful signal. In addition, a higher direct current at a PN junction causes shot noise which also has high-frequency

components, but this was small in our setup even in strong sunlight compared to other noise sources such as quantization noise or thermal noise of the components.

A more important source of interference are modulated light sources, which are modulated to adjust brightness. As described in Section 2.2.4, PWM has been established as a method for brightness adjustment. Typically, frequencies of up to 500 Hz are used. This is far below the frequencies used for communication, so a high-pass filter can eliminate these low frequencies. Since higher frequencies do not harm PWM for the purpose of brightness adjustment, PWM with higher frequencies also occurs. In addition, PWM are operated with a rectangular pulse shape, which means that the harmonic frequencies also disturb the communication. Such modulated light sources can have a negative influence on communication. To solve this problem, Section 5.1 introduces a spatially filtering receiver that receives desired signals depending on the location, while blocking unwanted interference.

Although V-VLC suffers less from multi-user interference than classic RF communication due to its propagation characteristics, it still occurs and needs to be addressed. Memedi, Sommer, and Dressler [72] evaluated simulations with realistic radiation patterns, with the finding that in common scenarios, a transmitted headlight signal is received by up to eight vehicles. This means that the number of multi-users is limited, but measures for multi-user access must be implemented. Established methods such as FDMA, TDMA, or Code Division Multiple Access (CDMA) can be used to provide multi-user access. However, these methods work at the expense of data rate and usually require an overhead for the allocation of the respective resources, which can cause complexity and latency.

In Section 5.2, an Space-Division Multiple Access (SDMA) approach is examined by modifying a special matrix headlight to transmit data in a small solid angle range to avoid interference and to enable reuse of resources of time, frequency or coding, locally, resulting in higher bandwidth efficiency. The approach from Section 5.1 can also help by filtering unwanted messages spatially on the receiver side. In this way, multi-user interference at the receiver can be suppressed.

5.1 Optical Spatial Receiver

Our field experiments showed the essential influence of receiver optics for successful V-VLC. Thus, the combination of two converging lenses in Section 4.2 could cause a signal amplification of the field strength by 11.6 dB. Apart from partially low signal strength caused by the regulated radiation characteristics, V-VLC has to deal with interference.

Shen and Tsai [92] showed in a field test with a drive through public streets in Taiwan that V-VLC worked properly in most of the cases, but failed, in terms of a

complete drop of PDR when LED road signs were nearby. These road signs probably were modulated with a frequency to regulate the brightness with a PWM matching the frequency of communication.

In the following chapter, a solution to this problem is examined where the interference is filtered already in the optical domain. Therefore, the novel Liquid Crystal based Optical Receiver (LC-Rx) is presented, simulated, implemented in a prototype, and evaluated. The switchable LC module allows the receiver to optimize the FoV adaptively to filter interference spatially and thus reduce the interference to a minimum. In addition to LED street signs, other sources of interference in the V-VLC environment are also present, which can be eliminated with the LC-Rx. Other sources of interference include other modulated light sources, such as billboards or PWM dimmed automotive lighting, the sun, or other VLC transmitters that send a message to a different addressee.

5.1.1 Background and Related Work of Receiver Optics

With V-VLC, the received signal in the form of light must be converted back into an electrical signal at the receiver in order to be processed further. For this purpose two technologies, photodiodes and camera sensors, have been established. Camera sensors have the advantage that they can differentiate signals locally because different angles of incidence are imaged on different pixels. Thus, signals from several transmitters can be received and distinguished simultaneously or sources of interference can be isolated. In certain cases, data rates can also be increased by Multiple-Input Multiple-Output (MIMO) [99].

However, camera sensors as receivers for VLC also have some disadvantages. Especially the bandwidth has to be mentioned here, which is comparatively low due to the limited readout rate of the individual pixels [62]. Usual readout rates are in the range of 30 frames per second. Also, the sensitivity is limited because the individual pixels have comparatively small active areas [62]. High-speed cameras with several hundred fps can achieve higher bandwidths and thus higher data rates [100]. However, these sensors are very expensive and prevent an application in the broad mass market.

Photodiodes on the other hand can offer a very high bandwidth in the range of GHz [101], [102]. This high bandwidth enables data rates of several gigabits under appropriate conditions. Photodiodes can also offer high sensitivities because large active areas are feasible. However, unlike camera sensors, photodiodes do not have a spatial separation. This leads to the fact that receivers with a photodiode either have a small field of view and can therefore only receive from a small operating angle, which is a disadvantage in dynamic channels as they occur in traffic or if the receiver optics have a larger field of view, more interference from other light

sources, ambient light or multi-user interference will be received. Another problem is that very high light levels can reach the receiver, which leads to saturation of the components, usually the photodiode itself, one of the amplifier stages, or the ADC. This can lead to a complete failure of the communication.

Using angular diversity to reduce interference based on photodiode arrays has already been demonstrated with prototypes using infrared [103], ultraviolet ,[104] and light communication [105]. Another novel approach is based on the use of a dynamic vision sensor [106], which reacts differentially to changes in the illumination of pixels and thus advises higher readouts or achieves bandwidths. However, these systems cause an increased system complexity or higher costs.

The idea of combining a single photodiode with an optical local filter originally comes from Kratochvil [107]. For the spatial filtering, he uses a DMD, which consists of many small mirrors that can be controlled individually. The coverage area is imaged on these micro-mirror surfaces and signals of relevance are transmitted via the mirrors to the receiver. Interference sources are diverted by the mirrors in a different direction and absorbed by an absorber. This method can greatly reduce noise and interference without bandwidth loss. However, the use of the DMD also causes difficulties. Because it is a reflective system, the optical axis is folded to save size in one dimension but increase size in the other dimension. Furthermore, DMDs are very limited in the acceptance of the angle of incidence. Therefore, either more complex or expensive optics are necessary or the field of view is limited. The control of DMD chips is mostly proprietary and relatively complex.

An alternative to the previously mentioned solutions is a locally filtered receiver with a single photodiode based on an LC module, explained in the following. In contrast to the DMD, however, the LC module can be placed in the optical axis, which simplifies the adjustment. By using Vertical Alignment (VA)-technology, higher angles of incidence are permitted, which reduces the demands on the optics and allows a large FoV. LC-modules are widely used so that they can also be controlled cost-effectively with relatively simple hardware, like a microcontroller. A further advantage is that pixels, unlike mirrors, can be switched on or off not only in binary but also in grayscale so that signals can be dimmed to reduce the dynamic bandwidth and thus prevent saturation. To our knowledge, our publication [25] was the first time a spatial filter receiver based on an LC module was presented. The benefits of this novelty were verified by simulations and measurements of the prototype.

5.1.2 System Design

Figure 5.1 illustrate the concept ouf our receiver. The left side shows the spatially distributed objects, which are located in the opening angle of the receiver. These are on the one hand the vehicle (a), which symbolizes the desired communication

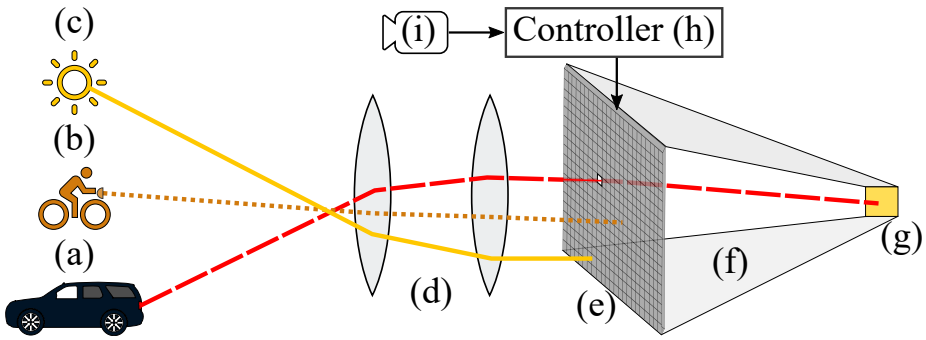

Figure 5.1 – Schematic layout of the receiver. (Reproduced from [25], © 2019 IEEE.)

partner, on the other hand, the bicycle (b), which represents an interference source with modulated light, and the sun (c), which represents the ambient light. This scenario is imaged on the LC panel (e) using the optics (d). The LC-panel is in the focus of the optics so that the light sources (a) to (c) are each imaged on a small area consisting of a few pixels in the plane of the LC-panel.

A camera (i) can additionally capture the scenario. A camera installed in the vehicle for other applications, such as Lane Assistant or High Beam Assistant, can be used, to prevent additional hardware costs. The camera data can be processed in an Electronic Control Unit (ECU) (h) in order to control the LC panel (e) according to the communication task. This could also include additional information from an ECU or Telematic Control Unit (TCU), such as information from a higher communication layer like the MAC. It is also conceivable that the information about the position of the light sources could be generated not only by a camera system but also by other sensors such as Light Detection and Ranging (LiDAR) or a fusion of several sensors.

In the simplest case, the pixels on which the desired light signal hits will be switched to transparent, while all other pixels will be switched to nontransparent, thus absorbing unwanted signals on this layer. The desired signal, shown as a red dotted line, is then passed through a light-carrying channel (f) to the photodiode (g), allowing the desired signal to be processed in isolation in the receiver. If the signal source (a) is very close to the receiver and clipping or saturation would occur, the corresponding pixels could also reduce the transmission according to a grayscale and thus reduce the dynamic range, which can counteract clipping or saturation.

5.1.3 Optical Design

The optical design of a receiver optic for V-VLC is always a matter of trade-offs. For example, the extent of the optics, luminous flux at the receiver, aperture angle, reception of interfering light, or, in the case of a locally filtering receiver, the resolu-

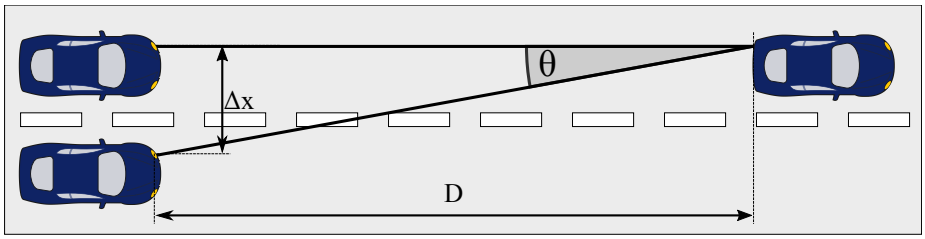

Figure 5.2 – Example scenario where one signal source and one interference source are present in a vehicular VLC application. (Reproduced from [25], © 2019 IEEE.)

tion of the receiver must be weighed up. In order to be able to make a meaningful assessment, applications were consulted, and a possible scenario was considered. As a possible scenario, a multi-lane roadway with a width for each lane of 3 meters was assumed. This scenario is shown in Figure 5.2. In addition, it was assumed that vehicles drive with the recommended minimum distance between them for 100 km/h (D_{100}). The recommended minimum distance in meters can be calculated by a rule of thumb by dividing the numerical value of the speed by two. This means that the recommended distance, in this case, is 50 m.

The requirements for the optics are, on the one hand, to be able to separate the signals of two vehicles driving next to each other with the distance D_100, which essentially places requirements on the angular resolution. On the other hand, the angle of beam spread should be large enough so that a vehicle approaching on the adjacent lane with a lateral distance of 0.5 m is still within the communication range if the longitudinal distance is more than 0.5 m. This geometrical dependence was chosen, for example, to be able to initiate a lane change or to inform a vehicle when entering the blind spot. This large FoV competes with the goal of high resolution, but the receiver should produce optimal results in a variety of possible situations, so matching both very different cases is a good compromise to the requirements.

The front optic was designed with ZEMAX. It must essentially fulfill three functions. First of all, it must perform basic imaging. However, there is a special feature compared to common imaging systems, such as cameras or projectors, that errors like distortion or astigmatism are less relevant in this application. The primary goal is to minimize the local spread of an image on the LC panel in order to make optimal use of the LC panel and achieve a high resolution. A further task is to achieve the largest possible pupil opening to capture more light and thus achieve high signal strengths. This can lead to a higher SNR since the signal is usually amplified more than the noise, which consists largely of thermal and quantization noise. The third requirement is the wide field of view, which should ensure that there is always a communication link, even in dynamic traffic scenarios. The scenarios considered

result in the desired field of view of 100°. In addition, a particular difficulty is to implement this requirement with the least possible use of optical elements to keep the losses at material transitions low on the one hand and to keep the costs low on the other hand. Since V-VLC is intended for the mass market, it is essential to create a financially attractive system for the automotive industry by using as few components as possible, which allows the system to be installed in all vehicle classes.

It was possible to implement the front optics with only two optical elements. The first element is a biconvex lens to concentrate the light. A biconvex lens is the best choice because it tends to have less spherical aberration. Since spot size is an important criterion to achieve high resolution and chromatic aberration is a cause for an enlarged sports size. A double lens was used as a second optical element to reduce chromatic aberration and paraxial spherical aberration. The doublet lens is also positive to support the focusing of the first lens.

Behind the front optics, the LC panel is arranged on which the scenario is imaged. The properties of the LC Panel are summarized in Table 5.1. It is a monochrome LC-panel, which on the one hand lets as much light through as possible, on the other hand, achieves the highest possible contrast to effectively filter out sources of interference and additionally guarantees high viewing stability to allow large angles of incidence. This is realized by VA-technology. In addition, the dimensions of the integration in a vehicle and the selected lenses must be appropriate. Furthermore, the resolution also ensures the targeted isolation of signal sources at great distances.

After the parameters of the optics had been optimized in simulations, they were replaced with COTS lenses with parameters as similar as possible. The result of this optics can be seen in Figure 5.3. The Figure shows the XZ-plane, where rays with different angles of incidence are displayed in different colors. These different beams cover angles of incidence of 0° to 50° in intervals of 10°. The lateral field of view is 100° as required. For the vertical FoV an opening of 60° was achieved, which should

Table 5.1 – Specifications of the LC panel (Reproduced from [25], © 2019 IEEE.)

Parameter	Value
Type	Monochrome
Display size	2.2-inch diagonal
Technology	α-Silicon, VA
Resolution	320×240
Pixel size	$141\,\mu m \times 141\,\mu m$
Transmittance	$\sim 20\,\%$
Contrast ratio	~ 3400
Operating temperature	$-20\,°C$ to $70\,°C$

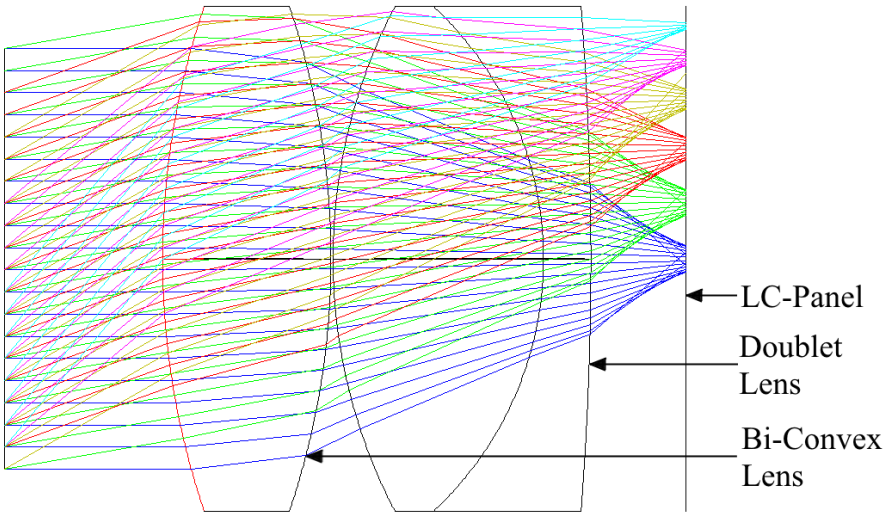

Figure 5.3 – Layout of the optical design in xz-plane. (Reproduced from [25], © 2019 IEEE.)

be sufficient for common traffic scenarios. The entrance pupil has a diameter of 40 mm, which results in a significant amplification of the signal.

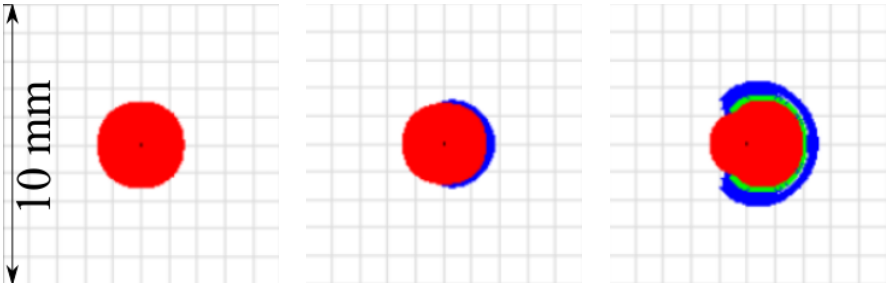

(a) $\theta = 0°$ **(b)** $\theta = 10°$ **(c)** $\theta = 20°$

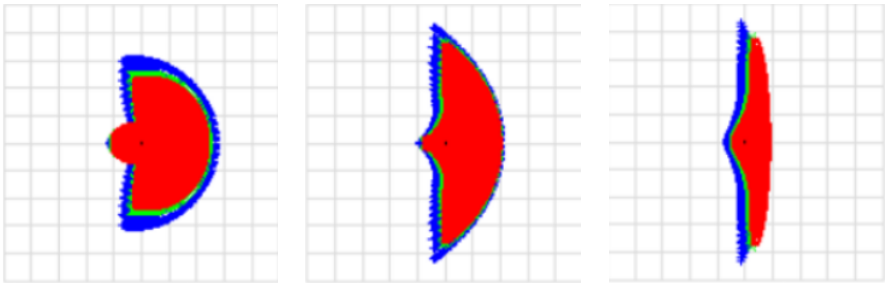

(d) $\theta = 30°$ **(e)** $\theta = 40°$ **(f)** $\theta = 50°$

Figure 5.4 – Spot diagram of the optics for different angle of incidence. (Reproduced from [25], © 2019 IEEE.)

The fulfillment of the requirement for a low spot size can be evaluated with a spot diagram. Spot diagrams for different angles of incidence resulting in different positions on the LCD are shown in Figure 5.4. The different colors show the spots of the different wavelengths. Deviations are caused by chromatic aberration, which cannot be completely prevented even with the doublet lens. The IMA, which indicates the position of the image on the imaging plane, matches the dimensions of the LC-panel, so that the maximum angle of incidence of 50° appears at the edge of the 2.2-inch panel, cf. Table 5.2. While the incidence on the optical axis results in an almost perfect circle (cf. Figure 5.4a), an increased angle of incidence causes the spot to be narrower in horizontal orientation but larger in vertical orientation, cf. Figures 5.4b to 5.4f. This effect increases with larger angle. So the spot becomes narrower and higher up to 50°, cf. Figure 5.4f. This behavior also becomes clear when the radii of the spot are compared. Table 5.2 shows that the Root-Mean Square (RMS) of the radius increases only slightly, while the Geometric Radius, which is the maximum radius of the spot measured by the centroid, increases more than three times as the angle of incidence increases. This trend of distortion harmonizes with typical traffic scenarios in which high resolution or separability is particularly important in the center, since large longitudinal and small lateral distances, i.e. small differences in angle, occur in this area. For large angles of incidence, distances are usually small, so that a high angular resolution is less important here.

This property is also supported by the type of mapping. While most lenses follow a mapping according to the formula [108]

$$f - \tan(\theta)\,, \tag{5.1}$$

the mapping law changes for lenses with a very large field of view. For those, the mapping can be estimated by what the increasing distance on the image plane corresponds to the increasing angle of the object plane. This causes a higher resolution in the region near the optical axis, i.e. in the center of the communication area.

Table 5.2 – Spot size in dependency of the angle of incidence (Reproduced from [25], © 2019 IEEE.)

Angle of incidence	0°	10°	20°	30°	40°	50°
RMS Radius in µm	923	885	862	960	1098	1101
Geo Radius in µm	1370	1673	2373	3055	4216	4310
IMA in mm	0	5.38	10.54	15.21	19.193	22.17

5.1.4 Analytical Evaluation of the LC-Rx

The novel receiver optics can be analyzed using the analytical model presented in Section 3.1. As the source of light, the high beam of a left headlamp was chosen. The radiation pattern of this headlamp is shown in Figure 3.4h. As photodiode, the Thorlabs PDA100A was used again. This has an active area of 10 mm by 10 mm and reacts to the entire range of the visible light spectrum. The integrated TIA of the photodiode was also taken into account. As in the system design description in Section 5.1.2, the light spatially filtered by the LC panel must be passed on to the photodiode. For the simulation, it is assumed that all light passing through the LC Panel is collected by the photodiode. The possibility of back reflection from the pyramid-shaped mirror arrangement is not taken into account, as this can be at least partially recycled by a transreflective film on the back of the LC panel.

With the help of the analytical model, two main scenarios are considered. The first scenario is an outdoor experiment with brightest sunlight which is 100 klx and homogeneously distributed in the room. The signal source, i.e. the left headlight is located centrally in front of the receiver. The signal to noise ratio can be calculated by

$$SNR = \frac{I_{signal}^2}{\sigma_{shot}^2 + \sigma_{thermal}^2} , \tag{5.2}$$

where I_{signal} is the photocurrent caused by the signal and σ_{shot} and $\sigma_{thermal}$ are the variances of the shot-noise and the thermal noise, respectively. A BER of 10^{-6} is assumed as the target for reliable communication. This corresponds to an SNR of 16.55 dB and 11.78 dB for OOK and 8 PPM modulation if the formulas from Section 3.1 and average available signal power are assumed. When a bare photodiode is used with neither optics nor LC panel, the SNR corresponds to the orange curve in Figure 5.5.

In comparison, the LC-Rx achieves significantly higher values in relation to the SNR, cf. Figure 5.5 blue dashed curve. This is partly due to increased input pupil provides more signal strength and partly due to the local filter reduces sunlight, which causes shot noise. This change in SNR has a direct effect on the communication range. Without optics and with simple OOK 64.7m can be reached, 85.1m can be reached with 8-PPM. The LC-Rx increases the ranges to 101.8m and 133.8m for OOK and 8-PPM, respectively. It should also be noted that direct sunlight with an illuminance of 100 klx already causes 271 mA. This is far above the saturation limit of the photodiode, which is specified as 6.67 mA. Therefore, no communication is possible with the bare photodiode and direct sunlight. The LC-Rx provides a solution by blocking the sunlight by a high amount.

The second scenario considers the case of several participants of the communication which can interfere with each other. In this case, two headlights are in the

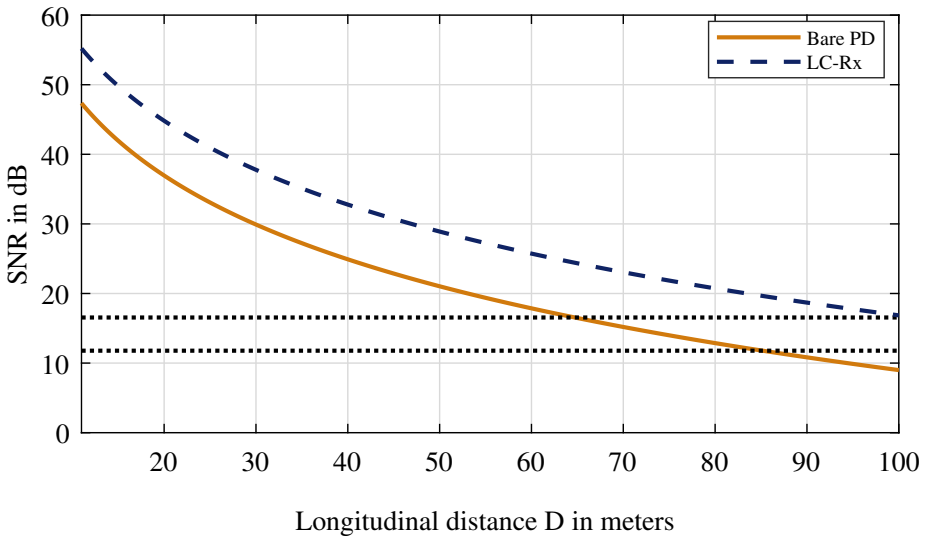

Figure 5.5 – SNR at the receiver. (Reproduced from [25], © 2019 IEEE.)

detection range of the receiver and communicate in the same frequency band at the same time. In this scenario, one headlight is considered as the desired transmitter. This is located centrally in front of the receiver. The second headlight is interpreted as an interference source and is located at a distance Δx from the headlight, as shown in Figure 5.2. The evaluation of the scenario is performed for three different distances D of 10 m, 25 m and 50 m. The Signal-to-Interference Ratio (SIR) is used as a metric, it is given by

$$SIR = \frac{I_s^2}{I_i^2}\,, \tag{5.3}$$

where I_s is signal-induced photocurrent and I_i is the interference-induced photocurrent at the PD. The SIR for the bare photodiode and LC-Rx receivers are shown for different distances in Figure 5.6. In the case of the bare photodiode (orange curves), the SIR starts at low values and then increases as the lateral distance between the transmitter and the interference source increases. This is due to the interference source emits less light away from the center, the effective receiver area decreases according to a cosine due to the increased angle of incidence, and the Euclidean distance increases. At a lateral distance which depends on the longitudinal distance, the interference source leaves the FoV of the receiver, causing the SIR to jump to infinity. For a longitudinal distance of D equal to 50 m and lateral distances of Δx equal to 0.5 m and Δx equal to 3 m, which on the one hand represent very close receivers driving side by side and on the other hand represent two vehicles in the middle of a 3 m wide roadway, SIRs of 0.7 dB and 12.62 dB are achieved. With non-adaptive optics, the SIR could be reduced depending on the angle of aperture,

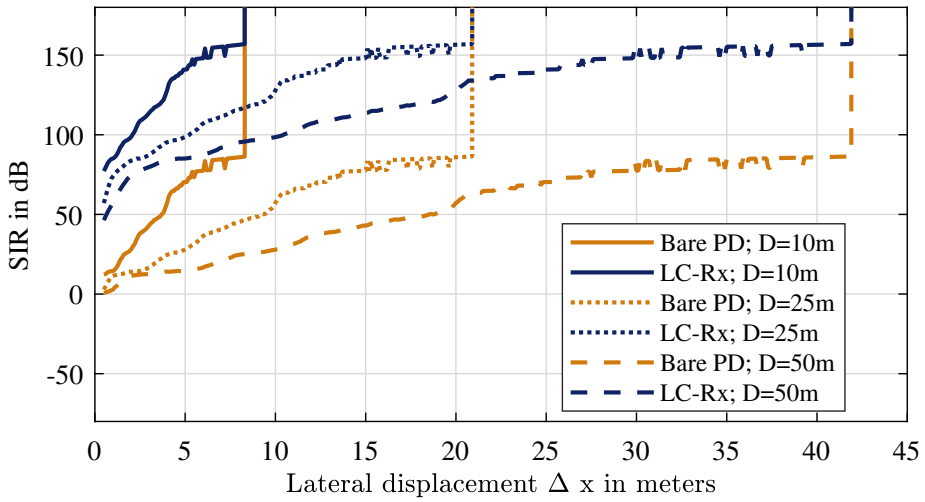

Figure 5.6 – SIR at the receiver at D = 10 m, 25 m and 50 m. (Reproduced from [25], © 2019 IEEE.)

either by having a vignette effect in the lens or by having a lower FoV. However, this is always accompanied by a shrinking reception range.

The combination of optics and LC panel in the LC-Rx, on the other hand, allows a large FoV and at the same time eliminates interference to a large extent by blocking the interference source with black pixels. This can be clearly seen as an increase of SIR in Figure 5.6. Unlike the bare photodiode, the SIR is large even at small lateral distances. In this case, the SIR is essentially determined by the contrast behavior of the LC panel. A good black level suppresses interference particularly well, while a high transmittance shows less attenuation. For the same reasons as with the bare photodiode, the SIR continues to rise with increasing lateral distance until the interference source leaves the FoV of the receiver and the SIR rises to infinity.

If we look closely at the SIR for a longitudinal distance of 50 m and lateral shifts of 0.5 m and 3 m, as we did with the bare photodiode, we also see a dramatic increase in the SIR, so that we reach 46.33 dB and 79.76 dB, respectively. This means that the LC-Rx can enable communication even in the presence of a strong interference source.

5.1.5 LC-Rx Prototype

In order to test the promising analytical results in reality, a prototype was developed, as shown in Figure 5.7. The lenses optimized in ZEMAX were used and a 3-D-printer was used to design a housing. The housing performs several tasks: on the one hand, it places the optical elements in the correct distance to each other and protects them, on the other hand, it shields stray light from other sides in front of the first lens, the

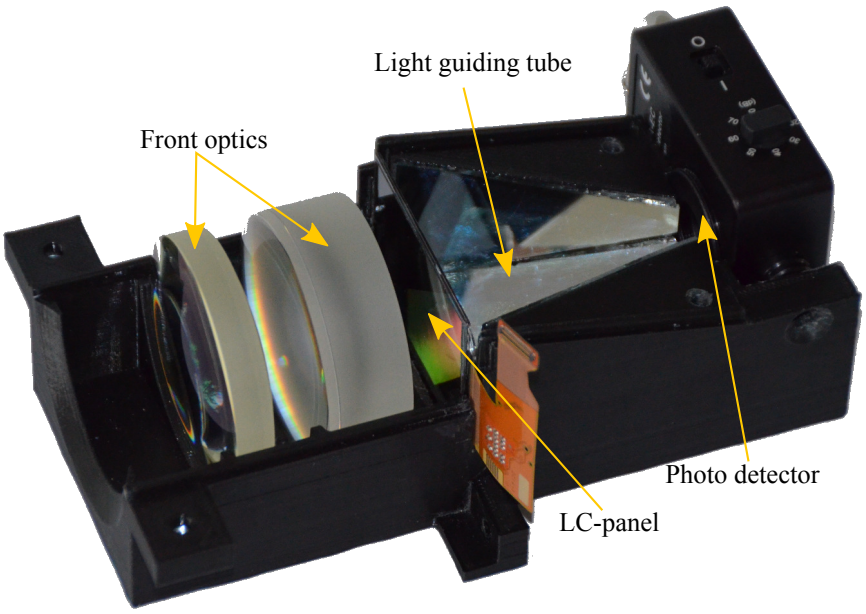

Figure 5.7 – The cross-sectional view of the prototype. (Reproduced from [25], © 2019 IEEE.)

construction served as an aperture to achieve the desired field of view, furthermore, it forms the pyramidic mirror arrangement in front of the photodiode which acts as a light guide.

The housing consists of two parts that can be clipped and screwed together. Figure 5.7 shows the optical components and the lower half of the housing. The dimensions of the prototype are 90 mm × 60 mm × 145 mm, which allows integration into a vehicle even in prototype status.

5.1.6 Evaluation of the Prototype

The practical measurement of the prototype took place on a parking lot during a very sunny day. The illuminance of the daylight varied continuously between 90 klx and 120 klx during the measurements. COTS-headlights were used, which were not optically modified. However, the control was modified so that high frequencies can also be driven using the OOK driver circuit from Section 2.2.4. The LC-panel was operated with a selection of eight static patterns, which could be selected according to the measurement with a controller. The headlights were modulated with a 200 kHz sine wave to distinguish the signal from ambient light, noise, or interference. The signal was detected by the PDA 100A photodiode, converted into a voltage by the integrated TIA and then recorded by an oscilloscope. With the help of an Fast Fourier Transform (FFT), the useful signal could be isolated.

When measuring with a bare photodiode and 0 dB amplification, the signal of 200 kHz could be identified at a distance of 5 m as long as no direct sunlight was shining on the sensor. In this case an SNR of 15 dB was achieved. At a distance of 10 m, the signal could no longer be detected with a bare photodiode. A higher gain of the TIA usually increases the SNR, but a higher gain combined with the strong ambient light caused the photodiode to saturate resulting in no signal being detected. This measurement already shows that a bare photodiode without any further modifications is entirely unsuitable as an V-VLC-receiver, since a high dynamic range of illumination is present in traffic scenarios, meaning that the problem of saturation can occur frequently. In contrast to the measurement setup, other sources of interference, such as modulated light sources, can also occur in traffic scenarios in addition to the sun, preventing a reliable communication link.

If the same photodiode was integrated into our newly designed prototype, however, the characteristics of the channel improved significantly. If the LC panel was controlled with a white rectangle on a black background, to pass only a part of the light through and block the rest by black pixels, the DC component dropped from 2.1 dB V to -12.5 dB V. This enables communication even under direct sunlight.

In addition, even during the day, higher amplifications on the TIA could be used without the problem of saturation. Also, the SNR increased significantly, so the SNR at a longitudinal distance of 5 m increased to 28.4 dB. Even at a distance of 10 m, where no signal could be detected with a bare photodiode, the SNR increased to 17.3 dB.

When comparing different patterns on the LC panel, it was found that a small rectangular area could reduce the DC component significantly compared to a completely white LC panel, but the noise was only slightly reduced. This indicates that the shot noise only plays a minor role in the composition of the noise and that thermal noise or quantization noise, for example, are more important. Nevertheless, the performance of the prototype was also far better than that of a bare photodiode in terms of SNR.

Apart from improving SNR, the LC-RX's greatest strength is its ability to suppress interference. Shen and Tsai [92] have already shown that modulated light sources within the reception range can lead to severe limitations in communication. In general, the presence of such interference sources is likely to occur in many scenarios. Possible sources of interference are artificial light sources such as lanterns, traffic lights, advertising signs, lighting on houses but also headlights, and taillights of other vehicles. To investigate the capability of local filtering of interference sources of the LC-Rx, first, the signal strength measurement of a headlamp with the distance D was performed, then the same headlamp was measured with the same modulation with the shift Δx. This second signal strength was interpreted as interference power. Good isolation of interference sources is therefore characterized by the fact that

the first signal is large, while the interference power is as low as possible. This is expressed by the signal to interference ratio which is given by Equation (5.3).

The results of these measurements with a lateral displacement of only 0.5 m are shown in Table 5.3. Lager lateral displacements are generally easier to separate, since the angle of arrival increases. If a bare photodiode is used, an SIR of only 0.6 dB is obtained for a distance of 5 m. This means that communication is almost impossible. If the interference is another source of communication, multi-user access technologies could be used to enable communication. However, multi-user access technologies such as TDMA, FDMA, CDMA usually require additional resources and thus reduce the usable data rate. With a longitudinal distance of 20 m, no SIR could be measured with the bare photodiode as no signal was detected.

In contrast, the LC-Rx offers significantly larger SIR when a proper pattern is used. At a longitudinal distance of 5 m, an SIR of 11.5 dB was achieved, at a distance of 20 m even 12.1 dB. This would allow multi-user scenarios to communicate without additional more user access technologies, thus saving bandwidth. It would also allow communication even during the presence of a modulated light source so that communication can be carried out even in the presence of LED signage.

Figure 5.8, which shows the received spectrum of the transmitter and the interference source, shows the effect of controlling the LC-Rx with different patterns. First of all, the entire LC panel was set to transparent, which means no locally filtering takes place, cf. Figures 5.8a and 5.8c. In contrast, the panel was switched to nontransparent except for a central transparent rectangle in Figures 5.8b and 5.8d. The first thing to notice is that the noise is always at about the same level, suggesting that the pattern has little effect on the SNR in this case. It can also be seen that the interference source is at about the same level as the signal source in the case of the transparent LC panel. In the case of the small transparent rectangle, the signal remains large, but the interference can be almost completely eliminated, thus achieving a large SIR.

An evaluation of the local resolution is shown in Figure 5.9. For this purpose, the signal strength was measured as a function of the angle of incidence for different patterns. The figure shows a very high resolution of about one degree can be

Table 5.3 – SIR performance in the outdoor experiment (Reproduced from [25], © 2019 IEEE.)

D	Δx	Receiver	SIR
5 m	0.5 m	PD	0.6 dB
20 m	0.5 m	PD	no signal detected
5 m	0.5 m	LC-Rx	11.4 dB
20 m	0.5 m	LC-Rx	12.1 dB

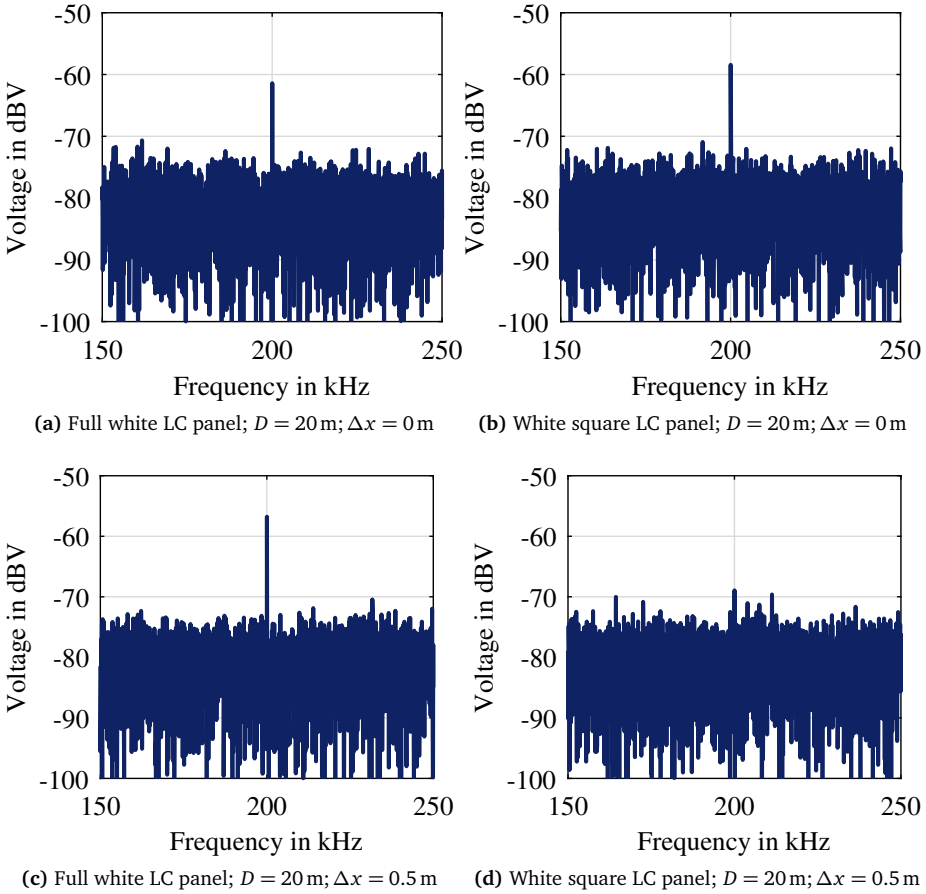

(a) Full white LC panel; $D = 20\,\text{m}$; $\Delta x = 0\,\text{m}$

(b) White square LC panel; $D = 20\,\text{m}$; $\Delta x = 0\,\text{m}$

(c) Full white LC panel; $D = 20\,\text{m}$; $\Delta x = 0.5\,\text{m}$

(d) White square LC panel; $D = 20\,\text{m}$; $\Delta x = 0.5\,\text{m}$

Figure 5.8 – Outdoor experiment with $D = 20\,\text{m}$ and $\Delta x = \{0\,\text{m}, 0.5\,\text{m}\}$. (Reproduced from [25], © 2019 IEEE.)

achieved, which means even closely spaced sources can be separated, allowing even demanding traffic scenarios to be handled. The figure shows additionally that by using a slightly wider pattern, more signal can be passed to the receiver, this could be used for example if there are no sources of interference in the immediate proximity of the transmitter to increase the range.

5.1.7 Conclusion

With the LC-Rx a prototype of a receiver was introduced, which can reduce the negative effects of interference to a minimum. It uses the directivity of light to filter spatially by an optical element according to the angle of incidence. This enables V-VLC even when strong sources of interference are present and furthermore offers the opportunity of using simple protocols which reduce overhead and latency. Simulations have extensively shown the possible reduction of interference and the

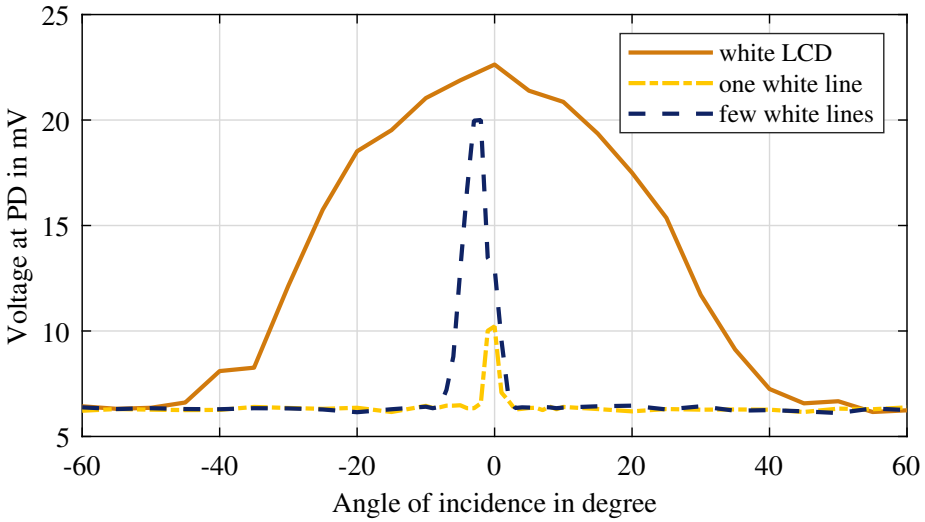

Figure 5.9 – Angular resolving capabilities of the LC based receiver with different patterns. (Reproduced from [25], © 2019 IEEE.)

increase of SNR by reducing shot noise. By implementing a prototype and subsequent validation, the suppression of interference in a field experiment was demonstrated. The interference could be reduced by more than 12 dB even in challenging scenarios. In summary, we consider the receiver as an important piece within an VLC solution to enable future heterogeneous intelligent transportation systems and cooperative driving.

However, aspects were also shown which can be improved in the future. First, the light-guiding mirror channel loses signal strength due to back reflections and directs less light to the photodiode, especially at large angles of incidence. This problem could be solved with a Compound-Parabolic-Concentrator (CPC). Secondly, a large part of the light is absorbed by the polarization filters of the LC panel. This reduces the signal strength. A potential future improvement would be the use of an electrostatic micro-shutter array, such as the one used in the James Webb Space Telescope from Nasa [109], which is an individually controllable micro-shutter with microscopic windows that open and close electrostatically to pass or block light. As this is a very new technology, the costs are still high, the operating temperature range is limited and the robustness is not yet clear. This is a barrier to commercialization in the near future. For this reason, LC panels may play an irreplaceable role for local filters in the next years.

5.2 Space-Division Multiple Access with Matrix Headlights

An advantage of V-VLC is that existing vehicle lighting hardware can be utilized to communicate in addition to illumination and signaling. As a result, the communication characteristics are also directly dependent on the characteristics of the vehicle lighting. Therefore, the low-pass behavior of the LEDs has an effect [67] on the usable bandwidth, and additionally, the safety regulations that determine the shape of the radiation characteristics [110] also have a direct influence on the received signal strength [22], [111]. As a result, the resources available for communication are limited and must be used as efficiently as possible. One way to use communications resources with high efficiency is to use spatial multiplexing and beamforming.

In recent years, the use of LEDs made it possible to implement many other new improvements in vehicle lighting technology in addition to communication. By using a multitude of LEDs in an array or matrix, which can be controlled individually, advanced AFS has become possible [112]. AFSs enable the targeted emission of light into areas where it is needed. Thus, the center of the light will follow the curve when passing through a curved road. At the same time, light is dimmed adaptively, firstly to avoid glare for other road users and secondly to avoid glare from reflections of road signs, for example. Due to the individual control and the sharply separated beam characteristics of the individual LEDs, AFS are very promising for spatial multiplex technologies in the context of V-VLC.

A conceptual demonstration using a high-end matrix LED spotlight Spatial Multiplexing is presented and examined in the next sections. Furthermore, the increased efficiency by SDMA is shown, which reduces multiple-user-interference by implementing multiple physical channels.

5.2.1 Background and Related Work of VLC-MIMO Systems

Since VLC is very attractive for the use of multiple transmitters and receivers, MIMO has often been considered in the domain of VLC. Luo, Ghassemlooy, et al. [113] investigated the increase in bandwidth efficiency by using two headlights as the signal source for vehicle-to-vehicle communication. In this analytical investigation, a model was used that consists of LOS and NLOS components, where the reflections of the NLOS component were assumed to be purely Lambertian. Monte Carlo simulations show that certain mounting heights of photodiodes reach data rates of 40 Mbit/s over a distance of 40 meters.

Turan, Ucar, et al. [114] used transmitter diversity to increase communication reliability. They used two fog lights, which were modulated with the same signal,

and a single photodiode as the receiver. A field test showed the increase of PDR for short distances, but a decrease due to interference at higher distances.

Narmanlioglu, Turan, et al. [65] investigated the feasibility of a MIMO system in an empirical study using multiple LED taillights as transmitters and multiple photodiodes as receivers mounted near the headlights of the following vehicles. The BER can be improved by MIMO dependent on the scenario and modulation order. However, using all LEDs was not necessarily the best solution when they compete for performance.

In contrast to the previously mentioned approaches, which rely on photodiodes as receivers, there are also several approaches that use camera sensors as receivers [115]. Usually, one camera sensor is used instead of several photodiodes and image processing algorithms are used to differentiate between transmitter sources [116]. For example, Goto, Takai, et al. [100] were able to prove the feasibility of such an approach by modulating a 4x5 LED array with the same OFDM signal for each LED and receiving the signal with a high-speed camera sensor specially designed for optical communication. A disadvantage of such a system is certainly the cost, but he was able to demonstrate a data rate of 54 Mbit/s in a laboratory environment.

In contrast, Luo, Zhang, et al. [117] showed a study with a system that did not rely on local separation but separation by wavelength on the one hand and on the other hand get along with a camera sensor with a standard frame rate by using a single RGB-LED. However, vehicle lighting generally does not use RGB LEDs, but phosphorus converted blue LEDs for front lighting and red LEDs for rear lighting.

In Section 5.1 and in [25] we presented an LC-based local filtering receiver, which can reduce interference and ambient light to a minimum by optical filtering.

While the studies mentioned above primarily focus on increasing date rate or reliability by MIMO, in the following we mainly investigate the use of Spatial Multiplexing (SM) to achieve the reduction of interference. In contrast to modulating multiple modules [65], [114] we modulate single LEDs in the following.

Where SM with the driving of single LEDs achieves a higher granularity than the use of single modules as in [65], [114].

By combining this with the sharply separating optics of a matrix headlight, this represents a novel implementation of spaital multiplexing for VLC, which was first presented in publication [26] the following chapter is based on.

5.2.2 Spatial Multiplexing with Matrix Headlights

The strong penetration of LEDs as light sources has also found its way into vehicle lighting and fundamentally changed it. LEDs are robust enough to last a vehicle's life, they are efficient and achieve high luminous intensity with small dimensions.

Adaptive headlights or AFS are enabled by quickly and individually controllable LEDs. This allows optimized illumination of the road for every driving situation. Among other things, glare-free high beam is even possible, in which the high beam is always on and individual channels are dimmed by controlling individual LEDs so as not to glare other road users.

A particularly advanced AFS is the Hella HD 84, in which 84 individual LEDs are arranged in a matrix and can be controlled individually. This high number of individually controllable LEDs results in a very high degree of freedom, which helps to optimize the beam pattern best suited to the situation. Thus, with a very high angular resolution, individual areas can be illuminated more or less strongly. To illustrate the difference to a traditional headlamp with high beam and low beam, the beam characteristics for a traditional static high beam and low beam as well as the beam characteristics of two neighboring LEDs (48 and 49) of the HD 84 are shown in Figure 5.10 as an iso-candela plot. In an iso-candela plot, levels of equal luminous intensity are represented by a line, where a blue line represents low intensity and a red line represents high intensity. The high beam has the highest intensities near the center and in addition, has high intensities above 0°. This means that the high beam reaches high illuminance densities even in the far central area in front of the vehicle.

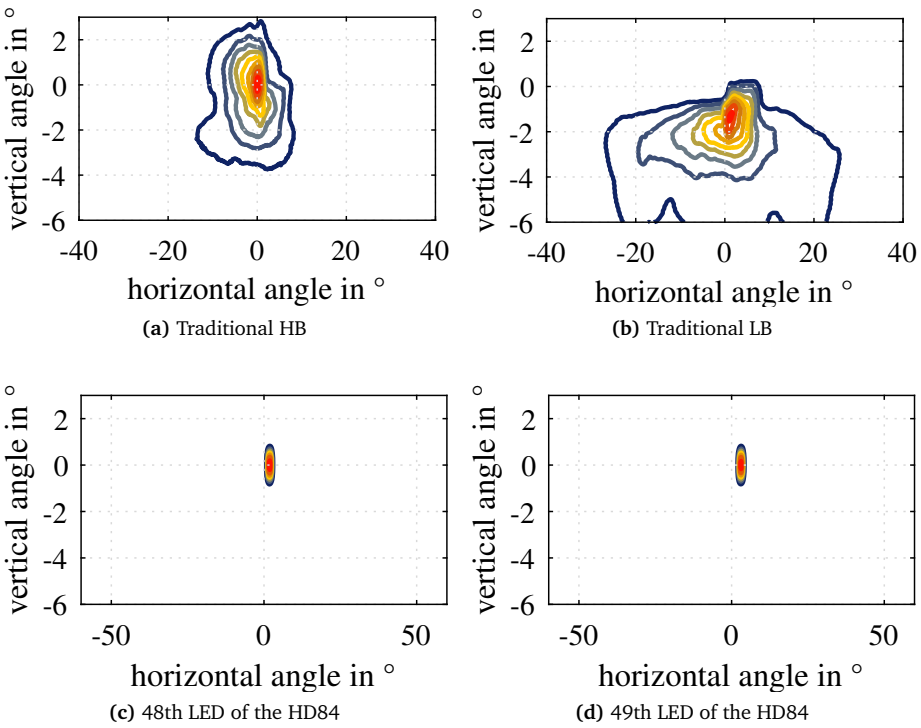

(a) Traditional HB **(b)** Traditional LB

(c) 48th LED of the HD84 **(d)** 49th LED of the HD84

Figure 5.10 – Isocandala pattern of different headlights; the red and blue colors represent high and low luminous intensities respectively. (Reproduced from [26], © 2019 IEEE.)

The low beam, on the other hand, has been optimized to illuminate your own road without glare to oncoming traffic. This results in an asymmetrical distribution with a sharp cut-off line. In contrast, the radiation characteristics of the LEDs of the HD 84 show strong intensities in a very small angle, which is different for each LED. This means that a single LED emits a high light intensity at a fixed solid angle and only a very small portion is scattered into other areas. By controlling multiple LED in combination, similar light distributions as for low beam and high beam can be achieved, but additionally, with a high degree of freedom, the light distribution can be optimized dynamically.

The LEDs are arranged according to Figure 5.11. The 84 LEDs are arranged in 3 rows. 30 LEDs in the bottom row are located above 28 or 26 LEDs in the top row. This arrangement was chosen because a wider illumination is useful at low vertical angles than at high vertical angles.

SM is a key to higher bandwidth efficiency in radio communications, several antennas or even antenna arrays are used to influence the direction of radiation. This allows resources in bandwidth and frequency to be reused and multi-user interference to be avoided. SM is also very attractive for light-based communication, which is due to the directionality of light and the fact that many LEDs are often already implemented for the lighting task and have sharply separated radiation patterns using special optics so that there is little local channel correlation. Especially the connection between matrix headlamps and SM is promising because the requirements of the AFS function on the headlamp harmonize with the requirements of SM, which are sharply separated channels that can be controlled according to the desired beam angle. Different from radio communication, the channel can be modulated much easier because in most cases the LOS component dominates and reflection can be neglected. Therefore the selection of the LED can be implemented by a geometrical consideration. This can eliminate the need for Channel State Information (CSI), resulting in less overhead and feedback. However, in this case, the exact positions between receiver and transmitter are necessary. In modern vehicles, this can often be determined precisely by Radio Detection and Ranging (RADAR), LiDAR, cameras, or by the communication itself.

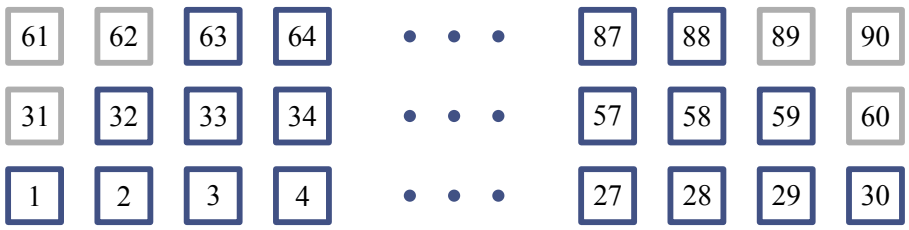

Figure 5.11 – Arrangement and the corresponding ID of the HD84 Matrix LEDs. (Reproduced from [26], © 2019 IEEE.)

5.2.3 Controlling the LED Matrix

When using a high-resolution matrix headlight system for SM, it is essential to modulate the right LED at the right time with the signal. This LED will be called optimal LED in the following. For our approach, we suggest modulating only the LED which causes the highest signal strength at the receiver. This LED will be chosen in the later application by the relative position and the resulting optimal LED, which has been calculated by pre-processing.

In our case, the relative position is determined by a camera system. For this purpose, we use the system of Hella Aglaia Mobile Vision GmbH, which is often integrated into vehicles with AFS. This approach allows a low-cost implementation, while the hardware is already integrated and saves overhead compared to a system with RSS feedback. Which LED causes the highest RSS depending on the angle can be determined in pre-processing by the model from Section 3.1 and optical simulations which determine the LED specific radiation characteristic of the HD 84.

If the headlight and receiver unit are at the same height, the dependence between relative angle and optimum LED is very simple. The optimal LED is always located in the middle row of LEDs and as the angle increases, so does the LED identification number, cf. Figure 5.12a. If the transmitter and receiver are at different heights, as shown in Figure 5.12b, there is also a dependency on distance in addition to the angle dependency. The example shows a headlight height of 65 cm and a receiver height of 20 cm, which corresponds to the minimum permitted mounting height of a license plate, i.e. a height difference (Δh) of 20 cm. Up to a distance of 46.9 m, the LEDs in the lowest row produce the highest signal strength, while for longer distances the middle row is optimal. This means that from a distance of 46.9 m on, the behavior of the two cases is the same as shown in Figure 5.13.

The selection of the optimal LED can be implemented with a simple controller using the following methods. A look-up table can be stored, which contains the

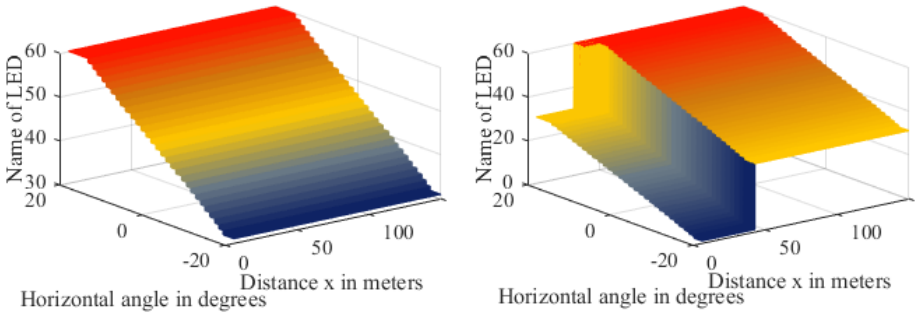

(a) PD and light source at same hight **(b)** light source 45 cm higher than PD

Figure 5.12 – Optimal LED in dependence of angle and distance. (Reproduced from [26], © 2019 IEEE.)

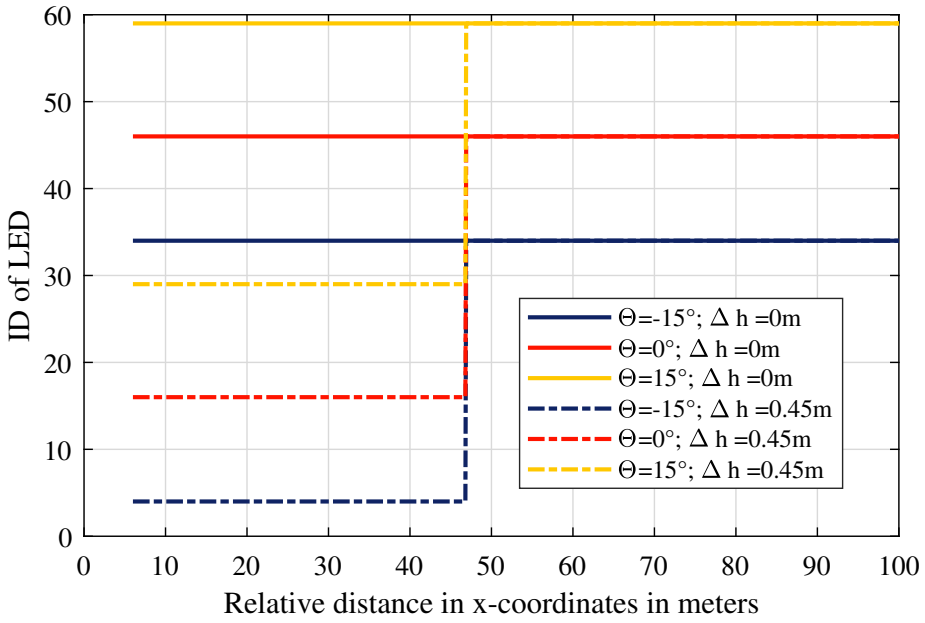

Figure 5.13 – Optimal LED depending on angle and distance for different heights between RX and TX. (Reproduced from [26], © 2019 IEEE.)

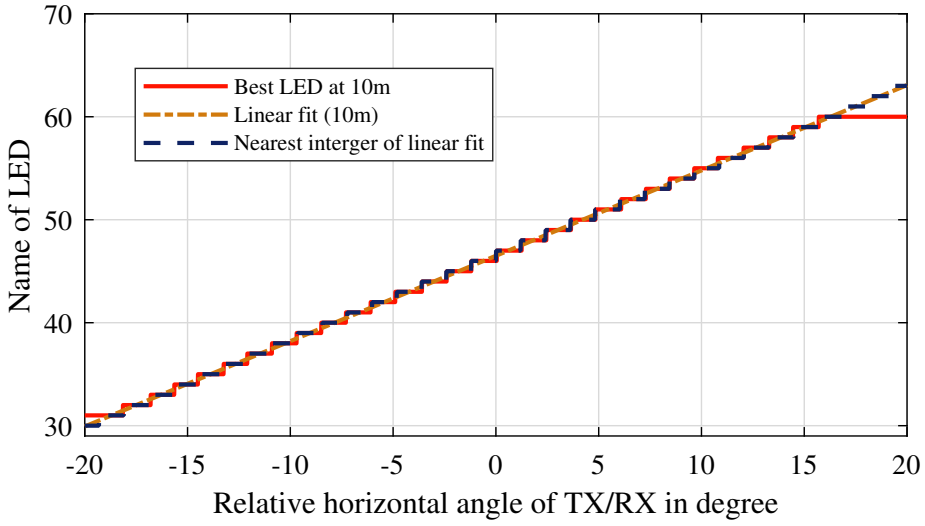

Figure 5.14 – Angular dependency of the optimal LED at a distance of 10 m. (Reproduced from [26], © 2019 IEEE.)

optimal LED for each position. Alternatively, the behavior can be described by a function. Since the relationship between the relative angle and the optimum LED is largely linear in the case that RX and TX are at the same level, a partially linear function is sufficient.

$$\text{LED} = \begin{cases} 32 & \text{for } \phi < -19° \\ \lfloor 0.829 \times \phi + 46.498 \rceil & \text{for } -19° \leq \phi \leq 16.5° \\ 59 & \text{for } \phi > 16.5° \end{cases} . \tag{5.4}$$

This function consists of three ranges, for angles smaller than −19° the LED furthest left is the optimum LED, for larger angles than 16.5° the LED far right is the optimum LED and in between the optimum LED is defined by the linear function. Figure 5.14 shows that the function corresponds very well with the optimal LED from the preprocessing so that the simplified representation employing a function does not result in a significant error.

However, this simple function only applies if the transmitter and receiver are at the same height; for other heights, either a more complex function or a larger look-up table would have to be used. Figure 5.12b gives an impression that even this complexity is manageable. Alternatively, several LEDs can be modulated simultaneously, so that instead of a single LED, whole columns can be switched to compensate for the height difference.

5.2.4 Evaluation

In order to investigate the effect of SDMA using matrix headlamps, the model from Section 3.1 is utilized and modified to take multi-user interference into account. The photometric radiation characteristics and the real specifications of the components are taken into account to calculate signal strengths and BER. The simulation parameters from Table 5.4 are applied for this analysis. In this case, the radiation characteristics are created by optical ray-trace-based simulations. For this purpose, over 25 million beams were simulated in the model of the HD 84. Even with this high number, the number is still finite, which results in areas with a signal strength of zero, since not a single ray hits the area under consideration. In reality, it can be assumed that this area does reach some light but has very low signal strength or illumination.

5.2.5 Channel Matrix for a Static Two-Lane Scenario

P-matrices are particularly suitable for evaluation in a two-lane scenario as it is shown in Figure 5.15. A P-matrix consists of several elements P_{ij}, each containing

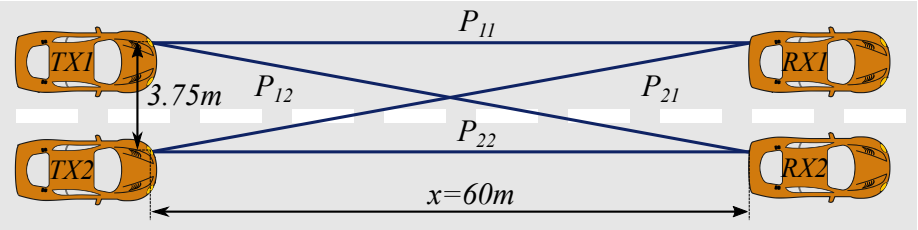

Figure 5.15 – Two lane scenario. (Reproduced from [26], © 2019 IEEE.)

the RSS for a specific connection.

$$\boldsymbol{P} = \begin{bmatrix} P_{11} & P_{12} \\ P_{21} & P_{22} \end{bmatrix}. \tag{5.5}$$

A P-matrix has elements on the diagonal which contain the communication to the vehicle in front on the same lane, compare P_{11} and P_{22}. Above the diagonal are the connections to vehicles driving further to the right (P_{12}) and below the diagonal to vehicles driving further to the left (P_{21}).

A large value of an element P_{ij} indicates that a lot of signal strength arrives at the receiver via this connection. A small value of P_{ij} means a low signal strength, which is desirable in case of interference. An ideal P-matrix, therefore, has a large value for the connection to the desired communication partner and as small values as possible for all other elements.

In the following, the P-matrices are examined for a distance (x) of 60 m. For the high beam, P_{HB} was calculated (compare Equation (5.6)). In this matrix, the elements on the diagonal are the largest. This means that the strongest signal strength in vehicles is achieved centrally in front of the transmitter. On the lanes to the left and right of the transmitter, about 10 dB less RSS is reached. Since the high beam is not adaptive, the P-Matrix is static and cannot be further adapted to communication. This is also the case with the low beam (Equation (5.7)), which achieves lower signal strengths overall and the highest signal strength on the right

Table 5.4 – Simulation parameters (Reproduced from [26], © 2019 IEEE.)

TX height	65 cm
RX height	65 cm
PD type	Thorlabs PDA100A
PD active area	10 mm × 10 mm
PD gain	0.75×10^3 V/A
Bandwidth	2 MHz
Illuminance of the sun	100 klx
Thermal noise	−58.893 dBm
Rays in optical simulation	25 484 095

lane. This is caused by the asymmetrical radiation behavior and has already been discussed in [111] and Section 3.3.

In contrast, the Matrix headlamp can be controlled adaptively for the communication task. For the scenario of several lanes in 60 m distance LED 46, 44, and 49 were calculated as optimal LEDs. LED 46 is the optimum LED for communication with a vehicle driving centrally in front. This is clearly shown by the fact that strong signal strengths are found on the diagonal of the P-matrix while the values off the diagonal are very low, cf. Equation (5.8). LED 44 is the optimal LED to communicate to a vehicle on the left lane at a distance of 60 m, because the element P_{21} is large and the other elements of the matrix are small, corresponding to Equation (5.9). LED 49 is the optimal LED to establish a communication link to a vehicle on the right lane at a distance of 60 m because element P_{12} is large and all other elements are low, as it is shown in Equation (5.10). In all three P matrices, the elements except the one corresponding to the communication partner are so low that they fall below the noise floor. This means that multi-user interference can be almost completely eliminated.

$$\boldsymbol{P}_{HB} = \begin{bmatrix} -41\,\text{dBm} & -53.7\,\text{dBm} \\ -47.2\,\text{dBm} & -41\,\text{dBm} \end{bmatrix} \tag{5.6}$$

$$\boldsymbol{P}_{LB} = \begin{bmatrix} -88\,\text{dBm} & -54.2\,\text{dBm} \\ -88.9\,\text{dBm} & -88\,\text{dBm} \end{bmatrix} \tag{5.7}$$

$$\boldsymbol{P}_{46} = \begin{bmatrix} -39.9\,\text{dBm} & 0 \\ -126.8\,\text{dBm} & -39.9\,\text{dBm} \end{bmatrix} \tag{5.8}$$

$$\boldsymbol{P}_{44} = \begin{bmatrix} -120.7\,\text{dBm} & -137.3\,\text{dBm} \\ -39.7\,\text{dBm} & -120.7\,\text{dBm} \end{bmatrix} \tag{5.9}$$

$$\boldsymbol{P}_{49} = \begin{bmatrix} -126.8\,\text{dBm} & -39.5\,\text{dBm} \\ -118.5\,\text{dBm} & -126.8\,\text{dBm} \end{bmatrix} \tag{5.10}$$

5.2.6 Dynamic Two-Lane Scenario

For vehicle communication, usually dynamic channels occur, therefore in further investigation the dynamic behavior is analyzed, which occurs when the distance of the vehicles varies. The same scenario as in Figure 5.15 was used for this purpose, but the parameter of distance x varies. It is assumed that *TX2* communicates to *RX1* while *RX2* is interfered by this transmission. The HD 84 is used, selecting the optimum LED for each position, as shown in Figure 5.16. The high beam, which is not adaptively switched, is used as a reference. The achieved RSS, the interference

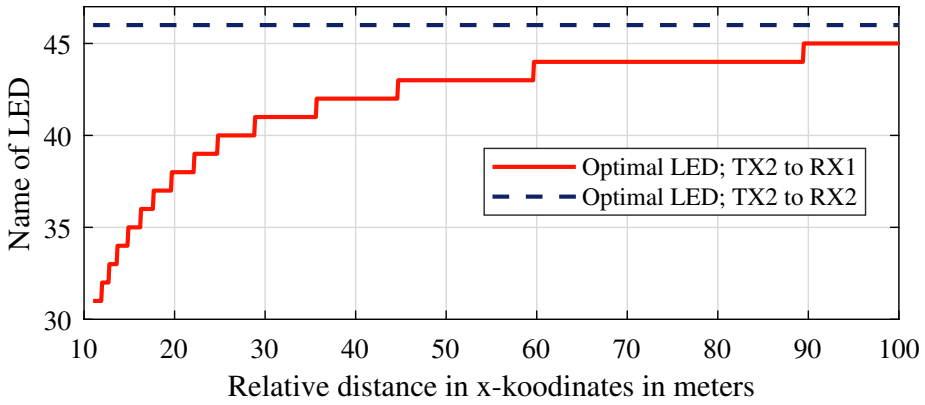

Figure 5.16 – The optimal LED for the dynamic two lane scenario. (Reproduced from [26], © 2019 IEEE.)

power, as well as the BER under consideration of noise and multi-user interference are evaluated.

Signal and Interference Power in a Dynamic Two-Lane Scenario

Figure 5.17 shows the RSS at *RX1* and the received interference power at *RX2* plotted over the distance x for the two headlights. The high beam shows a very high interference power. In fact, it is higher than the signal power of the high beam. This is since the high beam cannot be controlled adaptively and higher intensity is achieved in the center of the light distribution than on the left lane. Even if the receivers change roles and the useful signal is applied to *RX2* and the interference to

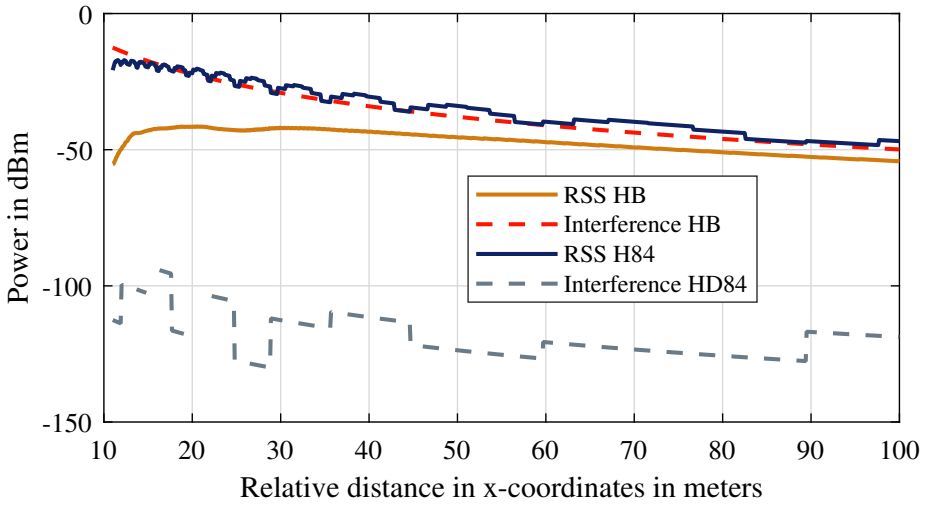

Figure 5.17 – Signal and interference power of the HB of HD84 in the two-lane scenario. (Reproduced from [26], © 2019 IEEE.)

RX1, there would still be a large influence of the interference since the signal and the interference power are relatively close to each other.

The interference power shows completely different behavior when using the HD 84 with SDMA. The optimum LED was used at all times, as shown in Figure 5.16. The interference power is very low, in the range of −100 dB, so that it is below the noise power of −58.893 dB and can usually be neglected. The signal power, on the other hand, is very high with the HD 84, and even on the adjacent lane, it is approximately equal to the signal power of the high beam in the center. This results in a high signal power on the one hand and a low interference power on the other hand. This means a high Signal-to-Interference-and-Noise Ratio (SINR) can be expected, resulting in reliable and well-performing communication.

Bit Error Ratio in a Dynamic Two-Lane Scenario

With the signal strengths calculated as mentioned above and with the addition of a noise model as presented in Section 3.4.1, the SINR can be determined. In this case, the thermal noise ($\sigma_{thermal}$) is the value from the datasheet of the photodiode Thorlabs PDA100A Table 5.4. The shot noise (σ_{shot}) is calculated according to Equation (3.9). This gives the SINR as

$$SINR = \frac{S}{\sigma_{thermal} + \sigma_{shot} + I} \,. \tag{5.11}$$

with the interference power (I) and es the signal strength (S). With the SINR, the analytical calculations for error probabilities according to the formulas Equations (3.11) and (3.12) can be performed. This shows the geometric dependence of the expected error probability.

Figure 5.18a shows the BER of the high beam over the distance x between transmitter and receiver. Since the interference power is high, no useful communication is possible. The BER decreases with increasing distance. The reason for this is that the interference power decreases faster than the signal power over the distance because the receiver vehicle reduces the relative angle to the transmitter with increasing distance and thus moves into the range of higher luminous intensity of the high beam. Nevertheless, the BER over the entire distance remains in a range that excludes meaningful communication.

When using the matrix headlight, as shown in Figure 5.18b, completely different behavior can be observed. Especially for small distances, the strong signal power in relation to low interference and noise power causes very low error probabilities.

With increasing distance, however, the signal strength decreases with the inverse square law of distance. This causes the SINR to decrease and thus the BER to increase. Nevertheless, the communication with the Matrix Searchlight and OOK

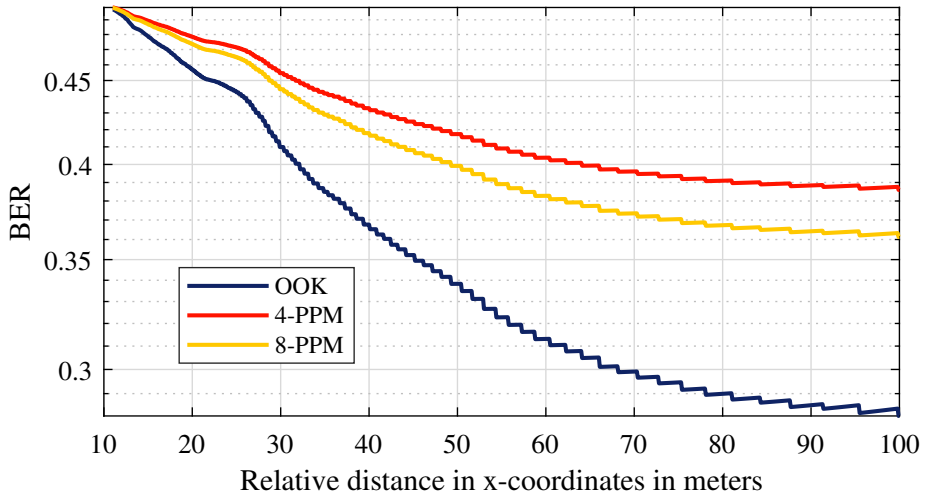

(a) BER curves for the HB over the distance

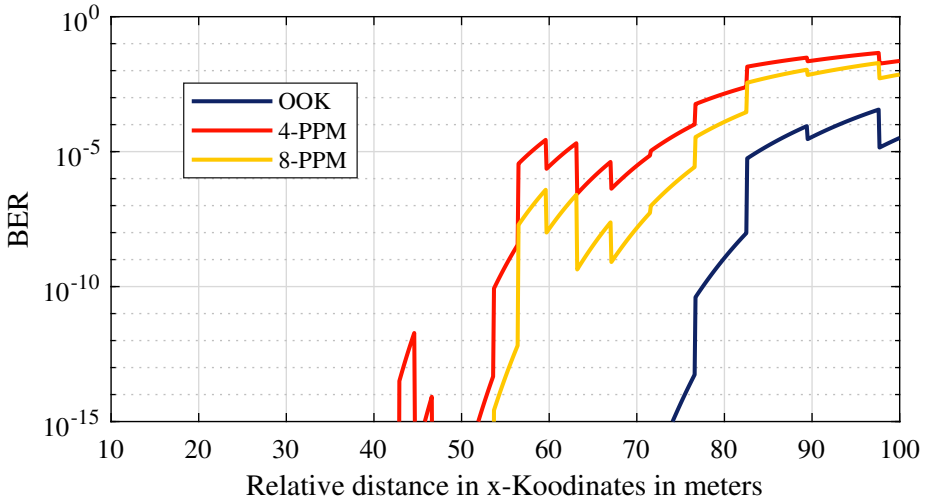

(b) BER curves for the HD84 headlight over the distance

Figure 5.18 – BER curves. (Reproduced from [26], © 2019 IEEE.)

reaches a low BER of less than 10^{-6} over a distance of 60 m. A further increase of the communication distance would be possible by a receiver optic as it was shown in the field test in Chapter 4.

The strong fluctuations in Figure 5.18b are due to the following causes. The step-like behavior results from the relatively coarse resolution of 0.2° that was selected for the HD 84 in the optical simulation. This choice was made to increase the accuracy in the areas of low illumination. The fluctuations with a longer period are caused by switching between the optimal LEDs, as these have the maximum in the center, drop off from the center and overlap a little (compare Figures 5.10c and 5.10d). One consideration would be to modulate two neighboring LEDs simultaneously with the signal to avoid fluctuations in signal strength even in the transition area. These influences can also be observed in Figure 5.17 but in a less pronounced form. It is also important to note that the graph is plotted on a logarithmic scale so that small deviations are clearly visible in the graph but do not necessarily have a large effect in reality. Overall, we concentrated on the noise which is caused by the first stage and consists of shot noise and thermal noise. In reality, noise sources of the following stages such as quantization noise of the ADC must also be considered. However, since these depend very much on the choice of hardware, we have not considered them in detail. On the other hand, the choice of hardware can further improve the communication, for example by signal amplifying optics and optical filtering, cf. Section 5.1. Furthermore, error-correcting codes can further reduce the BER. These methods can also be used to achieve larger communication distances and data rates.

5.2.7 Conclusion of SDMA based on AFS

In summary, SDMA based on AFS can dramatically improve the reliability of V-VLC by exploiting the selective driving of LEDs arranged in a matrix and the corresponding optics. Multi-user interference is minimized already at the transmitter by the fact that the signal is solely emitted in a small angular range, which allows other communication partners to achieve interference performance at the noise level. It has been shown that this method could increase the SINR elementary. This feature allows multi-user access in the spatial domain. On the one hand, this saves valuable communication resources such as bandwidth or time slots, which have to be expended in traditional multi-user access methods such as TDMA, CDMA or FDMA. This increases bandwidth efficiency. On the other hand, lightweight protocols become possible, as there is no need to coordinate resources of frequency bands, codes, or time slots. The very targeted transmission of data with a small angular range further increased the security level of the communication, which is already at a high level with VLC. This could be very attractive for the exchange of keys, for example.

Chapter 6

Conclusion

In this thesis, a step towards the feasibility of V-VLC was taken. First, challenges were analyzed and fundamental limits were determined by developing an analytical model. To solve the challenges, different approaches were investigated, implemented, and evaluated with prototypes. Field tests showed the general feasibility but also limits and potential for improvement.

The limited bandwidth of Intensity Modulation (IM) associated with the use of Commercial Off-The-Shelf (COTS) light sources from automotive applications was identified as a challenge. As a solution, slight adjustments were made to the LED boards and a linear and broadband driver was developed that can drive the relatively high power of a headlight while providing bandwidth-efficient modulation. The resulting driver is published as open-source to drive the development of advanced Visible Light Communication (VLC) systems, cf. Section 2.2.4.

The strict regulations of vehicle lighting are a further challenge for Vehicular Visible Light Communication (V-VLC). Especially the specified radiation characteristics determine the maximum achievable signal strengths. Within the scope of this thesis a model was developed which analytically calculates the local distribution of signal strength, channel capacity and with the corresponding Modulation and Coding Schemes (MCS) the error probability in dependence of real radiation characteristics, cf. Section 3.1. These calculations allow determining theoretical limits of V-VLC. For instance, the maximum possible data rates at a location can be determined as a function of the light distribution of a real headlamp. Additionally, a variety of effects such as pitching caused by braking can be investigated. Different light functions such as low beam, high beam, or the adaptive matrix light can also be compared and it can be weighed up which light function is useful for a specific application. The analytical model has been validated extensively and repeatedly in different scenarios. This analytical model was included in the open-source simulator VEINS [69] as the extension VLC-VEINS. This integration allows the large feature set of VEINS,

which includes network simulation based on OMNeT++ [70], road traffic simulation based on SUMO [71], and a large set of IVC models, to be used in the context of V-VLC. Even the investigation of concrete applications of connected vehicles such as platooning on a large scale are enabled. The simulation tool also supports the investigation of heterogeneous communication as a particularly interesting field for future studies. First studies show that heterogeneous communication is very promising for the networking of vehicles. Essentially, the disadvantages of the individual technologies and such as limited range for V-VLC or limited scalability for 802.11p can be compensated by the other communication, resulting in a very reliable and high-performance communication. Thus Schettler, Memedi, and Dressler [16] could show that in the case of platooning the combination of 802.11p and V-VLC increases the reliability of the application.

Using software-defined radios and a VLC driver allows to create very flexible prototypes for the communication with COTS vehicle light sources. Based on the GNU Radio implementation of 802.11 a/b high-performance OFDM transmission of more than 72 m was achieved in a field test, cf. Chapter 4. The high flexibility allows modulating a variety of light sources like low beam, daytime running light, brake light, or matrix headlights with a broad spectrum of modulation schemes like Pulse Position Modulation (PPM), Phase-Shift Keying (PSK), On-Off Keying (OOK) or Orthogonal Frequency Division Multiplexing (OFDM). A large variety of communication technology methods, such as equalization, synchronization, or diversity combining, can be flexibly introduced into the transmission chain, thus enabling further investigations and improvements.

V-VLC has a major advantage due to the propagation properties of light, which results in low multi-user interference and therefore high scalability so that reliable communication is possible even in dense traffic scenarios. However, interference is not negligible. Other communication sources as well as modulated light sources for dimming purposes can interfere with communication and cause high data loss. For this purpose, a novel spatially filtering receiver was designed, prototyped, and evaluated, cf. Section 5.1. By this design, interference could be reduced by more than 12 dB even in challenging scenarios.

Another measure to reduce multi-user interference is achieved by applying Space-Division Multiple Access (SDMA) with the utilization of matrix headlights, cf. Section 5.2. By the selective control of single LEDs of a modern matrix headlamp, the signal propagates in a sharply limited and defined solid angle. Other solid angles are not modulated with the information and can either remain unmodulated or be modulated with information for another receiver. By this method, the multi-user interference is reduced to a level that is lower than the noise level. For an advanced two-track scenario, the signal-to-interference ratio is in the range of 80 dB. This allows bandwidth-efficient communication that does not suffer from a reduced usable

data rate due to methods like Frequency Division Multiple Access (FDMA), Code Division Multiple Access (CDMA) or Time Division Multiple Access (TDMA). When utilizing the sensor data available in the vehicle, the allocation of communication resources can take place without additional overhead or a centralized unit. In addition, very secure communication is possible, which is robust against eavesdropping, since the information is only available in a very limited local area.

In summary, the hypothesis of achieving V-VLC feasibility can be answered based on the specific goals.

- **Communicate over a typical distance occurring in traffic of 50 m with a bit error probability of less than 10^{-6}.**
  First, based on the radiation pattern of a real headlamp and the corresponding Received Signal Strength (RSS) in Section 3.4.3, the theoretical feasibility of a bit error rate below 10^{-6} over the distance of more than 50 m was shown analytically even without the utilization of any receiver optics. In Chapter 4, a stable communication link, which fulfills the BER-requirement was calculated over the entire measured distance of more than 72 m based on the measured RSS with a dependency on the used MCS. Furthermore, a PDR of over 95% was shown over a distance of 59 m with real transmitted data.

- **Achieve a data rate that can send all vehicle data relevant to cooperative driving with a sufficient update interval.**
  In Section 3.4.2, the maximum achievable data rate was determined in detail in the form of the channel capacity, which strongly depends on the positioning between transmitter and receiver. This observation was confirmed in field tests. In the field tests, a data rate of 150 kbit/s was measured at a distance of 72 m. Data rates of up to 8.1 Mbit/s were achieved with the setup. It should be noted that the development of the prototype does not focus on a high data rate but on the use of application-oriented hardware. In combination with the opportunity of a lean protocol with little overhead, the possibility of sending simple vehicle data, such as speed, direction, and position over common vehicle distances is therefore offered. Over short distances or with the implementation of further improvements, the transmission of more complex data, such as raw sensor data, is achievable.

- **Performing the communication task while maintaining the main task of vehicle illumination and meeting acceptable component cost.**
  The prototype shown in Chapter 4 is based on a series headlight. In order to achieve linear modulation over a wider bandwidth, capacitors were removed and a driver was developed which uses exclusively components that are within the usual cost range for automotive electronics components. However, to achieve the flexibility needed for research purposes, USRPs were used for

signal processing, which would currently exceed the cost of a series application. This could be solved by performing signal processing on Application-Specific Integrated Circuits (ASICs), which can be produced for reasonable costs, if sufficient quantities are requested, or by integrating the VLC signal processing as an additional function into an existing Telematic Control Unit (TCU) and thus benefiting from synergies with other communication technologies. In addition, a trend of lower-cost SDRs can be observed, which may also allow the application of V-VLC in series production in the future.

- **Robust communication in real traffic scenarios.**
  During the dissertation, robust indoor and outdoor V-VLC with realistic distances and environments were successfully performed. However, sources of interference were identified, which can negatively impact communication. Perhaps the most obvious source of interference is the saturation due to the very high intensity of the sun, which was solved by optical concepts and high-pass filters. Furthermore, multi-user interference and Power Width Modulation (PWM) modulated light sources were identified as sources of interference. Possible solutions to avoid these sources of interference were presented in Chapter 5. These results indicate robust communication in real traffic scenarios, but extended test drives are necessary to sufficiently consider the numerous influencing factors such as region, environment, or dynamics with many participants.

This gain in knowledge allows a broad variety of applications to be enabled by V-VLC in the future. For a broad application, further steps are necessary. These steps contain standardization, cost reduction, for example by using ASICs, and consideration of the communication task as an additional function of the light modules already at the design phase instead of a modification. This includes using fast switching drivers, reserving power when selecting the Light Emitting Diodes (LEDs) to have more freedom for dimming, avoiding parasitic capacitors and inductances.

Many technologies can be transferred from the RF domain to V-VLC. Thus MCS can be utilized with just minor modifications, also technologies like Multiple-Input Multiple-Output (MIMO) or diversity combining are possible. Transferring these methods offers a lot of room for further improvements. However, to exploit the full potential of V-VLC, it is particularly important to take advantage of the special features of VLC. These are based especially on the propagation of light. 5.1.5 gives an impression of the importance of receiving optics. Precise shaping of light allows precise reception characteristics to be created to allow even adaptive local reception characteristics. Also, a combination of VLC specific properties and state-of-the-art Radio Frequency (RF) technologies is very promising and worth looking into in detail in the future. Several receivers could be combined via diversity combining.

This would allow by the combination of optics with high Field of View (FoV) and optics with strong concentration to enable communication in a wide near field as well as for a long distance. A closer look at the possible sources of interference can also bring further advantages. For example, characteristic PWM signals, which are usually characterized by a square wave signal, could be detected and suppressed to achieve higher robustness against artificial light sources.

In terms of hardware, improving the receiver side offers further potential. An AGC stage could show improvements by compensating the dynamic range of the received signal strength by an adaptive gain, thus utilizing the ADC more effectively, which would lead to lower quantization noise.

This work was able to show the feasible use of V-VLC in static realistic scenarios. First, dynamic drives have already been performed by Shen and Tsai [92]. To identify any unexpected sources of interference and to better examine the influence of dynamic channels, large-scale dynamic test drives must be carried out in addition to simulations. This is the only way to ensure that the high demands on the reliability of communication are fulfilled in all situations.

The gain of a combination of radio and light combination could already be shown simulatively. For the practical implementation of the combination of the two technologies, the potential for optimization is high. The most straightforward implementation is a redundant use of the technologies. A fallback level is also conceivable; thus VLC can be used as the default communication to keep the load on the radio channel low. If the VLC channel fails, for example, due to obstruction, the less loaded radio channel is available. More advanced systems could already consider the different channels during Forward Error Correction (FEC) and divide the redundancy of the information according to the available data rates of the channels. This can allow the reconstruction of the information even in cases where both channels are disturbed. At the same time, resources are fully utilized. These ideas should first be tested in depth analytically and simulatively. Subsequently, practical implementation and testing are particularly of interest in order to discuss the interaction of the multitude of dynamic influencing variables.

All in all, this thesis and many publications have shown that V-VLC has the potential to support vehicular connectivity. For the broad application in the field, further improvements can be achieved as described in this thesis and large-scale simulations and evaluations would be needed to show limits in a fully comprehensive way, but an important next step would be a commitment from industry to use the technology.

List of Abbreviations

ACC	Adaptive Cruise Control
ACO-OFDM	Asymmetrically Clipped Optical OFDM
ADAS	Advanced Driver Assistance System
ADC	Analog-to-Digital Converter
ADO-OFDM	Asymmetrically Clipped DC Biased Optical OFDM
AFS	Adaptive Front-Lighting System
ASIC	Application-Specific Integrated Circuit
AWGN	Additive White Gaussian Noise
BER	Bit Error Rate
BPSK	Binary Phase-Shift Keying
BRDF	Bidirectional Reflectance Distribution Function
C-V2X	Cellular V2X
CAD	Computer Aided Design
CAP	Carrier-less Amplitude Modulation
CDM	Color Domain Modulation
CDMA	Code Division Multiple Access
COTS	Commercial Off-The-Shelf
CPC	Compound-Parabolic-Concentrator
CPM	Collective Perception Message
CSI	Channel State Information
CSK	Color Shift Keying
DC	Direct Current
DCO-OFDM	Direct Current-Biased Optical OFDM
DMD	Digital Micromirror Device
DSRC	Dedicated Short Range Communication
DSSS	Direct-Sequence Spread Spectrum
ECE	Economic Comission for Europe
ECU	Electronic Control Unit
EMC	Electromagnetic Compatibility
ESD	Electrostatic Discharge

ETSI	European Telecommunications Standards Institute
FDMA	Frequency Division Multiple Access
FEC	Forward Error Correction
FFT	Fast Fourier Transform
FoV	Field of View
FPGA	Field-Programmable Gate Arrays
FSK	Frequency Shift Keying
HB	High Beam
HCM	Hadamard Coded Modulation
HNI	Heinz Nixdorf Institut
IM	Intensity Modulation
IM/DD	Intensity Modulation and Direct Detection
IR	Infrared
ITS	Intelligent Transportation System
IVC	Inter-Vehicle Communication
L-PPM	Pulse Position Modulation
LACO-OFDM	Layered ACO-OFDM
LC	Liquid Crystal
LC-Rx	Liquid Crystal based Optical Receiver
LED	Light Emitting Diode
LiDAR	Light Detection and Ranging
LiFi	Light Fidelity
LOS	Line of Sight
MAC	Medium Access Control
MCM	Multicarrier Modulation
MCS	Modulation and Coding Schemes
MIMO	Multiple-Input Multiple-Output
mmWave	Millimeter-Wave
MOSFET	Metal-Oxide-Semiconductor Field-Effect Transistor
NLOS	Non Line Of Sight
OFDM	Orthogonal Frequency Division Multiplexing
OOK	On-Off Keying
OWC	Optical Wireless Communications
PAM	Pulse Amplitude Modulation
PD	Photo-Detector
PDP	Power Delay Profile
PDR	Packet Delivery Ratio
PER	Packet Error Rate
PHY	Physical Layer
PPM	Pulse Position Modulation

PSK	Phase-Shift Keying
PWM	Power Width Modulation
QAM	Quadrature Amplitude Modulation
QPSK	Quadrature Phase-Shift Keying
RADAR	Radio Detection and Ranging
RF	Radio Frequency
RGB	Red-Green-Blue
RLL	Run Length Limited
RMS	Root-Mean Square
RMSE	Root-Mean Squared Error
RS	Reed-Solomon
RSS	Received Signal Strength
RX	Receiver
SAE	Society of Automotive Engineers
SCM	Single Carrier Modulation
SDMA	Space-Division Multiple Access
SDR	Software Defined Radio
SINR	Signal-to-Interference-and-Noise Ratio
SIR	Signal-to-Interference Ratio
SM	Spatial Multiplexing
SNR	Signal-to-Noise Ratio
SUV	Sport Utility Vehicle
TCA	Transconductance Amplifier
TCU	Telematic Control Unit
TDMA	Time Division Multiple Access
TIA	Transimpedance Amplifier
TX	Transmitter
USRP	Universal Software Radio Peripheral
UV	Ultraviolet
V-PPM	Variable Pulse Position Modulation
V-VLC	Vehicular Visible Light Communication
V2I	Vehicle-to-Infrastructure
V2V	Vehicle-to-Vehicle
V2X	Vehicle-to-Everything
VA	Vertical Alignment
VLC	Visible Light Communication
WiFi	Wireless Fidelity
WPDM	Wavelet Packet Division Multiplexing

List of Figures

List of Tables

Bibliography

[1] W. Robertson, "Reducing death on the road: the effects of minimum safety standards, publicized crash tests, seat belts, and alcohol.," *American Journal of Public Health*, vol. 86, no. 1, pp. 31–34, Jan. 1996.

[2] A. T. McCartt and S. Y. Kyrychenko, "Efficacy of Side Airbags in Reducing Driver Deaths in Driver-Side Car and SUV Collisions," *Taylor & Francis Traffic Injury Prevention*, vol. 8, no. 2, pp. 162–170, Jun. 2007.

[3] B. Reimer, "Driver Assistance Systems and the Transition to Automated Vehicles: A Path to Increase Older Adult Safety and Mobility?" *Public Policy & Aging Report*, vol. 24, no. 1, pp. 27–31, Feb. 2014.

[4] A. Linder, A. Kircher, A. Vadeby, and S. Nygårdhs, "Intelligent Transport Systems (ITS) in passenger cars and methods for assessment of traffic safety impact : a literature review," Swedish National Road and Transport Research Institute, Linköping, Sweden, technical report 604A, Dec. 2007.

[5] C. Sommer, R. Krul, R. German, and F. Dressler, "Emissions vs. Travel Time: Simulative Evaluation of the Environmental Impact of ITS," in *71st IEEE Vehicular Technology Conference (VTC 2010-Spring)*, Taipei, Taiwan: IEEE, May 2010.

[6] H. Hartenstein and K. Laberteaux, Eds., VANET - Vehicular Applications and Inter-Networking Technologies, ser. Intelligent Transport Systems. Chichester, United Kingdom: Wiley, 2010, p. 466.

[7] J. B. Kenney, "Dedicated short-range communications (DSRC) standards in the United States," *Proceedings of the IEEE*, vol. 99, no. 7, pp. 1162–1182, Jul. 2011.

[8] X. Wang, S. Mao, and M. X. Gong, "An Overview of 3GPP Cellular Vehicle-to-Everything Standards," *GetMobile: Mobile Computing and Communications*, vol. 21, no. 3, pp. 19–25, Sep. 2017.

[9] B. Toghi, M. Saifuddin, H. N. Mahjoub, M. O. Mughal, Y. P. Fallah, J. Rao, and S. Das, "Multiple access in cellular V2X: Performance analysis in highly congested vehicular networks," in *10th IEEE Vehicular Networking Conference (VNC 2018)*, Taipei, Taiwan, Dec. 2018, pp. 1–8.

[10] M. Gonzalez-Martín, M. Sepulcre, R. Molina-Masegosa, and J. Gozalvez, "Analytical Models of the Performance of C-V2X Mode 4 Vehicular Communications," *IEEE Transactions on Vehicular Technology (TVT)*, vol. 68, no. 2, pp. 1155–1166, Feb. 2019.

[11] J. Heinovski, F. Klingler, F. Dressler, and C. Sommer, "Performance Comparison of IEEE 802.11p and ARIB STD-T109," in *8th IEEE Vehicular Networking Conference (VNC 2016)*, Columbus, OH: IEEE, Dec. 2016, pp. 1–8.

[12] F. Dressler, H. Hartenstein, O. Altintas, and O. K. Tonguz, "Inter-Vehicle Communication – Quo Vadis," *IEEE Communications Magazine (COMMAG)*, vol. 52, no. 6, pp. 170–177, Jun. 2014.

[13] X. Li, R. Zhang, and L. Hanzo, "Cooperative load balancing in hybrid visible light communications and WiFi," *IEEE Transactions on Communications*, vol. 63, no. 4, pp. 1319–1329, Apr. 2015.

[14] M. Ayyash, H. Elgala, A. Khreishah, V. Jungnickel, T. Little, S. Shao, M. Rahaim, D. Schulz, J. Hilt, and R. Freund, "Coexistence of WiFi and LiFi toward 5G: concepts, opportunities, and challenges," *IEEE Communications Magazine (COMMAG)*, vol. 54, no. 2, pp. 64–71, Feb. 2016.

[15] A.-M. Cailean, B. Cagneau, L. Chassagne, V. Popa, and M. Dimian, "A survey on the usage of DSRC and VLC in communication-based vehicle safety applications," in *IEEE 21st Symposium on Communications and Vehicular Technology in the Benelux (SCVT 2014)*, Delft, Netherlands: IEEE, Nov. 2014, pp. 69–74.

[16] M. Schettler, A. Memedi, and F. Dressler, "Deeply Integrating Visible Light and Radio Communication for Ultra-High Reliable Platooning," in *15th IEEE/IFIP Conference on Wireless On demand Network Systems and Services (WONS 2019)*, Wengen, Switzerland: IEEE, Jan. 2019, pp. 36–43.

[17] M. Giordani, A. Zanella, and M. Zorzi, "Millimeter wave communication in vehicular networks: Challenges and opportunities," in *6th International Conference on Modern Circuits and Systems Technologies (MOCAST 2017)*, Thessaloníki, Greece: IEEE, May 2017, pp. 1–6.

[18] L. Cheng, W. Viriyasitavat, M. Boban, and H.-M. Tsai, "Comparison of Radio Frequency and Visible Light Propagation Channels for Vehicular Communications," *IEEE Access*, vol. 6, pp. 2634–2644, May 2018.

[19] M. Uysal, Z. Ghassemlooy, A. Bekkali, A. Kadri, and H. Menouar, "Visible Light Communication for Vehicular Networking: Performance Study of a V2V System Using a Measured Headlamp Beam Pattern Model," *IEEE Vehicular Technology Magazine (VTMag)*, vol. 10, no. 4, pp. 45–53, Dec. 2015.

[20] P. H. Pathak, X. Feng, P. Hu, and P. Mohapatra, "Visible Light Communication, Networking, and Sensing: A Survey, Potential and Challenges," *IEEE Communications Surveys & Tutorials*, vol. 17, no. 4, pp. 2047–2077, Feb. 2015.

[21] S. Kruse, C. Kress, A. Memedi, C. Tebruegge, M. S. Amjad, C. Scheytt, and F. Dressler, "Design of an Automotive Visible Light Communications Link using an Off-The-Shelf LED Headlight," in *16th GMM/ITG-Symposium ANALOG 2018*, Munich, Germany: VDE, Sep. 2018.

[22] A. Memedi, C. Tebruegge, J. Jahneke, and F. Dressler, "Impact of Vehicle Type and Headlight Characteristics on Vehicular VLC Performance," in *10th IEEE Vehicular Networking Conference (VNC 2018)*, Taipei, Taiwan: IEEE, Dec. 2018.

[23] C. Tebruegge, A. Memedi, and F. Dressler, "Empirical Characterization of the NLOS Component for Vehicular Visible Light Communication," in *11th IEEE Vehicular Networking Conference (VNC 2019)*, Los Angeles, CA: IEEE, Dec. 2019, pp. 64–67.

[24] M. S. Amjad, C. Tebruegge, A. Memedi, S. Kruse, C. Kress, C. Scheytt, and F. Dressler, "An IEEE 802.11 Compliant SDR-based System for Vehicular Visible Light Communications," in *IEEE International Conference on Communications (ICC 2019)*, Shanghai, China: IEEE, May 2019.

[25] C. Tebruegge, Q. Zhang, and F. Dressler, "Optical Interference Reduction with Spatial Filtering Receiver for Vehicular Visible Light Communication," in *22nd IEEE International Conference on Intelligent Transportation Systems (ITSC 2019)*, Auckland, New Zealand: IEEE, Oct. 2019.

[26] C. Tebruegge, A. Memedi, and F. Dressler, "Reduced Multiuser-Interference for Vehicular VLC using SDMA and Matrix Headlights," in *IEEE Global Communications Conference (GLOBECOM 2019)*, Waikoloa, HI: IEEE, Dec. 2019.

[27] M. S. Amjad, C. Tebruegge, A. Memedi, S. Kruse, C. Kress, C. Scheytt, and F. Dressler, "Towards an IEEE 802.11 Compliant System for Outdoor Vehicular Visible Light Communications," *IEEE Transactions on Vehicular Technology (TVT)*, vol. 70, no. 6, pp. 5749–5761, Jun. 2021.

[28] ETSI, TCITS, "Intelligent transport systems (ITS); vehicular communications; basic set of applications; definitions," *Tech. Rep. ETSI TR 102 6382009*, 2009.

[29] A. Buchenscheit, F. Schaub, F. Kargl, and M. Weber, "A VANET-based emergency vehicle warning system," in *1st IEEE Vehicular Networking Conference (VNC 2009)*, Tokyo, Japan: IEEE, Oct. 2009, pp. 1–8.

[30] R. Braun, F. Busch, C. Kemper, R. Hildebrandt, F. Weichenmeier, C. Menig, I. Paulus, and R. Presslein-Lehle, "TRAVOLUTION – Netzweite Optimierung der Lichtsignalsteuerung und LSA-Fahrzeug-Kommunikation," *Strassenverkehrstechnik*, vol. 53, pp. 365–374, Jun. 2009.

[31] J.-B. Tomas-Gabarron, E. Egea-Lopez, and J. Garcia-Haro, "Vehicular Trajectory Optimization for Cooperative Collision Avoidance at High Speeds," *IEEE Transactions on Intelligent Transportation Systems (TITS)*, vol. 14, no. 4, pp. 1930–1941, Dec. 2013.

[32] H.-J. Gunther, O. Trauer, and L. Wolf, "The potential of collective perception in vehicular ad-hoc networks," in *14th International Conference on Intelligent Transportation Systems Telecommunications (ITST 2015)*, Copenhagen, Denmark: IEEE, Dec. 2015.

[33] Europisches Parlament, "Verordnung (EU) 2015/758 des Europäischen Parlaments und des Rates vom 29. April 2015 über Anforderungen für die Typgenehmigungen zur Einführung des auf dem 112-Notruf basierenden bordeigenen eCall-Systems in Fahrzeugen und zur Änderung der Richtlinie 2007/46/EG," *Rat der Europäischen Union (2011)*, 2011.

[34] J. Schütze, Modellierung von Kommunikationsprozessen in KMU-Netzwerken. Springer, 2009.

[35] A. G. Bell, "Selenium and the Photophone," *Nature*, vol. 22, no. 569, pp. 500–503, 1880.

[36] F. R. Gfeller and U. Bapst, "Wireless in-house data communication via diffuse infrared radiation," *Proceedings of the IEEE*, vol. 67, no. 11, pp. 1474–1486, 1979.

[37] H. Elgala, R. Mesleh, and H. Haas, "Indoor optical wireless communication: potential and state-of-the-art," *IEEE Communications Magazine (COMMAG)*, vol. 49, no. 9, pp. 56–62, 2011.

[38] D. G. Pelka and K. Patel, "An overview of LED applications for general illumination," in *Design of Efficient Illumination Systems*, R. J. Koshel, Ed., vol. 5186, San Diego, CA: SPIE, Nov. 2003, pp. 15–26.

[39] R. Schedel, "LED headlamps gain market share," *ATZ elektronik worldwide*, vol. 109, no. 11, pp. 2–3, Nov. 2007.

[40] C. DiLouie, Advanced Lighting Controls. Boca Raton, FL: CRC Press, 2014.

[41] H. Burchardt, N. Serafimovski, D. Tsonev, S. Videv, and H. Haas, "VLC: Beyond point-to-point communication," *IEEE Communications Magazine (COMMAG)*, vol. 52, no. 7, pp. 98–105, Jul. 2014.

[42] "IEEE Standard for Local and metropolitan area networks–Part 15.7: Short-Range Optical Wireless Communications," *IEEE Std 802.15.7-2018 (Revision of IEEE Std 802.15.7-2011)*, pp. 1–407, Apr. 2019.

[43] S. Dimitrov and H. Haas, Principles of LED Light Communications: Towards Networked Li-Fi. Cambridge University Press, 2015.

[44] M. Zhang and Z. Zhang, "An Optimum DC-Biasing for DCO-OFDM System," *IEEE Communications Letters*, vol. 18, no. 8, pp. 1351–1354, Aug. 2014.

[45] J. Armstrong and B. J. Schmidt, "Comparison of asymmetrically clipped optical OFDM and DC-biased optical OFDM in AWGN," *IEEE Communications Letters*, vol. 12, no. 4, pp. 343–345, Apr. 2008.

[46] M. S. Islim and H. Haas, "Modulation Techniques for Li-Fi," *ZTE Communications*, vol. 14, pp. 29–40, Apr. 2016.

[47] M. Noshad and M. Brandt-Pearce, "Hadamard-Coded Modulation for Visible Light Communications," *IEEE Transactions on Communications*, vol. 64, no. 3, pp. 1167–1175, Jan. 2016.

[48] Q. Wang, Q. Chen, X. Guo, Z. Wang, D. G. Cunningham, and I. H. White, "Layered ACO-OFDM for intensity-modulated direct-detection optical wireless transmission," *Optics Express*, vol. 23, no. 9, pp. 12 382–12 393, May 2015.

[49] S. D. Dissanayake and J. Armstrong, "Comparison of ACO-OFDM, DCO-OFDM and ADO-OFDM in IM/DD Systems," *Journal of Lightwave Technology*, vol. 31, no. 7, pp. 1063–1072, Apr. 2013.

[50] Y. Wang, L. Tao, X. Huang, J. Shi, and N. Chi, "8-Gb/s RGBY LED-Based WDM VLC System Employing High-Order CAP Modulation and Hybrid Post Equalizer," *IEEE Photonics Journal*, vol. 7, no. 6, Oct. 2015.

[51] "IEEE Standard for Local and metropolitan area networks – Part 15.7: Short-Range Wireless Optical Communication Using Visible Light," IEEE, Std 802.15.7-2011, Sep. 2011.

[52] A.-M. Cailean and M. Dimian, "Impact of IEEE 802.15.7 Standard on Visible Light Communications Usage in Automotive Applications," *IEEE Communications Magazine (COMMAG)*, 2017.

[53] B. Turan, G. Gurbilek, A. Uyrus, and S. Coleri Ergen, "Vehicular VLC Frequency Domain Channel Sounding and Characterization," in *10th IEEE Vehicular Networking Conference (VNC 2018)*, Taipei, Taiwan: IEEE, Dec. 2018.

[54] K. H. Loo, Y. M. Lai, S.-C. Tan, and C. K. Tse, "Stationary and Adaptive Color-Shift Reduction Methods Based on the Bilevel Driving Technique for Phosphor-Converted White LEDs," *IEEE Transactions on Power Electronics*, vol. 26, no. 7, pp. 1943–1953, 2011.

[55] S. Lee, J. K. Kwon, S.-Y. Jung, and Y.-H. Kwon, "Evaluation of visible light communication channel delay profiles for automotive applications," *EURASIP Journal on Wireless Communications and Networking*, vol. 9, no. 1, Dec. 2012.

[56] J. B. Carruthers and J. M. Kahn, "Multiple-subcarrier modulation for nondirected wireless infrared communication," *IEEE Journal on Selected Areas in Communications (JSAC)*, vol. 14, no. 3, pp. 538–546, 1996.

[57] J. Kahn and J. R. Barry, "Wireless Infrared Communications," *Proceedings of the IEEE*, vol. 85, no. 2, pp. 265–298, Feb. 1997.

[58] T. Komine and M. Nakagawa, "Fundamental analysis for visible-light communication system using LED lights," *IEEE Transactions on Consumer Electronics*, vol. 50, no. 1, pp. 100–107, Feb. 2004.

[59] Z. Ghassemlooy, L. N. Alves, S. Zvanovec, and M. A. Khalighi, Visible light communications: theory and applications. Boca Raton, FL: CRC Press, 2017.

[60] J. Grubor, S. Randel, K.-D. Langer, and J. W. Walewski, "Broadband information broadcasting using LED-based interior lighting," *Journal of Lightwave Technology*, vol. 26, no. 24, pp. 3883–3892, 2008.

[61] T. Yamazato, I. Takai, H. Okada, T. Fujii, T. Yendo, S. Arai, M. Andoh, T. Harada, K. Yasutomi, K. Kagawa, et al., "Image-Sensor-Based Visible Light Communication for Automotive Applications," *IEEE Communications Magazine (COMMAG)*, vol. 52, no. 7, pp. 88–97, Jul. 2014.

[62] D.-R. Kim, S.-H. Yang, H.-S. Kim, Y.-H. Son, and S.-K. Han, "Outdoor visible light communication for inter-vehicle communication using controller area network," in *4th International Conference on Communications and Electronics (ICCE 2012)*, Hue, Vietnam, Aug. 2012, pp. 31–34.

[63] M. Werkstetter, S. Weber, F. Hirth, and C. Amann, "Laserlicht im BMW i8 Ansteuerung und E/E-Integration," *ATZelektronik*, vol. 9, no. 4, pp. 26–31, Aug. 2014.

[64] J. Hansen, "Remote-Laser-Lichtquelle für ein hochaufgelöstes Scheinwerfersystem," PhD Thesis, Technische Universität Berlin, Berlin, Germany, Mar. 2019.

[65] O. Narmanlioglu, B. Turan, S. Coleri Ergen, and M. Uysal, "Cooperative MIMO-OFDM based inter-vehicular visible light communication using brake lights," *Elsevier Computer Communications*, vol. 120, no. C, pp. 138–146, May 2018.

[66] W. Viriyasitavat, S.-H. Yu, and H.-M. Tsai, "Channel Model for Visible Light Communications Using Off-the-shelf Scooter Taillight," in *5th IEEE Vehicular Networking Conference (VNC 2013)*, Boston, MA: IEEE, Dec. 2013, pp. 170–173.

[67] H.-Y. Tseng, Y.-L. Wei, A.-L. Chen, H.-P. Wu, H. Hsu, and H.-M. Tsai, "Characterizing link asymmetry in vehicle-to-vehicle Visible Light Communications," in *7th IEEE Vehicular Networking Conference (VNC 2015)*, Kyoto, Japan: IEEE, Dec. 2015, pp. 88–95.

[68] G. Gurbilek, M. Koca, A. Uyrus, B. Soner, E. Basar, and S. Coleri, "Location-Aware Adaptive Physical Layer Design for Vehicular Visible Light Communication," in *11th IEEE Vehicular Networking Conference (VNC 2019)*, Los Angeles, CA: IEEE, Dec. 2019.

[69] C. Sommer, R. German, and F. Dressler, "Bidirectionally Coupled Network and Road Traffic Simulation for Improved IVC Analysis," *IEEE Transactions on Mobile Computing (TMC)*, vol. 10, no. 1, pp. 3–15, Jan. 2011.

[70] A. Varga, "The OMNeT++ Discrete Event Simulation System," in *European Simulation Multiconference (ESM 2001)*, Prague, Czechia, Jun. 2001.

[71] D. Krajzewicz, G. Hertkorn, C. Rössel, and P. Wagner, "SUMO (Simulation of Urban MObility); An Open-source Traffic Simulation," in *4th Middle East Symposium on Simulation and Modelling (MESM 2002)*, Sharjah, UAE, Sep. 2002, pp. 183–187.

[72] A. Memedi, C. Sommer, and F. Dressler, "On the Need for Coordinated Access Control for Vehicular Visible Light Communication," in *14th IEEE/IFIP Conference on Wireless On demand Network Systems and Services (WONS 2018)*, Isola 2000, France: IEEE, Feb. 2018, pp. 121–124.

[73] B. Heißing, M. Ersoy, and S. Gies, Fahrwerkhandbuch - Grundlagen · Fahrdynamik · Komponenten · Systeme · Mechatronik · Perspektiven. Heidelberg, Germany: Springer-Verlag Berlin Heidelberg, 2013.

[74] J. Kardelke, O. Diederichsen, and M. Weinberger, "Hoehenaenderungen von Pkw-Karosserien beim Bremsen," *Verkehrsunfall und Fahrzeugtechnik*, vol. 42, no. 3, 2004.

[75] N. Lourenco, D. Terra, N. Kumar, L. N. Alves, and R. L. Aguiar, "Visible Light Communication System for outdoor applications," in *8th International Symposium on Communication Systems, Networks & Digital Signal Processing (CSNDSP 2012)*, Poznań, Poland: IEEE, Jul. 2012.

[76] K. Cho and D. Yoon, "On the general BER expression of one-and two-dimensional amplitude modulations," *IEEE Transactions on Communications*, vol. 50, no. 7, pp. 1074–1080, 2002.

[77] C. Heegard and S. B. Wicker, Turbo coding. Springer Science & Business Media, 2013, vol. 476.

[78] J. W. Craig, "A new, simple and exact result for calculating the probability of error for two-dimensional signal constellations," in *Military Communications Conference (MILCOM 91)*, McLean, U.S. Virgin Islands, Nov. 1991, pp. 571–575.

[79] M. Jacobsson and C. Rohner, "Link quality estimation for arbitrary packet sizes over wireless links using packet reception events," *International Journal of Communication Systems*, vol. 32, no. 16, pp. 609–612, 2019.

[80] X. Huang, S. Chen, Z. Wang, J. Shi, Y. Wang, J. Xiao, and N. Chi, "2.0-Gb/s Visible Light Link Based on Adaptive Bit Allocation OFDM of a Single Phosphorescent White LED," *IEEE Photonics Journal*, vol. 7, no. 5, pp. 1–8, Oct. 2015.

[81] P. Luo, Z. Ghassemlooy, H. Le Minh, E. Bentley, A. Burton, and X. Tang, "Performance analysis of a car-to-car visible light communication system," *Applied Optics*, vol. 54, no. 7, pp. 1696–1706, Mar. 2015.

[82] C. Wynn, "An introduction to BRDF-based lighting," *Nvidia Corporation*, 2000.

[83] F. Miramirkhani, "Channel modeling and characterization for visible light communications: indoor, vehicular and underwater channels," PhD Thesis, Özyeğin University, Çekmeköy, Istanbul, Turkey, Jun. 2018.

[84] S. Köhler and C. Neumann, "Luminance coefficients of road surfaces for low angles of illumination," *Lighting Research & Technology*, vol. 45, no. 5, pp. 599–613, 2013.

[85] H. Elgala, R. Mesleh, and H. Haas, "Practical considerations for indoor wireless optical system implementation using OFDM," in *10th International Conference on Telecommunications (ConTEL 2009)*, Zagreb, Croatia, Jun. 2009, pp. 25–29.

[86] C. G. Gavrincea, J. Baranda, and P. Henarejos, "Rapid prototyping of standard-compliant visible light communications system," *IEEE Communications Magazine (COMMAG)*, vol. 52, no. 7, pp. 80–87, Jul. 2014.

[87] N. Kumar, N. Lourenço, D. Terra, L. N. Alves, and R. L. Aguiar, "Visible Light Communications in Intelligent Transportation Systems," in *IEEE Intelligent Vehicles Symposium (IV 2012)*, Alcalá de Henares, Spain: IEEE, Jun. 2012.

[88] W. Liang, C.-W. Chow, Y. Liu, and C.-H. Yeh, "Multi-Gbit/s phosphor-based white-light and blue-filter-free visible light communication and lighting system with practical transmission distance," *Optics Express*, vol. 28, no. 5, pp. 7375–7381, Mar. 2020.

[89] A. H. Azhar, T. Tran, and D. O'Brien, "A Gigabit/s Indoor Wireless Transmission Using MIMO-OFDM Visible-Light Communications," *IEEE Photonics Technology Letters*, vol. 25, no. 2, pp. 171–174, Jan. 2013.

[90] I. Stevanović, "Light Fidelity (LiFi)," *Federal Office of Communications OFCOM Licences and Frequency Management Division Radio Technology Section*, 2016.

[91] H. Haas, L. Yin, Y. Wang, and C. Chen, "What is LiFi?" *Journal of Lightwave Technology*, vol. 34, no. 6, pp. 1533–1544, Mar. 2016.

[92] W.-H. Shen and H.-M. Tsai, "Testing Vehicle-to-Vehicle Visible Light Communications in Real-World Driving Scenarios," in *9th IEEE Vehicular Networking Conference (VNC 2017)*, Turin, Italy: IEEE, Nov. 2017, pp. 187–194.

[93] J. Koepe, C. Kaltschmidt, M. Illian, R. Puknat, P. Kneuper, S. Wittemeier, A. Memedi, C. Tebruegge, M. S. Amjad, S. Kruse, et al., "First Performance Insights on Our Novel OFDM-based Vehicular VLC Prototype," in *10th IEEE Vehicular Networking Conference (VNC 2018), Poster Session*, Taipei, Taiwan: IEEE, Dec. 2018.

[94] B. Bloessl, M. Segata, C. Sommer, and F. Dressler, "An IEEE 802.11a/g/p OFDM Receiver for GNU Radio," in *ACM SIGCOMM 2013, 2nd ACM Software Radio Implementation Forum (SRIF 2013)*, Hong Kong, China: ACM, Aug. 2013, pp. 9–16.

[95] L. Chia-Horng, "On the design of OFDM signal detection algorithms for hardware implementation," in *IEEE Global Telecommunications Conference (GLOBECOM 2003)*, San Francisco, CA: IEEE, Dec. 2003, pp. 596–599.

[96] E. Sourour, H. El-Ghoroury, and D. McNeill, "Frequency Offset Estimation and Correction in the IEEE 802.11a WLAN," in *60th IEEE Vehicular Technology Conference (VTC 2004-Fall)*, Los Angeles, CA: IEEE, Sep. 2004, pp. 4923–4927.

[97] M. L. Cedervall and R. Johannesson, "A fast algorithm for computing distance spectrum of convolutional codes," *IEEE Transactions on Information Theory*, vol. 35, no. 6, pp. 1146–1159, 1989.

[98] T. R. Roshna, R. Nivin, J. Sherly, J. AprenT, and V. Alex, "Design and implementation of digital Costas loop and Bit synchronizer in FPGA for BPSK demodulation," in *2013 International Conference on Control Communication and Computing (ICCC)*, Thiruvananthapuram, India: IEEE, Dec. 2013.

[99] H. Nishimoto, T. Yamazato, H. Okada, T. Fujii, T. Yendo, and S. Arai, "High-speed transmission of overlay coding for road-to-vehicle visible light communication using LED array and high-speed camera," in *IEEE Global Communications Conference (GLOBECOM 2012)*, Anaheim, CA: IEEE, Dec. 2012, pp. 1234–1238.

[100] Y. Goto, I. Takai, T. Yamazato, H. Okada, T. Fujii, S. Kawahito, S. Arai, T. Yendo, and K. Kamakura, "A New Automotive VLC System Using Optical Communication Image Sensor," *IEEE Photonics Journal*, vol. 8, no. 3, pp. 1–17, Jun. 2016.

[101] D. Tsonev, H. Chun, S. Rajbhandari, J. J. McKendry, S. Videv, E. Gu, M. Haji, S. Watson, A. E. Kelly, G. Faulkner, et al., "A 3-Gb/s Single-LED OFDM-Based Wireless VLC Link Using a Gallium Nitride μ-LED," *IEEE Photonics Technology Letters*, vol. 26, no. 7, pp. 637–640, Apr. 2014.

[102] B. Fahs, A. J. Chowdhury, and M. M. Hella, "A 12-m 2.5-Gb/s lighting compatible integrated receiver for OOK visible light communication links," *Journal of Lightwave Technology*, vol. 34, no. 16, pp. 3768–3775, 2016.

[103] J. B. Carruther and J. M. Kahn, "Angle diversity for nondirected wireless infrared communication," *IEEE Transactions on Communications*, vol. 48, no. 6, pp. 960–969, Jun. 2000.

[104] M. A. El-Shimy and S. Hranilovic, "Spatial-Diversity Imaging Receivers for Non-Line-of-Sight Solar-Blind UV Communications," *Journal of Lightwave Technology*, vol. 33, no. 11, pp. 2246–2255, Jun. 2015.

[105] Z. Chen, D. A. Basnayaka, X. Wu, and H. Haas, "Interference Mitigation for Indoor Optical Attocell Networks Using an Angle Diversity Receiver," *Journal of Lightwave Technology*, vol. 36, no. 18, pp. 3866–3881, Sep. 2018.

[106] W.-H. Shen, P. W. Chen, and H.-M. Tsai, "Vehicular Visible Light Communication with Dynamic Vision Sensor: A Preliminary Study," in *10th IEEE Vehicular Networking Conference (VNC 2018)*, Taipei, Taiwan: IEEE, Dec. 2018.

[107] J. Kratochvil, "Exterior lighting used for C2C communication – High Speed & High Resolution Smart Detector," in *12th International Symposium on Automotive Lighting (ISAL 2017)*, Darmstadt, Germany: Herbert Utz Verlag GmbH, Sep. 2017, pp. 575–578.

[108] C. B. Martin, "Design issues of a hyperfield fisheye lens," in *Novel Optical Systems Design and Optimization*, vol. 5524, Denver, CO: SPIE, Oct. 2004.

[109] M. J. Li, A. D. Brown, D. E. Burns, D. P. Kelly, K. Kim, A. S. Kutyrev, S. R. McCandliss, S. H. Moseley, V. Mikula, and L. H. Oh, "Electrostatic microshutter arrays," in *19th International Conference on Solid-State Sensors, Actuators and Microsystems (TRANSDUCERS 2017)*, Kaohsiung, Taiwan: IEEE, Jun. 2017, pp. 2235–2238.

[110] "Uniform Provisions Concerning the Approval of Motor Vehicle Headlamps Emitting an Asymmetrical Passing Beam or a Driving Beam or Both and Equipped with Filament Lamps," United Nations, Tech. Rep. Regulation No. 112 - Revision 1, Oct. 2006.

[111] A. Memedi, H.-M. Tsai, and F. Dressler, "Impact of Realistic Light Radiation Pattern on Vehicular Visible Light Communication," in *IEEE Global Communications Conference (GLOBECOM 2017)*, Singapore, Singapore: IEEE, Dec. 2017.

[112] G. Elger, B. Spinger, N. Bienen, and N. Benter, "LED matrix light source for adaptive driving beam applications," in *63rd IEEE Electronic Components and Technology Conference (ECTC 2013)*, Las Vegas, NV, May 2013, pp. 535–540.

[113] P. Luo, Z. Ghassemlooy, H. L. Minh, E. Bentley, A. Burton, and X. Tang, "Bit-error-rate performance of a car-to-car vlc system using 2×2 mimo," *The Mediterranean Journal of Computers and Networks (MEDJCN)*, vol. 11, no. 2, pp. 400–407, Apr. 2015.

[114] B. Turan, S. Ucar, S. Coleri Ergen, and O. Ozkasap, "Dual Channel Visible Light Communications for Enhanced Vehicular Connectivity," in *7th IEEE Vehicular Networking Conference (VNC 2015)*, Kyoto, Japan: IEEE, Dec. 2015, pp. 84–87.

[115] A. Ashok, M. Gruteser, N. Mandayam, J. Silva, M. Varga, and K. Dana, "Challenge : Mobile Optical Networks Through Visual MIMO," in *16th ACM International Conference on Mobile Computing and Networking (MobiCom 2010)*, Chicago, IL: IEEE, Sep. 2010.

[116] I. Takai, T. Harada, M. Andoh, K. Yasutomi, K. Kagawa, and S. Kawahito, "Optical Vehicle-to-Vehicle Communication System Using LED Transmitter and Camera Receiver," *IEEE Photonics Journal*, vol. 6, no. 5, pp. 1–14, Oct. 2014.

[117] P. Luo, M. Zhang, Z. Ghassemlooy, H. Le Minh, H.-M. Tsai, X. Tang, L. C. Png, and D. Han, "Experimental Demonstration of RGB LED-Based Optical Camera Communications," *IEEE Photonics Journal*, vol. 7, no. 5, Oct. 2015.